



HAL
open science

Synthesis of layered double hydroxides through continuous flow processes: A review

Didier Tichit, Géraldine Layrac, Corine Gerardin

► To cite this version:

Didier Tichit, Géraldine Layrac, Corine Gerardin. Synthesis of layered double hydroxides through continuous flow processes: A review. *Chemical Engineering Journal*, 2019, 369, pp.302-332. 10.1016/j.cej.2019.03.057 . hal-03090844

HAL Id: hal-03090844

<https://cnrs.hal.science/hal-03090844v1>

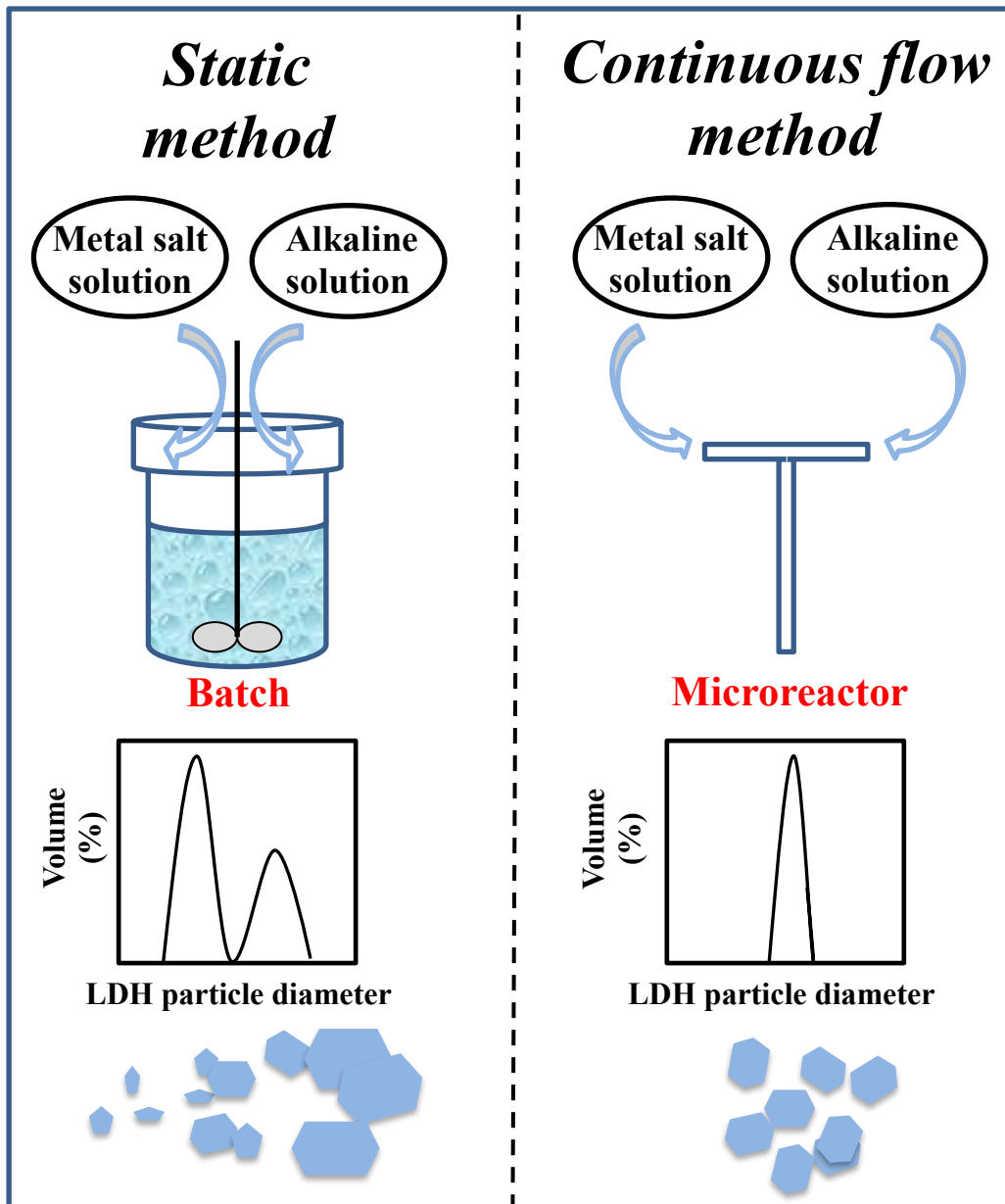
Submitted on 30 Dec 2020

HAL is a multi-disciplinary open access archive for the deposit and dissemination of scientific research documents, whether they are published or not. The documents may come from teaching and research institutions in France or abroad, or from public or private research centers.

L'archive ouverte pluridisciplinaire **HAL**, est destinée au dépôt et à la diffusion de documents scientifiques de niveau recherche, publiés ou non, émanant des établissements d'enseignement et de recherche français ou étrangers, des laboratoires publics ou privés.

Highlights

- Continuous flow processes allow scaling-up of LDH production with constant quality
- Morphology and size of particles are controlled
- Evolution of the reactor design from tank to microfluidic technology is evidenced
- Heat and mass transfers are improved, and residence times are reduced
- Nanosheets, LDH-based hybrids and nanocomposites are obtained



Graphical abstract

Different continuous flow processes allow the production of LDHs particles with controlled size and morphology or individual nanosheets, and of LDH-based hybrids and nanocomposites.

Synthesis of layered double hydroxides through continuous flow processes: A review

Didier Tichit*, Géraldine Layrac^a and Corine Gérardin

ICGM, Univ. Montpellier, CNRS, ENSCM, 240 Avenue du Professeur Emile Jeanbrau, 34296
Montpellier Cedex 5, France

Abstract

Continuous production processes allow scaling up of layered double hydroxides (LDHs) and avoid the drawbacks induced by conventional coprecipitation. These drawbacks result from variable supersaturation rate due to non constant pH and concentration of the solutions and from long residence times hindering a fine control of the size and morphology of the particles. Continuous flow processes allow reducing the residence time and maintaining almost constant supersaturation producing LDHs in large amounts with constant quality. We report here the different continuous flow methods for the production of LDHs particles with controlled size and morphology or individual nanosheets, and of LDH-based hybrids and nanocomposites. The paper will focus on the design of the reactors showing a decrease of their volume and an improvement of the mixing and heat and mass transfers. Cylindrical tank under steady-state conditions lead to particles with a narrower size distribution than in batch reactor. Then processes with vigorously stirred microreactors in the so-called in-line dispersion-precipitation method were developed. Counter-current flow reactors with particles formed at the interface of solutions flowing up and down were further used to obtain ultra-fine LDH nanoplates and efficient surface modification with surfactants. Hydrothermal continuous or co-flow reactors exhibit great versatility allowing the preparation of exfoliated or functional LDHs, LDH nanoplates on alumina-coated substrates, and reduced graphene oxide/LDH nanocomposite

films. The microfluidic technology is very promising for preparing LDHs of different compositions and functionalities. The reaction conditions as well as the structural and morphological properties of the materials are discussed and applications are reported.

*Corresponding author: ICGM, Equipe MACS, Ecole Nationale Supérieure de Chimie de Montpellier, 240 Avenue du Professeur Emile Jeanbrau, 34296 Montpellier Cedex 5, France.

E-mail address: didier.tichit@enscm.fr

^a Present address: ICPEES, Institut de Chimie et Procédé pour l'Energie l'Environnement et la Santé, CNRS UMR 7515, ECPM-Université de Strasbourg, 25 rue Becquerel, 67087 Strasbourg Cedex 2, France (E-mail : layrac@unistra.fr)

Key words: Layered double hydroxides, continuous-flow, tubular reactor, counter-current reactor, microreactor.

Abbreviations:

AFM: atomic force microscopy; BET: Brunauer, Emmett, Teller; BJH: Barrett, Joyner, Halenda; CFR: continuous flow reaction; DDA: dodecanedioic acid; DLS: Dynamic light scattering; DS: dodecyl sulfate; EDX: Energy-dispersive X-ray spectroscopy; DSC: Differential scanning calorimetry; Et: ethanol; FTIR: Fourier Transform Infrared spectroscopy; GO: graphene oxide; Hb: hemoglobin; HCFR: hydrothermal continuous flow reactor; HPLC: High performance liquid chromatography; IEP: isoelectric point; ILDP: in-line dispersion-precipitation; LDH: Layered double hydroxide; MEG: monoethylene glycol; MOFs: Metal organic frameworks; NCs: Nanocrystals; NPS: nanoparticles; NSs: nanosheets; OER: oxygen evolution reaction; OPD: *o*-phenylenediamine; PA: polyacrylate; PE: polyethylene glycol; PEA: Poly(ethylene-co-acrylic acid); PEs: polyelectrolytes; PS: Particle size; PSD: Particle size distribution; PWD: Precipitation, water-washing, dispersion; Re : Reynolds number; S:

supersaturation; SEM: Scanning electron microscopy; SHR: Static hydrothermal reactor; TEM: transmission electronic microscopy; TK: transketolase; UV-vis: Ultraviolet/visible spectroscopy; XPS: X-ray photoelectron spectroscopy; XRD: X-ray diffraction

1. Introduction

The industrial demand for different types of inorganic materials makes essential the development of scalable, cost-effective and versatile methods of production to replace the conventional static, batch or multiple step processes. In addition to be hardly scalable, these latter suffer from irreproducibility of particles size, size distribution and quality of the products from batch to batch. Over the past twenty five years continuous-flow synthesis methods have been investigated for the controlled production of a wide variety of inorganic nanomaterials including metal oxides, sulfides and phosphates, metal nanoparticles, silicates, zeolites and also metal-organic frameworks, core-shell particles, among others. There are a number of recent and particularly excellent reviews on the synthesis of these different sorts of nanomaterials using continuous flow processes [1-4]. A consequent number of other interesting reviews is devoted to the different types of reactors implemented for the continuous flow method with a peculiar attention to microfluidic devices which include continuous flow and segmented flow approaches. Continuous flow reactors allow improving heat and mass transfers, and due to the reduction of transport process, they allow performing faster chemical reaction in comparison with conventional reactors . However, they also exhibit inherent disadvantages or difficulties. For continuous-flow microreactors, blockage of the channels and contamination of their walls by adhesion of the particles increase the polydispersity. For segmented microreactors using either bubbles or liquid drops to produce segments, it is difficult to control the coalescence of droplets and their stability [5-7].

Lots of monoatomic or heteroatomic metal oxides have been prepared using continuous-flow methods but scarce examples of preparation of metal hydroxides or oxohydroxides are reported [1]. Layered double hydroxides (LDH) are a class of bidimensional materials which attract increasing attention due to their wide variety of compositions and multiple applications.

LDH also known as hydrotalcite-like compounds or anionic clays are described by the general formula $[M(II)_{1-x}M(III)_x(OH)_2]_n[(A^{n-})_{x/n} \cdot m H_2O]_n$, where M(II) and M(III) are divalent and trivalent cations, A^{n-} is a charge compensating interlayer anion, m the number of water molecules and x the molar fraction of trivalent cations ($0.2 < x < 0.4$). The LDH layer structure is similar to that of $Mg(OH)_2$ where edge-sharing octahedra of divalent cations in the central site are surrounded by six hydroxyl groups giving rise to infinite sheets. In the LDH, some divalent cations are isomorphically substituted by cations of higher charge and rather similar ionic size, often trivalent cations, so the brucite-like layers become positively charged. Charge compensating and exchangeable anions are intercalated between the layers in order to balance the positive charge [8, 9]. A main characteristic of LDH materials is their versatile chemical composition as they can be formed with a huge variety of divalent (Mg^{2+} , Ni^{2+} , Zn^{2+} , Cu^{2+} , Mn^{2+} , Fe^{2+} , Co^{2+} , Ca^{2+} , etc) and trivalent cations (Al^{3+} , Fe^{3+} , Cr^{3+} , Mn^{3+} , Ga^{3+} , Co^{3+} , V^{3+} , etc). Structures with monovalent (Li^+) [10], tetravalent cations, i.e. Zr^{4+} [11-14], Sn^{4+} [15, 16], Ti^{4+} [17-20] and rare-earth cations [21, 22] have also been claimed, although introduction of these cations in the brucite-like layer is still controversial [17, 23]. The successive LDH layers are held together by weak hydrogen bonds provided by molecular water surrounding the intercalated anions. The nature of interlayer anions is very diverse. Beside common inorganic (halides, CO_3^{2-} , NO_3^- , SO_4^{2-} , etc) and organic anions [24-27], many other negatively charged species like polyoxometalates [28-31], biomolecules [32], polymers [33-35], coordination compounds [36-38], anionic drugs [39-41] have been also intercalated.

LDH have very high potentialities for industrial applications if one considers the huge amount of publications dealing with synthesis and applications at the laboratory scale in relevant domains such as catalysis, biomedicine, energy, waste treatment, additive of polymers etc. However, developments in industry require scalable production of particles with constant quality, i. e. controlled mean size and distribution, aspect ratio and shape. The control of morphological properties of LDH in order to improve efficiency has been largely demonstrated for applications such as adsorbent [42], fire retardant [43], support and precursor of catalysts [44-46], drug and gene delivery [47-50]. A wider potential emerges through nanohybrids- and nanocomposites-based LDH which gain attention for incorporation in polymers as flame retardants and for improving mechanical and barrier properties, [43, 51-53] drug delivery, imaging, targeting, bio-sensing and anti-microbial formulation [39, 40, 54-59], environmental remediation [60-62], catalysis [63-66] among others.

Thereby, the required physico-chemical and morphological properties of pristine LDH and LDH nanosheets acting as host structures or building blocks for nanohybrids or nanocomposites boosted investigations on the syntheses through continuous flow methods allowing to avoid several drawbacks resulting from conventional coprecipitation in batch reactors. This latter is generally achieved by addition of metal salts and alkaline solutions at variable or constant pH, generally described by nucleation and growth/aging theory. Such procedure is time and energy consuming with inherent supersaturation gradients due to limitations in mixing and heat transfer. This has dramatic consequences on nucleation and growth which both largely overlap. Indeed, along the addition of precursor solutions, nucleation of LDH seeds being very rapid [67, 68], large discrepancies of growth and size occur between particles obtained from nuclei precipitated first, staying longer time in the mother liquor, and particles growing from nuclei formed later. Nuclei with different Mg:Al spatial distribution have been revealed at different stages of the nucleation step, which also implies inhomogeneous composition of the final

crystallites. The difference in composition induces different growth speeds of the particles, the Mg-rich ones growing faster [69]. In addition, it must be pointed out that ageing of the particles in the mother liquor is generally achieved in order to improve crystallinity. This involves growth, aggregation, breakage and Ostwald ripening of the particles. Aggregation is a major drawback for several relevant applications of LDH, because it hinders accessibility to the most active sites of low coordination at the surface of the crystallites, decreases anionic exchange rate and prevents diffusion of anionic species in the interlayer domain. Aggregation is mainly induced by residual electrolytes adsorbed on the surface of the particles [70] and/or by a small amount of an amorphous phase [71]. Washings steps are necessary to remove residual electrolytes in all the synthesis methods. They require large amounts of water which is a major drawback.

Although several methods have been implemented to rule out these drawbacks, obtaining in a simple process, poorly aggregated LDH particles with controlled size and narrow size distribution still remains a challenge. Without particular care, batch or semi-batch coprecipitation leads to LDH aggregates which lie, roughly, in the range 1 – 10 μm , with a huge number of sheet-like LDH nanocrystallites. Among the methods implemented to overcome one or several of the previous drawbacks, one must consider the separation of nucleation and aging steps [72], the coprecipitation through thermally controlled hydrolysis of urea [49, 73], the mechanochemistry [74], the delamination and restacking of the pristine LDH layers, the reconstruction of the lamellar structure by rehydration of thermally decomposed LDH (the so-called memory effect) [75-77], the syntheses in confined reactors such as water droplets of reverse microemulsion media [78] or in close nanoreactors obtained from double-hydrophilic block copolymers [79]. However, these methods can hardly be scaled up because they involve complex operations, highly polar solvents or organic compounds, purification of aqueous

wastes, use of protective inert gas atmosphere in order to avoid the presence of carbonate, microwave or ultrasound treatments to break agglomerates, etc.

Lots of the inconveniences resulting from coprecipitation in batch reactor are avoided achieving LDH synthesis via continuous flow methods where residence times of the reactants can be finely tuned, and where the thermodynamic driving force, i. e. supersaturation, can be maintained at a constant level. Consistently an increasing amount of attention is given to the intensification of LDH preparation using methods in continuous flow. This is achieved following different processes and types of LDH and more recently LDH-based nanohybrids and nanocomposites. Our aim in this review article was to provide a broad description of the continuous flow methods and of the different setups used for the preparation of LDH and LDH-based hybrids and composite materials. They account for the wide variety of approaches of this spreading investigation field. The different processes which are reviewed differ by the design of the reactors and the tuning of several main synthesis parameters, i. e. residence time, mixing intensification and concentrations of the solutions, pH, flow rates, temperature, pressure, etc. Continuous flow methods have been applied to the preparation of various kinds of LDH materials as depicted in Figure 1. Pioneer approaches were mainly devoted to the control of nanostructure, particle size and morphology, while obtaining stable suspensions of LDH nanosheets had rapidly become a main concern. In steps forward, procedures were achieved for the preparation of functional LDH through synthesis of nanohybrids and nanocomposites. This evolution reveals the versatility of the continuous flow methods. These different aspects incite us to herewith categorize the review into two main parts dealing with (i) the control of the particle size and morphology of LDH nanoparticles, (ii) the production of functional LDH and LDH-based composite materials.

The main parameters of the different processes depicted in the review are reported in Table 1. Physico-chemical and morphological properties of the LDH and LDH-based samples and, when available, examples of applications are reported in Table 2.

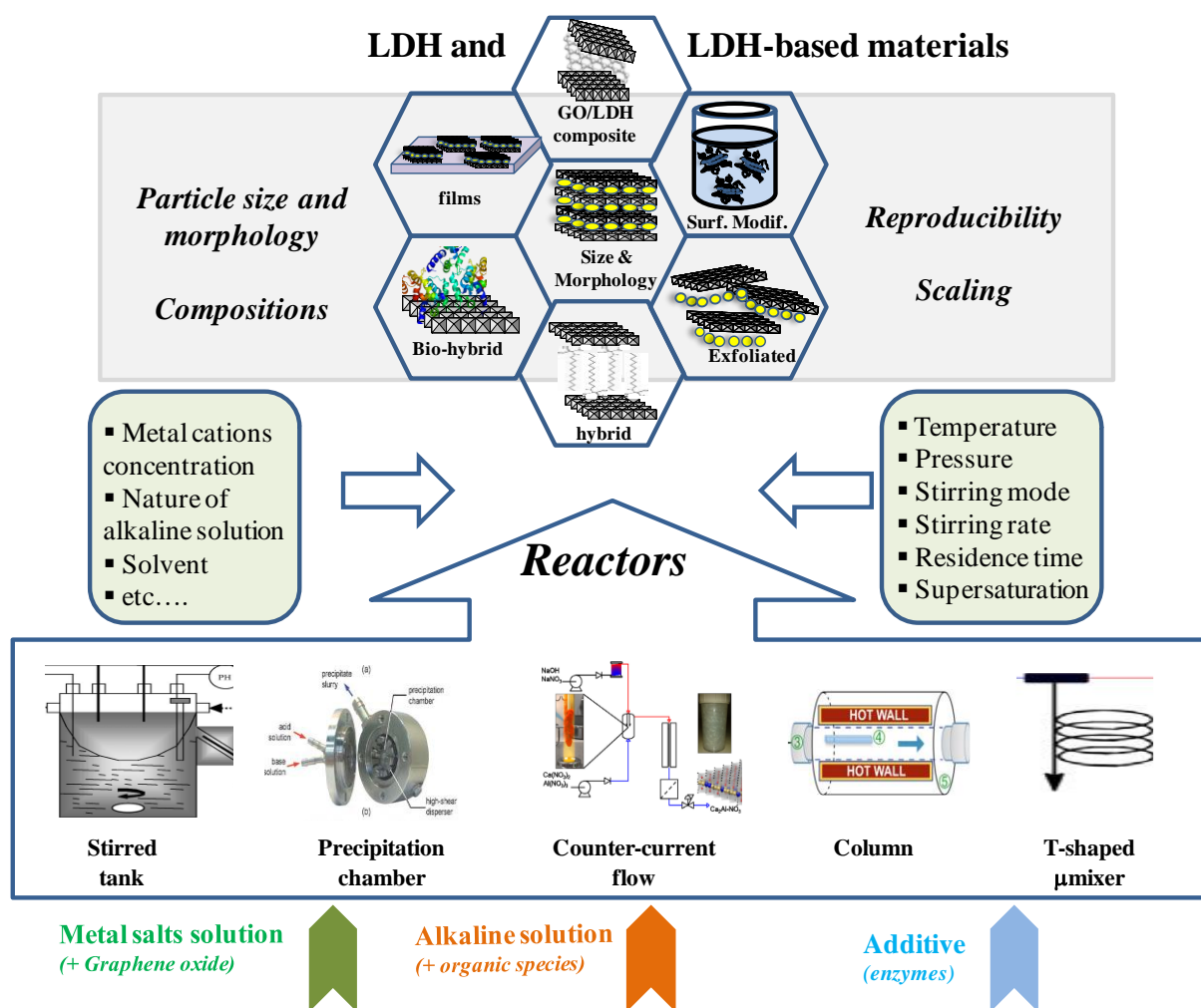


Figure 1: Overview of the continuous flow processes reviewed and the type of LDH-based materials prepared.

2. Continuous production of LDH particles: Control of the composition, particle size and morphology

The main objective of the continuous flow syntheses of LDH materials is to obtain constant and tunable particle properties through highly reproducible and scalable intensified methods. The

approaches implemented about 15 years ago started with transposition to continuous flow of the traditional coprecipitation in cylindrical tank reactor of large volume by adaptation to steady-state conditions [80]. This system ensures constant supersaturation and allows reducing residence time in comparison to batch or semi-batch syntheses. Afterwards the approaches emphasize preferentially on intensification of mixing and shortening of residence time. Indeed a net decrease of reactor volume and improvement of mixing were achieved in the in-line dispersion-precipitation (ILDp) and with counter-current flow methods. In these approaches mixing of solutions was achieved with rotating elements and in the highly turbulent contact region of the up and down flows, respectively [67, 81-83]. Another approach uses a meso-scale flow reactor where co-precipitation was performed at a residence time close to the micromixing time in order to improve the control of particle formation and to obtain high reproducibility of the syntheses [84].

The opportunities provided by the development of microreaction technologies led to exploit such methods in the synthesis of LDH in order to intensify heat and mass transfer capabilities able to reduce time and energy consumptions, and to improve reproducibility and scalability [68, 85, 86]. It is noteworthy that these processes were all achieved without aging and washing steps. So an approach which deserves interest was developed with the objective to include *in situ* cleaning of the LDH particles in the continuous flow procedure, although it leads to a more complex process in two steps [87].

The different achievements reported in the literature have essentially concerned MgAl, CaAl, NiAl, ZnAl LDH largely synthesized through conventional coprecipitation methods with different physico-chemical and morphological properties. Interestingly, they have also concerned less common NiCo LDH [88] and multicationic LDH [68, 84]. All these works will be considered in the following part.

2. 1. Synthesis using magnetically stirred tank reactor

A pioneering work dealing with coprecipitation of ZnAl LDH in continuous flow under steady-state conditions was reported in 2005 by Z. Chang et al [80]. Syntheses are achieved using a cylindrical tank (~ 230 mL) where reactants (metal cations and alkaline solutions) injected with peristaltic pumps above the central zone of the reactor were magnetically stirred (300 rpm). The pH (equal to 7, 9 or 11) is maintained constant during coprecipitation. After a residence time varying between 5 and 15 min, the effluent containing the coprecipitated LDH particles is collected continuously through an over-flow pipe going out of the upper part of the reactor (Figure 2).

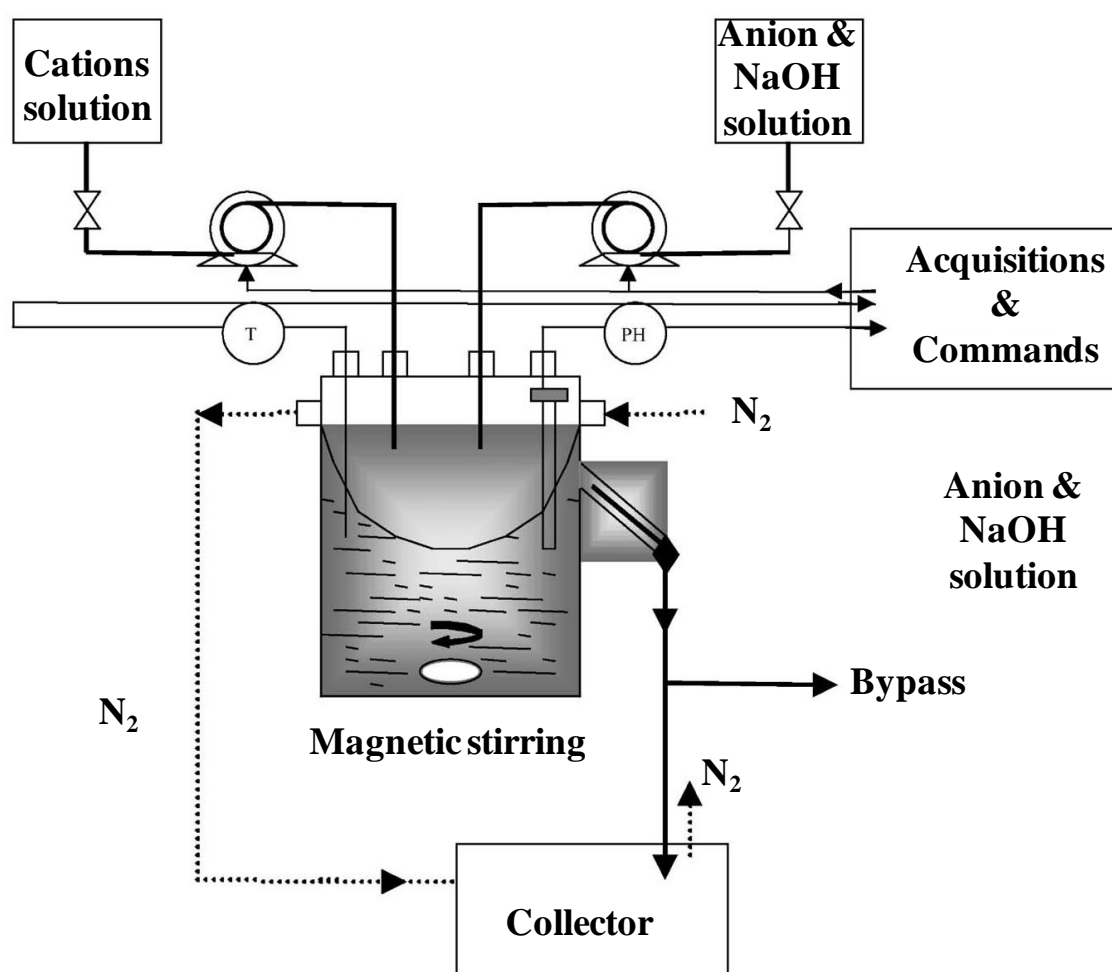


Figure 2: Experimental setup for the continuous coprecipitation of LDH samples under steady-state conditions (Reproduced with permission from Ref. [80]).

In this steady-state coprecipitation, gradients must inherently exist even though supersaturation is maintained roughly constant all along the experiment. The authors indeed suggest that higher supersaturation is generated in the vortex region where the two injected solutions collide and where nucleation occurs compared to the periphery where growth, agglomeration and Ostwald ripening must take place. These gradients impede very fine control of the particle size and particle size distribution. Moreover, mixing of the reactants is poorly efficient and short residence times (< 5 min) are hardly obtained.

The influence of several main parameters of preparation on the structural and textural properties of the ZnAl LDH has been studied, i. e. total metallic cations concentration ($3 \cdot 10^{-1}$ - $3 \cdot 10^{-3}$ mol.L⁻¹); nature of the solvent (H₂O, mixtures ethanol/H₂O (Et/H₂O), monoethylene glycol/H₂O (MEG/H₂O), polyethylene glycol/H₂O (PE/H₂O)); residence time; pH and nature of the anion (CO₃²⁻, acetate, benzoate). The obtained results can be summarized as follows.

Zn/Al molar ratios in the solids are about 2 which is consistent with the values in solution and CO₃²⁻ is the compensating anion. The sample prepared at higher metal salt concentration ($3 \cdot 10^{-1}$ mol.L⁻¹) is poorly crystallized, even though mixture of LDH, zinc hydroxide and aluminium hydroxide can be identified, while the LDH phase is conversely only present at lower metal salt concentrations ($3 \cdot 10^{-2}$ mol.L⁻¹ and $3 \cdot 10^{-3}$ mol.L⁻¹). Mean particle size and crystallinity decrease when concentration increases both in H₂O, e.g. from 200 to 160 nm, and in MEG/H₂O, e. g. from 110 to 80 nm (measured by TEM), in experiments at pH 9 and 15 min residence time. Accordingly, specific surface areas concurrently increase. Such a behavior is consistent with the increase of supersaturation with the total metal salt concentration leading to smaller crystallites. Regarding the influence of the solvent, crystallite sizes obtained in water-organic solvents are smaller than in water, and they decrease when the volume ratio of organic solvent

increases giving more uniform particles. This accounts for the increase of supersaturation in organic-water solvent mixture due to the lower solubility of metallic salts. This is also related to the increase of viscosity which has a negative effect on mixing and ion diffusivity near the surface of crystallites. It then modifies supersaturation and reduces growth rate favoring particle size reduction. The residence time controls the growth rate whereas nucleation is known to be very rapid. Both in water and organic solvents the crystallinity and the average size of the particles increase with the residence time, this effect being slightly higher in viscous media as growth rate is very rapid in water. pH 7 is too low to obtain the ZnAl LDH phase and in these steady-state conditions higher values (pH 9 and 11) have little influence on crystallinity and particle size. The organic anions, acetate and benzoate, are intercalated and lead to LDH crystallite sizes in water or organic solvents which are smaller than those obtained with CO_3^{2-} , with in addition pronounced agglomeration in the case of acetate due to its well known complexing property. It is suggested that, contrary to conventional coprecipitation, the molar ratio between anions and metallic salts is maintained constant in continuous flow experiments. Then intercalation could slow down the LDH coprecipitation which occurs simultaneously leading to smaller particles.

A comparison with the samples obtained using the standard preparation method in batch reactor (pure water and long aging period) is provided. Larger platelets of ~ 81 nm, instead of 20 – 60 nm, are obtained ; they exhibit a high degree of crystallinity and a lower specific area of $6 \text{ m}^2\text{g}^{-1}$ instead of $16 - 62 \text{ m}^2\text{g}^{-1}$ in continuous flow (Table 3, entry 1). This pioneer approach has clearly demonstrated that continuous coprecipitation under steady-state conditions has intrinsic advantages in comparison to conventional batch experiments for adjusting particle size and particle size distribution. These main advantages are the almost constant supersaturation rate, pH and residence time all along the experiment, though improvements are needed that will be achieved later in different publications by the same authors, and others, particularly through

better mixing and reduction of residence time. It must also be pointed out that the absence of aging decreases three- to tenfold the experiment time to prepare a same quantity of LDH in the continuous flow method compared to the batch reactor in the above study. This is highly relevant for scalability of LDH production.

2. 2. Synthesis using a coprecipitation chamber

In the frame of an extensive study which represents two original publications [67, 81] Abelló and Pérez-Ramírez introduce an in-line dispersion-precipitation (ILDp) process. It uses a precipitation chamber which is a microreactor (ca. 6 mL) that incorporates a rotating element with a high-speed disperser (up to 24 000 rpm). This setup ensures high degree of mixing of the two reacting solutions (metal cations and base solutions) leading to Reynolds numbers (Re) up to 10^5 , and residence times are in the range 1 – 36 s. The pH is maintained constant at 10 in the slurry by regulating the flows of the peristaltic pumps which provide the solutions. For this purpose, one of the pumps is connected to an in-line probe measuring the pH of the slurry at the outlet of the microreactor (Figure 3). A high level of constant supersaturation is maintained within the reactor during these experiments. Importantly, the precipitates are immediately collected by filtration of the slurry, without aging and washing. This rapid quenching is particularly interesting for studying LDHs obtained at very low residence times which will be one of the most relevant aspects of these publications.

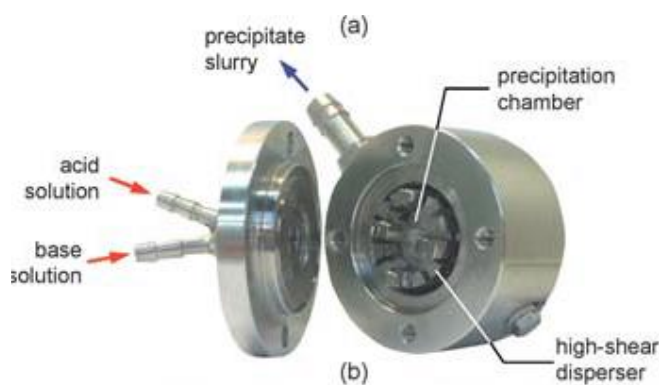


Figure 3: Photograph of the ILDP reactor (Reproduced with permission from Ref. [67]).

In the initial publication in 2006 [81], MgAl LDH were prepared by the ILDP method varying the residence time τ ($\tau = 1$ to 36 s) of the feed solutions and the stirring speed ω ($\omega = 13\,500$ to 24 000 rpm) in the microreactor in order to vary the characteristics (particle size, composition, porous and mechanical properties) of the final product. These operating parameters indeed play a role on the interconnected nucleation-growth-aggregation processes. The objective was also to demonstrate the potential of this highly intensified method for obtaining reproducible LDH materials with tunable properties. In all cases the degree of precipitation was almost complete. The solids have Mg/Al molar ratios of 2.6 – 2.8 close to the nominal value of 3 and exhibit typical XRD patterns of hydroxycalcite. The average crystallite size in the c direction (Scherrer equation applied to 003 reflection) was almost similar at ca. 4 - 5 nm for τ ranging from 1 to 18 s and increased to 11 nm at $\tau = 36$ s ($\omega = 24\,000$ rpm). The complete precipitation observed for $\tau = 1$ s termed flash precipitation by the authors, and the great increase of particle size from 5 to 11 nm when τ increases from 18 to 36 s, show that nucleation is a very fast process and that it rapidly overlaps with crystal growth and agglomeration. The aspect ratios (diameter to thickness) are in agreement with the platelet-shape morphology of the particles as average crystallite sizes in the 110 direction are larger than those in the 003 direction. There is then a clear influence of the residence time on the nucleation, growth and agglomeration processes.

This is more pronounced for a reference sample prepared by batch coprecipitation of the metal salts and alkaline solutions during 1 h whose crystallite size reaches ca. 40 nm (Table 3, entry 2). An influence of the stirring speed which contributes to maintain constant the supersaturation degree can also be anticipated. However, at low residence time ($\tau = 4.5$ s), there is almost no effect of the stirring speed (13500 or 24000 rpm) on the crystallite size (ca. 5.5 nm), while it increases from 6.4 to 11.0 nm at high residence time ($\tau = 36$ s). This unexpected result is assigned to local heating of the microreactor volume favoring crystal growth and agglomeration. Consistently, randomly distributed aggregates of fibrous particles (~ 80 nm) are observed by TEM at $\tau = 36$ s and $\omega = 13500$ rpm and larger agglomerates at $\tau = 36$ s and $\omega = 24\ 000$ rpm with an edge-face arrangement in all cases. Remarkably, particles with poorly defined shape and face-to-face agglomerates are likely observed at high nucleation rate by flash precipitation ($\tau = 1$ s and $\omega = 24\ 000$ rpm).

The porous properties of the materials prepared by the ILDP method with high productivity were carefully examined since they are crucial for industrial applications. Nitrogen adsorption-desorption isotherms of all samples (type IIb) were characteristic of LDHs with slit-shaped pores between aggregates of the platelet particles. The specific surface area versus the residence time goes through a maximum of $130\ \text{m}^2\ \text{g}^{-1}$ for $\tau = 12$ s according to the smaller crystallite size of this sample ($D_{003} = 5.2$ nm). Consistently the surface area decreases (from 130 to $85\ \text{m}^2\ \text{g}^{-1}$) when increasing the average crystallite size due to the increase of the residence time from 12 to 36 s. An unexpected behavior was observed when the residence time decreases from 10 to 1 s (flash coprecipitation) with no increase of surface area. Moreover, at $\tau = 1$ s the sample exhibits crystallites with average size of 4 nm, but both surface area and pore volume are close to zero. The short residence time and the high degree of supersaturation lead to small crystallites extremely well packed into non porous polycrystalline assemblies. A relevant practical interest of the highly intensified ILDP method is that, in spite of the small volume of the coprecipitation

chamber (6 mL), as a result of the short residence times, reproducible LDH particles with crystallite size in the range 4 – 11 nm can be obtained with productivities of several tons per hour and cubic meter of reactor.

As previously shown, the MgAl LDH sample prepared by flash precipitation exhibits unprecedented textural and morphological properties, particularly zero surface area and tight association of small crystallites. However, this sample was not extensively investigated. This incited the authors in a further study to get more insights into the effect of the residence time using the ILDP method. Characteristics of LDHs of different compositions (NiAl, MgAl and MgFe LDH) prepared by flash precipitation ($\tau = 1$ s) were investigated and compared to those obtained with a larger residence time of 12 s [67]. The influence of the residence time is already revealed by the visual aspect of the slurry and of the dried materials giving a precipitate and a dull with a fine grain texture at $\tau = 12$ s, while a stable colloidal suspension giving translucent and hard dried material is obtained at $\tau = 1$ s. The chemical composition of all samples is close to the nominal metal ratio of 3. Remarkably, all samples precipitated at 1 and 12 s residence times exhibit identical XRD patterns and the composition deduced by application of the Vegard's law to the lattice a parameter is in agreement with the results of bulk chemical analysis. These results point out on one hand, the rapid coprecipitation of the metal cations, and on the other hand their homogeneous distribution within the LDH layers, particularly in the flash experiment, the residence time having little influence on the composition. The aspect ratios are approximately 2 with D_{003} and D_{110} in the range 4 – 7 nm and 8 – 14 nm, respectively. Then, as expected, small particles are obtained using such synthesis conditions. Morphologies of the NiAl LDH particles obtained at $\tau = 1$ and 12 s confirm the differences of properties. TEM images of the samples obtained at $\tau = 12$ s show particle aggregates with plate-like and fibrous aspects as usually found for LDH prepared by conventional coprecipitation in batch reactor. For $\tau = 1$ s, AFM analysis reveals tight association of small particle subunits greatly aligned

into large agglomerates of low porosity. This is confirmed by TEM showing tightly aggregated polycrystalline particles (Figure 4).

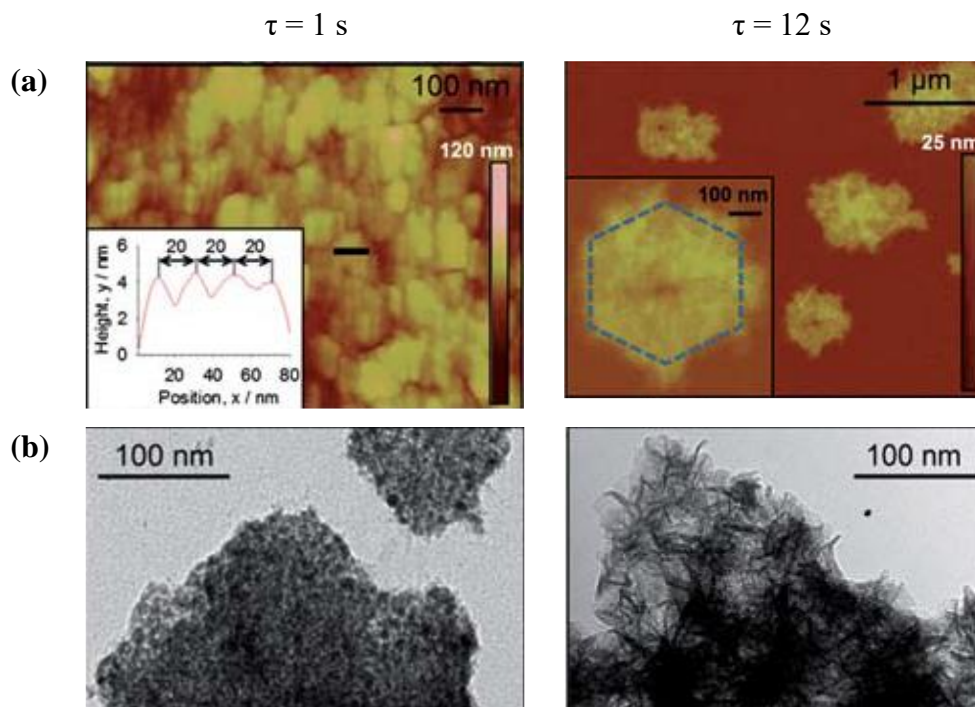


Figure 4: Images of the NiAl LDH coprecipitated with $\tau = 1$ and 12 s by (a) AFM, and (b) TEM. In AFM, the position of the height profile (inset) is marked with the horizontal line (Reproduced with permission from Ref. [67]).

The different aggregation mode of the particles is consistently reflected in the porosity. First NiAl and MgAl LDH samples prepared with $\tau = 1$ s have lower densities than those obtained with $\tau = 12$ s, which is attributed to occluded pores within the structure in the former case. Second, the N_2 adsorption-desorption isotherms are dramatically different. Type IIb adsorption isotherm and H3 hysteresis loop characteristic of slit-shape pores between LDH particles of plate-like morphology are observed for $\tau = 12$ s. Total pore volumes and surface areas range from 0.17 to 0.27 $\text{cm}^3 \text{g}^{-1}$ and from 48 to 61 $\text{m}^2 \text{g}^{-1}$, respectively, contrary to the behavior observed at $\tau = 1$ s with no N_2 uptake and no detectable surface area and porosity. This is in

agreement with the results of the previous work. Hg porosimetry confirms these results. Large mesopores and/or macropores with no intrusion are observed for $\tau = 1$ s while a pore size distribution centered at 100 nm is present for $\tau = 12$ s. The main difference between $\tau = 1$ and 12 s is the faster nucleation in the former case; and the above results show that this feature induces a peculiar behavior with tight packing of the small crystallites. A main consequence of the absence of porosity in the samples prepared with $\tau = 1$ s is the increase of thermal stability revealed by thermogravimetric analysis. For example, collapse of the structure is shifted of ca. 50 K toward higher temperature for the NiAl LDH obtained at $\tau = 1$ s in comparison to that obtained at $\tau = 12$ s obviously due to the impeded release of CO₂ and H₂O in the former. It is noteworthy that after thermal decomposition at 723 K when the materials transform into mixed oxides by dehydroxylation and decarbonation, there is a remarkable increase of porosity and surface area. However, NiAl and MgAl LDHs have different behaviors. Porosity and surface area have similar values (~ 0.20 cm³ g⁻¹ and ~ 200 m² g⁻¹, respectively) for NiAl LDH at $\tau = 1$ and 12 s, but larger values at $\tau = 12$ s (0.36 cm³ g⁻¹ and 235 m² g⁻¹) than at $\tau = 1$ s (0.06 cm³ g⁻¹ and 102 m² g⁻¹) for MgAl LDH. The porosity of the mixed oxide is more dependent of the crystal arrangement of the as-prepared LDH in the case of MgAl than in the case of NiAl LDH. In the ILDP experiments the high degree of supersaturation is maintained constant due to the high pH value (pH 10) and the intense mixing of the two feed solutions. Therefore, nucleation occurs instantly as revealed by the XRD patterns and the composition of the samples obtained at $\tau = 1$ s is homogeneous. This means that a variation of the residence time predominantly influences the crystallite growth. A main breakthrough provided by the studies of Abello et al. is the evidence of an unprecedented regime for the samples obtained by flash coprecipitation ($\tau = 1$ s) with the formation of stable colloidal suspensions of small crystallites (4 - 7 nm) so tightly packed after drying that porosity vanishes. This reveals that the operating mode favors strong face-to-face orientation of the particles, contrary to the common weak face-to-edge

arrangement of LDH nanoplates leading to mesoporosity. Such feature was never observed in standard batch experiments.

2. 3. Synthesis using counter-current flow method

Q. Wang et al. [82] developed a synthesis method using a counter-current continuous-flow reactor (Figure 5). In the reactor a down-flow of base aqueous solution (20 ml min^{-1}) pumped through a pre-heater regulating the temperature meets an up-flow of metal precursor aqueous solution (10 ml min^{-1}). This allows maintaining a very short contact time of 4 s. Experiments where crystallinities of MgAl LDH and CaAl LDH have been controlled using temperature ($75 - 400 \text{ }^\circ\text{C}$) and pressure (50 or 240 bar) have been achieved.

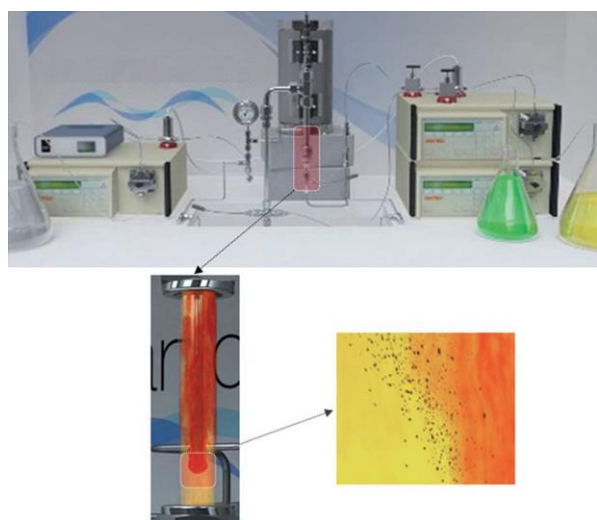


Figure 5: Images depicting the continuous hydrothermal rig. The reactor section is highlighted, showing the heated downflow (red) mixing with the ambient upflow (yellow), leading to nanoplatform formation (Reproduced with permission from Ref. [82]).

MgAl-CO₃ LDH (Mg/Al = 3) crystallite size reached ca. 10 nm in the *c* direction, whatever the synthesis temperature and pressure, both being then of little influence, while this size varies more largely from 25 to 62 nm for CaAl-NO₃ (Ca/Al = 2). TEM images and AFM analysis

reveal very thin nanoplates with thickness of 10 nm for CaAl-NO₃ and 4 - 5 nm for MgAl-CO₃, both synthesized at 50 bar and 75 °C (Figure 6). Aspect ratios of 3 - 4 are obtained for MgAl-CO₃ LDH particles their lateral width dimension being of ca. 30 - 40 nm. An increase of synthesis temperature at 150 °C favors the growth of particles. The shuttle-like CaAl-NO₃ LDH particles have a width of ca. 50 nm and a length of ca. 200 nm and the lateral dimension of the MgAl-CO₃ LDH particles is of ca. 50 - 70 nm. The latter give long nanowires at synthesis temperature of 250 °C, while CaAl-NO₃ LDH starts to decompose. Using this counter-current continuous-flow hydrothermal method the pressure has a lower influence than the temperature on the particles size and morphology. LDH yields are not reported but through the tuning of temperature, pressure and contact time the authors claimed a constant quality of products.

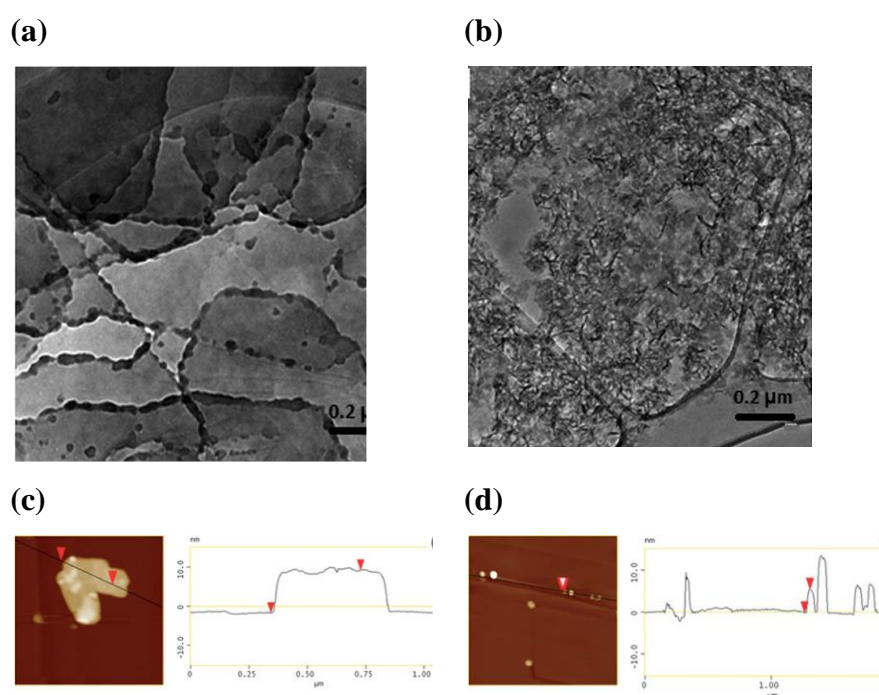


Figure 6: TEM images of CaAl-NO₃ LDH (a), MgAl-CO₃ LDH (b); and AFM images of CaAl-NO₃ (c), MgAl-CO₃ LDH synthesized at 50 bar and 75 °C (Reproduced with permission from Ref. [82]).

The continuous-flow hydrothermal synthesis using counter-current flow reactor has been also employed by I. Clark et al. [83] to prepare CaAl-NO₃ LDHs (Ca/Al = 2). Their study focuses on the influences of temperature (75 - 200 °C), pressure (50 - 200 bar) and NaOH concentration (0.01 - 1 mol.L⁻¹) on crystal sizes (*c* direction and *ab* lattice plane), and on surface areas. The mixed Ca and Al nitrates solution was flowed up (10 mL min⁻¹) while the heated NaOH and NaNO₃ solution was flowed down (20 mL min⁻¹) into the counter-current flow reactor where pressure was maintained constant by a back pressure regulator (Figure 7).

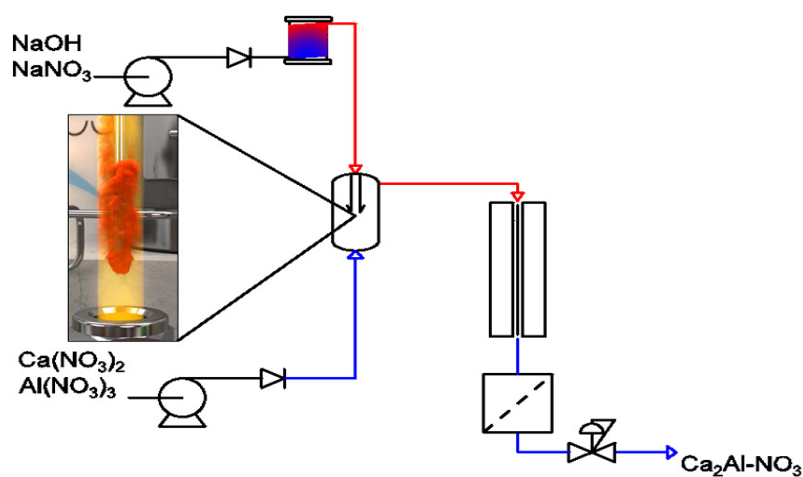


Figure 7: Schematic of counter-current flow reactor for CaAl LDH synthesis (Reproduced with permission from Ref. [83]).

The effects of temperature and pressure were examined in a narrower range than in the previous study of Q. Wang et al. [82] accounting for their results which reveal that CaAl-NO₃ LDH starts to dissociate and decompose when the synthesis temperature is too high (e. g. 250 °C) and that at 400 °C a large amount of AlOOH/Al(OH)₃ impurities are formed. Clark et al. [83] found a different effect of pressure for synthesis temperature ranges 75 - 100 °C and 150 - 200 °C. At low temperatures (< 150 °C) the crystal domain length calculated from the Scherrer equation in the *c* direction increases from ~ 50 to 75 nm when the pressure increases from 50 to 150 bar

(Figure 8). This size is larger than that reported by Wang et al. [82] (25 – 62 nm). For synthesis temperature ≥ 150 °C crystal sizes in the c direction are smaller (55 – 65 nm) and go through a maximum value at 100 bar (~ 63 nm). The crystal sizes in the (a,b) plane vary in a larger range (65 to 120 nm) than in the c direction, but irregularly as a function of the temperature and pressure. The largest sizes are obtained at 75 °C in all pressure ranges with a maximum at 150 bar (120 nm). Then, contrary to the general tendency observed by Wang et al., a variation of the pressure allows varying the crystal size in the c and (a,b) directions from ~ 50 to 80 nm and a variation of the temperature from ~ 65 to 120 nm, respectively. Nevertheless, a greatest effect of pressure is observed for a synthesis temperature below 150 °C affecting thus more largely the nucleation and growth rates. At high temperature the low residence time and turbulent mixing inside the reactor impede fine control of the crystal sizes. There is no product of the synthesis when NaOH concentration is below 0.1 mol.L^{-1} . Higher NaOH concentration increases more largely the nucleation than the growth rate. For concentration higher than 0.2 M the crystal size in the c direction decreases from ~ 55 nm at 75 °C to 30 - 40 nm at 100 °C and the crystal size in the (a,b) plane goes through a maximum with NaOH 0.5 mol.L^{-1} (80 - 90 nm). At a too high OH concentration (NaOH 1 mol.L^{-1}) additional Ca(OH)_2 phase is formed. According to the high crystallinity of the samples, surface areas of the CaAl LDH obtained by the continuous-flow method are very low ($4 - 7 \text{ m}^2\text{g}^{-1}$). A comparison can be made with CaAl- NO_3 LDHs ($\text{Ca/Al} = 2$) nanoplatelets synthesised using a rapid mixing followed by rapid precipitation method where the metal salts and the alkaline solutions were added using a colloidal mill (rotor speed of 2000 rpm for 90 s) by M. Yang et al [89]. TEM data showed that the as-prepared nanoplatelets have an average particle size of 250 nm with a large standard deviation of 106 nm. The crystal size along the c and the (a, b) direction is of 14.7 and 10.7 nm, respectively, and the BET surface area is $17.95 \text{ m}^2\text{g}^{-1}$. Therefore, higher size and stacking of

the particles are observed using the counter-current flow method in place of the colloid mill (Table 3, entry 3).

Further improvements are needed regarding the synthesis of these hydrocalumite materials using the continuous-flow method, particularly in order to reduce the particle size and greatly increase the specific surface areas.

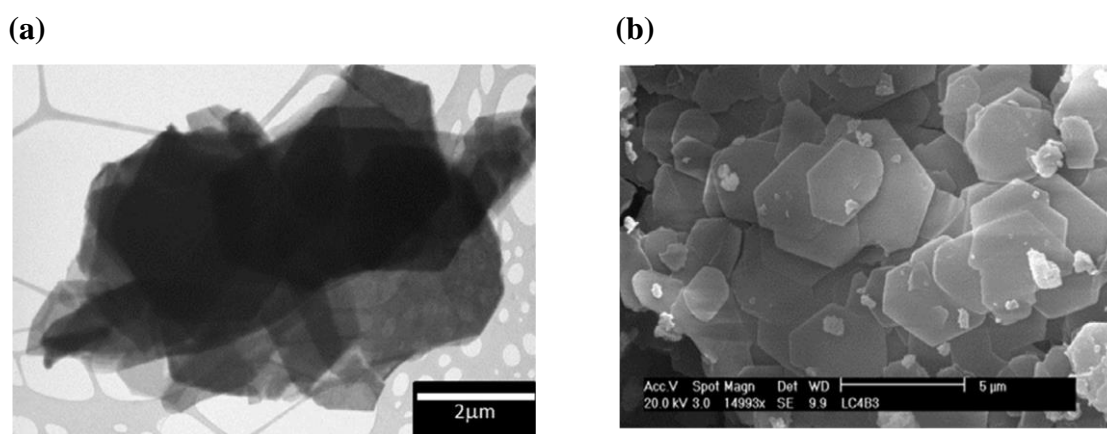


Figure 8: TEM image of the CaAl-NO₃ LDH prepared at 100 °C and 50 bar (a) and SEM image of the CaAl-NO₃ LDHs prepared at 100 °C and 150 bar (b) (Reproduced with permission from Ref. [83]).

2. 4. Synthesis using a meso-scale flow reactor in a two-step process

P. Yaseneva et al [84] synthesized transition metal cation-containing LDHs (MgAlM with M = Fe, Co, Ni, Cu and Zn; $M^{2+}/M^{3+} = 3$) in a two-step co-precipitation and aging process using a meso-scale flow tubular reactor and a thermostated beaker. The operating conditions are chosen in order to obtain similar residence (0.34 s) and micromixing times (0.4 s) in the reactor. The mixing time is indeed longer than the characteristic nucleation time of MgAl LDH then allowing the control of the growth rather than that of the nucleation rate of the crystallites. Smaller particles and narrower distribution size than in a magnetically stirred batch reactor should be obtained. Practically the co-precipitation is achieved under continuous flow

conditions in a tubular reactor ($\phi = 2$ mm) where the metal salts and the alkaline solutions both delivered by syringes placed on a syringe pump are mixed after being introduced through a Y-connector (flow rate: 4 mL min^{-1}). In these conditions the pH is not controlled. Aging was then done by dripping the mixture at the outlet of the reactor into the stirred thermostated beaker at the set of temperature in the range $65 - 95$ °C for 2 h (Figure 9).

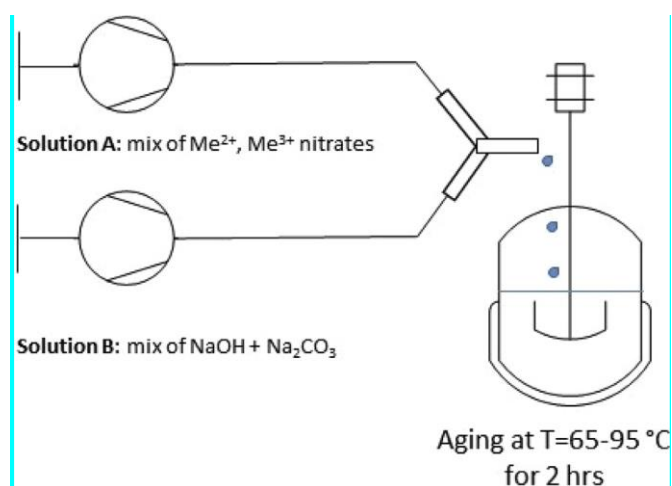


Figure 9: Schematic diagram of the two-step process of synthesis involving coprecipitation in a meso-scale reactor followed by aging in a thermostated beaker (Reproduced with permission from Ref. al [84]).

The paper focuses particularly on the reproducibility of the LDH syntheses and on the mechanistic insights into the formation of their pore structures. This is mainly examined through the analysis of the nitrogen adsorption-desorption isotherms of the different LDHs. The isotherms are in all cases of type IV with an H3 hysteresis loop consistent with a mesoporous structure. Standard deviations below $6.05 \text{ m}^2\text{g}^{-1}$ are observed for the BET surface areas of the MgAl, MgFeAl and MgNiAl LDHs synthesized through the continuous flow method and aged at 65 °C. Generally the specific surface areas are lower for the LDH samples obtained by the conventional batch co-precipitation method with mean value of $73 \pm 28 \text{ m}^2\text{g}^{-1}$ than by continuous flow method which are in the range of $80 - 150 \text{ m}^2\text{g}^{-1}$. Comparison of the surface areas of the MgAl LDH emphasizes the reproducibility of the two-step continuous flow co-

precipitation and the aging method developed in the paper. These surface areas are between 139 and 148 m^2g^{-1} for the samples synthesized in four replicates in continuous flow but between 27 and 110 m^2g^{-1} in six replicates for those synthesized in batch reactor and aged at 65 °C in all cases. This reveals the improved reproducibility of the LDHs syntheses done through flow experiments due to a better control of the co-precipitation in a short residence time. Moreover, when the particles are obtained by flow process aging in the thermostated beaker crystal growth and aggregation are quenched by dilution. For all flow-synthesized LDHs of the study, the surface areas are not significantly varied when increasing the aging temperature from 65 to 80 °C, while on the contrary great differences are observed as a function of the compositions; they increase from 79 m^2g^{-1} for MgAlCo LDH to 140 m^2g^{-1} for MgAlCu LDH aged at 65 °C. However, the influence of both composition and aging temperature is more pronounced on the size distribution of the mesopores which are formed between the agglomerated particles as revealed by TEM. TEM images of MgAl LDH indeed show hexagonal platelets with a diameter 20 - 30 nm larger than the value of 10 - 12 nm determined by XRD, confirming the agglomeration of the primary crystallites. It must be underlined that in spite of the aging treatment, though agglomeration takes place, the lateral size of the primary crystallites and the number of stacked layers are very comparable to those obtained using counter-current flow reactors or T-shape micromixers (Table 2). For the different LDHs the pore sizes in the range 3.5 – 7.3 nm and the pore volumes in the range 0.17 – 0.41 cm^3g^{-1} both increase with the aging temperature. This increase varies differently with the composition which is consistent with the values of the sizes of the agglomerates. A correlation is found between the pore size and the thermal stability investigated by TG analysis of the LDHs. The samples with smaller pores, i. e. MgAl, MgAlNi and MgAl Cu LDHs, exhibiting small pores attributed to smaller agglomerates of primary crystallites are also more stable. It is noteworthy that the compositions of the LDHs obtained with the two step process of co-precipitation in continuous flow and aging

are close to the theoretical ones. The variations of the lattice a parameters determined by XRD between the different LDHs are consistent with the different ionic sizes of the cations in the brucite-like layers.

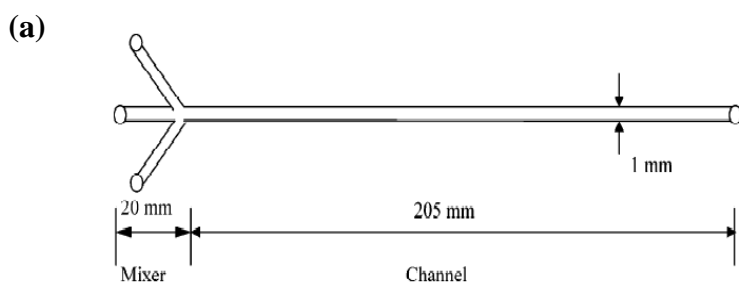
This study shows that in the two step process of co-precipitation in continuous flow using a meso-scale reactor followed by aging, the choice of a residence time close to the micromixing time allows to obtain with high reproducibility well crystallized transition metal cation-containing LDHs whose crystallite size and porosity depend on the composition and the aging temperature.

2. 5. Synthesis using microreaction technology

The above ILDP and counter-current flow processes through intense mixing ensure good heat and mass transfers. Tuning of particle size and morphology was achieved and high LDH yields with constant compositions and morphologies were obtained mainly through the control of temperature, pressure, residence time and stirring rate. Particles with high aspect ratios were generally obtained. However, improvements in heat and mass transfers and better control of aspect ratio already obtained with the meso-scale flow reactor can be better contemplated using microreactors with channel scales in the sub-millimeter range (size \ll 1 mm). They indeed have large surface-to-volume ratio and short transport path which greatly intensify the heat and mass transfer capabilities. Moreover, microreaction technology ensures excellent mixing effectiveness of reactants due to dissipation of kinetic energy leading to small size and constant morphological and composition of the particles. The coprecipitation in microreactor is less energy demanding than the reaction in conventional batch or semi-batch reactor, and scaling-up can be easily achieved by multiplying the number of reactors. Then it provides many potential opportunities which have been already exploited for different sorts of compounds. For example microreactors are increasingly used in chemical process and intensification

developments for synthesis of organic molecules [90, 91], inorganic materials such as CaCO_3 [92], $\text{Mg}(\text{OH})_2$ [93], BaSO_4 [94], hydroxyapatite [95, 96], NaA zeolite [97], $\text{AlPO}_4\text{-5}$ [98], metal–organic frameworks (MOFs) [99], various nanoparticles such as Au, Ag, Ni, Pd, Co, Cu, CdS, CdSe, CdSe/ZnS, TiO_2 [6, 7, 100-104] among others. Lastly breakthroughs have been made in the design of microreactors and experimental methods available for characterizing the mixing of liquids and the gas–liquid flows able to improve organic reactions and synthesis of inorganic materials [7, 105]. Compared to all previous processes, i.e. tank reactor, ILDP method, counter-flow reactor, the conditions encountered in microreactor limit to a larger extent and almost avoid the growth of the particles. However, washing steps are always needed to reduce agglomeration as polyelectrolytes are obviously present in the synthesized materials.

In 2005 V. S. Shirure et al. investigated the intensification of parent $\text{Mg}(\text{OH})_2$ preparation using narrow channel reactors [93]. They extended this approach in 2007 to the synthesis of MgAl LDH. They carried out a fundamental study which compares the effect of the mixing parameters on the particle size and particle size distribution measured by light scattering of MgAl- CO_3 LDH precipitated in conventional stirred batch reactor and in segmented-flow narrow channel reactor [85]. The batch reactor (3 L) is a stirred cell equipped with four baffles where stirring is achieved with impellers (330 - 900 rpm). The narrow channel reactor consists of two independent parts: a Y or a cross mixer where mixing and segmentation take place, and the channel with two cross-sectional areas (1 and 2 mm^2) where the reaction proceeds (Figure 10).



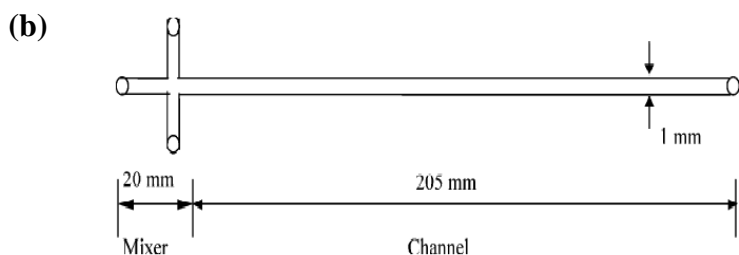


Figure 10: Schematic diagram of Y mixer (a) and cross-mixer narrow channel reactors (b) (Reproduced with permission from Ref. [85]).

The influence of several main parameters during coprecipitation in the stirred semi-batch reactor of the two aqueous solutions of precursors (magnesium and aluminium salts; NaOH and Na_2CO_3) was first investigated. The two feed streams were added at 8 mL min^{-1} in the cell while the pH value was maintained around 10 - 11. Adjustment of the following parameters: feed point location, temperature, stirring rate, supersaturation ratio is able to decrease the particle size, as determined by light scattering analysis in the turbulent flow conditions of the experiments. It is observed that the mean particle size (PS) decreases when both solutions are streamed in the discharge of the impeller where the regime is more turbulent than when one solution is added in the discharge and the other one in the bulk, or both solutions added in the bulk. The mean PS also decreases when the temperature, the stirring rate and the supersaturation ratio increase accounting for the increase of nucleation rate and power input. It must be noted that the mean PS ranges from 10 to $50 \mu\text{m}$. The study on the influence of the operating parameters in the case of the segmented-flow narrow channel reactor reveals several important features. For practical use it is worth noting that segmentation of the reactant streams by injection of air, which creates individual microvolumes of reactants and narrows the residence time distribution, does not change the mean PS compared to segmentation-free experiments. The advantage of segmentation is to avoid blockage of the channels. This is important for uninterrupted operation leading to uniform product with narrow size distribution. Parameters

influencing the mean PS and particle size distribution (PSD) were identified and carefully examined, i. e. the Reynolds number (Re) depending on the flow rate and the cross-sectional area of the channel, the supersaturation ratio (S) and the channel cross-section. It is observed that the mean PS and the PSD decrease when Re increases (1600 to 4600) for all S values. For example the mean PS decreases from ~17 to ~8 μm at S = 450. The PSD becomes sharper as Re increases and mixing is improved. This behavior is due to the rapid nucleation leading to nuclei of small size and to growth limitation resulting from the short residence time in the reactor. When S increases, the mean size of the individual crystallites measured by light scattering decreases. For example the mean PS are ~32 and ~17 μm for S = 50 and 450, respectively, at Re = 1600. But SEM analysis shows a strong tendency to agglomeration of the small particles leading to an apparent particle size of 200 μm at S = 450. The high tendency toward agglomeration at higher S values was confirmed by an agglomeration model with a good agreement between experimental and predicted PSD curves. Finally the mean PS decreases when the cross-sectional area of the microchannel decreases (from 2 to 1 mm^2) due to better mixing. There is also an influence of the shape of the narrow-channel reactor. Lower mean PS is obtained using the cross mixer rather than the Y mixer with intrinsic particle size of 11.2 and 14.1 μm , respectively. Micro mixing is better in the former reactor where the two streams collide with high power dissipation than in the latter where they flow parallel. The cross mixer thus leads to nucleation of finer particles. However, the very large dimension in the *ab* plane (Table 2 entry 6) accounts for the important agglomeration of the small particles resulting from high supersaturation ratio and low residence time in the experiments. Formula giving the specific power input per unit mass of solid produced for the stirred batch reactor and the continuous narrow-channel reactor were established. The average PS decreases as the power input increases in both cases, but it is smaller for the narrow-channel reactor (7 μm versus 15 μm) always giving smaller particles in the supersaturation range studied. For industrial

applications it is noteworthy that the micro-channel reactor requires a specific power input, which is an order of magnitude lower than with the stirred batch reactor. Production of 5 tons of LDH requires 3 stirred batches of 0.7 m^3 each with power consumption of 3283 kW, while they are provided by 25 narrow channels of $0.205 \times 10^{-6} \text{ m}^3$ each and with a power consumption of 280 kW (Table 3, entry 4).

M. Ren et al. extended the use of the microreaction technology to the preparation of different kinds of binary LDHs, i. e. MgAl, MgFe, NiAl LDH, and for the first time with continuous flow approach to the preparation of multicationic LDH, i. e. MgAlFe, MgZnAl and CuCoZnAl LDH [68]. Another main originality of their approach is the preparation of pure MgAl-NO₃ and MgAl-Cl LDH without inert gas protection usually necessary to avoid contamination by CO₂ which is a main constraint in batch experiments. This could be achieved benefiting of the very small reaction space and the extremely short residence time in the reaction channel. It is worth emphasizing on the peculiar operating parameters of the experiments using the T-type microchannel reactor. Flow velocity up to 7.8 m s^{-1} indeed leads to a total flow rate of ca. 18 L h^{-1} and Re up to 6200 when using water. The theoretical mixing time of 0.5 ms at this Re value accounts for a highly efficient mixing in the turbulent regime (Table 1, entry 9). An extremely short residence time of 1.3 ms is achieved in the reaction channel. For comparison, in the previous study of V. Shirure et al. [85] flow velocity and Re were in the range $1.44 - 5.40 \text{ L h}^{-1}$ and 1600 – 4600, respectively, the lower Re being consistent with the lower flow rate of reactants. It must also be noted that, although in a very different reactor type, the term “flash coprecipitation” was employed in the ILDP method for a residence time of 1 s.

The T-type microreactors described in papers of V. Shirure and M. Ren et al. have also different characteristics and configurations [68, 85]. In the former the two inlet channels have a length of 20 mm and the reaction channel a length of 205 mm with square configuration and cross-sectional areas of 1 or 2 mm^2 . In the latter, the microchannel reactor is composed of two sealed

microchannel plates with two inlet channels and a reaction channel of 800 μm (width) x 800 μm (depth) x 10 mm (length) with a rectangular cross section.

The XRD pattern of the as-prepared MgAl LDH (Mg/Al = 3) typical of the hydrotaalcite structure with a crystallite size of 5 nm (from the 003 reflection using the Scherrer's equation) reveals two uncommon features resulting from the synthesis via microreaction technology. Nucleation of the hydrotaalcite is extremely fast, the residence time being 1.3 ms, and the crystallite size is the smallest obtained using continuous flow processes due to growth inhibition. It must be noted that in these experiments aging is not performed. Unfortunately, the crystallite size of the other as-prepared multicationic LDHs is not reported which impedes confirmation of this interesting behaviour for other LDH compositions. Hydrothermal treatments of the MgAl LDH slurry obtained at the outlet of the microreactor were carried out in order to improve crystallinity. Results show that the temperature and duration of the treatment must be controlled because decomposition occurs for shorter treatment time as the temperature increases from 100 to 180 $^{\circ}\text{C}$. The particle size was 100 – 1000 nm for the slurry just put at 150 $^{\circ}\text{C}$, without aging. This shows that the very small particles are agglomerated due to the high surface energy and the presence of electrolytes. Particle size in the range 30 - 110 nm with hexagonal plate-like morphology was obtained after 2 h of hydrothermal treatment at 150 $^{\circ}\text{C}$ accounting for dissolution-recrystallization of the as-synthesized particles. TEM images of the MgAl LDH of Mg/Al molar ratio of 2 to 4 and hydrothermally treated at 150 $^{\circ}\text{C}$ show in all cases narrow particle size distribution and regular shape assigned to the uniform size of the initial particles formed in the microchannel. The results reported in this study deserve particular attention because they demonstrate that different kinds of LDHs containing several types of divalent and trivalent cations, but also a unique charge-compensating anion (CO_3^{2-} , Cl^- or NO_3^-) can be prepared with high slurry throughput and with a very short residence time in

microchannel reactors. Moreover, narrow particle size distribution with good reproducibility is achieved, thus offering great industrial potentialities.

Preparation of well-dispersed LDH nanosheets is an important methodological challenge which offers exciting potentialities because nanosheets can be used as positive building blocks for constructing functional 2D hybrid materials by direct co-assembly. The most commonly used method leading to LDH nanosheets goes through initial delamination in a well adapted solvent using organic species in order to overcome the strong electrostatic interactions between highly charged brucite-like layers and compensating anions. A main drawback of this approach is that the obtained nanosheets are coated with organic species or are dispersed in organic media. However, more eco-friendly methods recently implemented delamination in water using lactate or NO_3^- anions [106, 107]. Several microemulsion methods lead to interesting results but exhibit drawbacks similar to those of the delamination method in organic solvents [78]. The group of W. Hou [108] has developed a method in three steps termed the PWD route overcoming several of the previous drawbacks [108]. It includes aqueous coprecipitation, then intermediate water-washing of the precipitate and finally redispersion in water yielding LDH single-layer nanosheets with a solid content of ~8.5 wt%. All the process was achieved at ambient temperature. This PWD method leading to naked LDH nanosheets with average lateral size of ~80 nm was achieved in a beaker under magnetic stirring. Interestingly, this approach follows a previous one of the same group achieving preparation of naked LDH nanosheets in bulk aqueous solution using a T-shaped microchannel reactor (reaction channel: 1 mm (width) x 0.2 mm (depth) x 20 mm (length)) on which we will focus in the present review [86]. In this experiment the mixed Mg and Al salts solution (0.3 mol.L^{-1} ; Mg/Al = 2) and the alkali solution ($\text{NH}_3\cdot\text{H}_2\text{O}$; ~ 7 wt%) were pumped into the T-type microreactor through two inlets ($20 \text{ mL}\cdot\text{min}^{-1}$ each). Importantly, the suspension collected at the reactor outlet was immediately centrifuged (12000 rpm) and washed by redispersion and centrifugation. The solid content in the gel-like

LDH nanosheet sample thus recovered is *ca.* 7.0% (w/w). The absence of (00*l*) reflections in the XRD pattern and the presence of only a weak (110) reflection clearly indicate the lack of stacking in the *c* direction in the diluted suspension (7.0% (w/w)) (Figure 11). AFM analysis confirms that LDH nanosheets had thickness 0.68 - 1.13 nm consistent with the presence of 1 - 2 superimposed brucite-like layers (Figure 11). Their lateral size is 20 - 30 nm and it is lower than that of ~80 nm obtained using the PWD method (Table 3, entry 5). Accordingly, the average particle hydrodynamic radius is *ca.* 13 nm. When the solid concentration increases to 46% (w/w) after centrifugation (80000 rpm), the XRD pattern exhibits the characteristic reflections of LDH with an average crystallite size in the *c* direction of 12.1 nm showing the stacking of *ca.* 11 brucite-like layers. Crystallinity is further increased upon peptization at 60 °C with an average crystallite size in the *c* direction reaching 18.7 nm which represents *ca.* 21 stacked layers and an average particle hydrodynamic radius of *ca.* 45 nm (Figure 11).

It is worth mentioning that all the well-known arrangements generally observed in the case of post-synthesis treatments of the initially well dispersed LDH nanosheets are obtained. Indeed the well-crystallized LDH nanosheets directly formed at the T-type reactor outlet are aggregated upon centrifugation and concentration increase (from 7% to 46%), and finally they are self-assembled into 3D crystallites and grown by Ostwald ripening upon peptization. Therefore, the 1 - 2 LDH nanosheets in the fresh transparent colloidal suspension stable for 16 h at room temperature result from several features of the synthesis procedure. A high nucleation rate is maintained in the T-type microchannel reactor. Further electrolytes in excess are removed by washings in water and finally the LDH aggregates are gradually disaggregated by the low solid concentration in the dispersion. It must be emphasized that this continuous flow method allows obtaining for the first time LDH nanosheets dispersed in aqueous media, which compulsorily implies a diluted suspension (7% w/w). LDH yields are lower than in continuous flow experiments previously examined but this method gives unique outlooks for several

applications such as flame retardant, stabilization of polymers, catalysis and preparation of functional hybrids. Besides, in the publication of X. Pang et al., co-assembly of the LDH nanosheets from the fresh colloidal suspensions and dodecyl sulfate (DS) has been successfully achieved leading to DS-LDH nanohybrids similar to those obtained by direct coprecipitation.

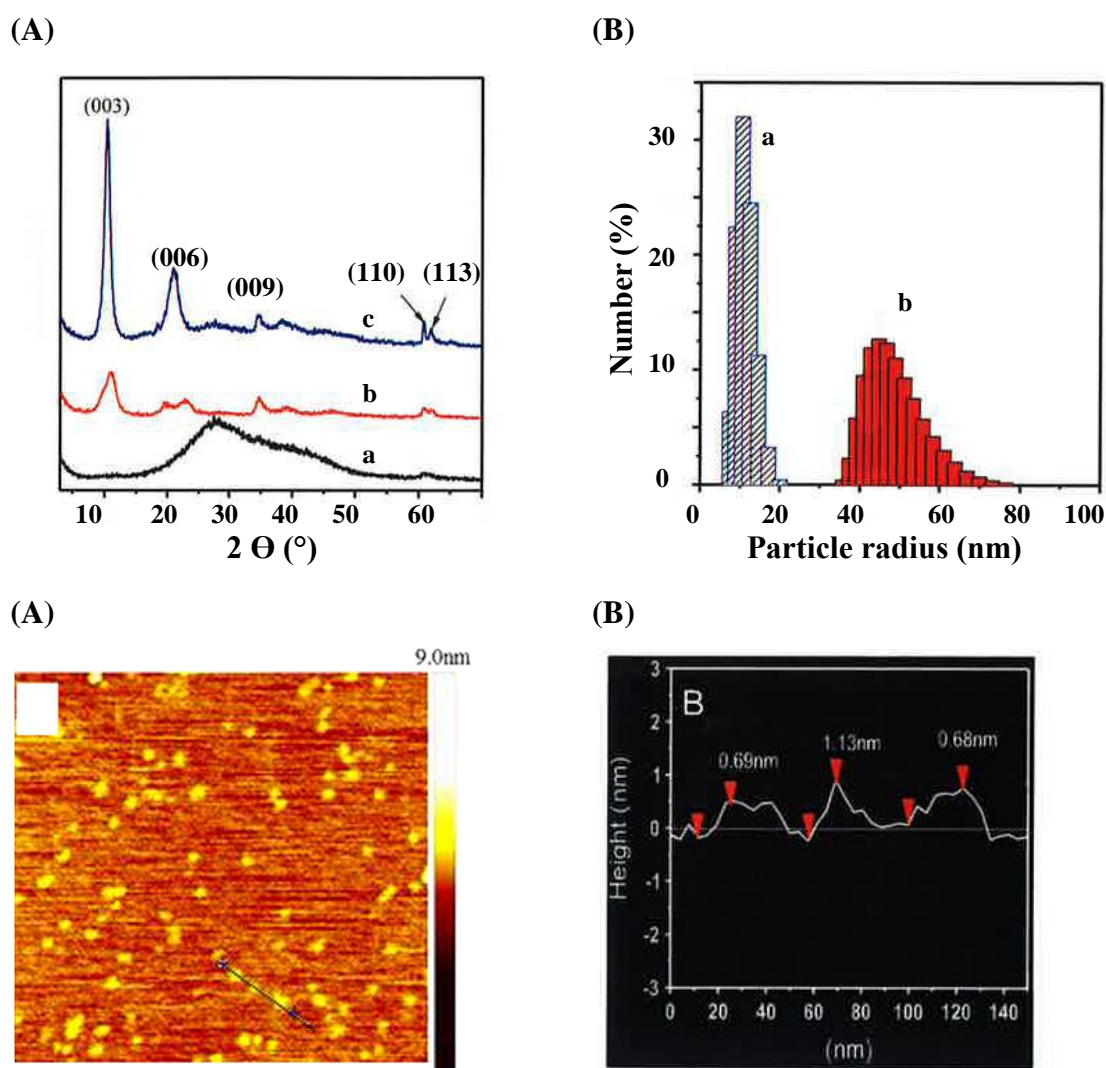


Figure 11: (top) (A) XRD patterns of freshly prepared LDH (a), LDH centrifuged at 80,000 rpm for 2 h (b), and LDH peptized at 60 °C for 24 h (c); (B) Particle size distribution of freshly prepared LDH (a), and LDH peptized at 60 °C for 24 h (b); (bottom) (A) AFM images and height scale of LDH nanosheets; and (B) sectional analysis along the black line marked in (A) (Reproduced with permission from Ref. [86]).

2. 6. Synthesis by coprecipitation and coupled cleaning

It has been underlined several times that in the previous methods the LDH particles were characterized after being harvested at the outlet of the reactor without any washing step. This indeed explains that agglomeration mainly due to the presence of residual electrolytes is generally observed leading in most cases to a large discrepancy between crystallite size measured by XRD and size of the agglomerates measured by microscopy or light scattering.

Also the approach developed by A. Flegler et al. [87] deserves a great attention because LDH were prepared for the first time by a combination of a continuous coprecipitation followed by down-stream separation and washing in a semi-continuous tubular centrifuge [87]. Coprecipitation is achieved in a static spiral mixer consisting of 30 mixing elements rotating spirally by 180° in an alternating way to the right and left side. Then the outgoing gel solution of the static spiral mixer is pumped into the semi-continuous tubular centrifuge.

The reactor volume is obviously larger than the channels of the microreactors and the residence time of the mixed solution is larger making heat and mass transfer probably less efficient, and allowing more growth of the particles. It must also be pointed out that the final cleaned LDH particles are obtained in one-go but using a two step process. However, the immediate washing of the precipitated product on the flow allows its quenching. The method is then close to the method separating nucleation and aging steps developed by Y. Zhao et al. [72] but with continuous coprecipitation of LDH particles. The study of Flegler et al. focused on the influence of precursor concentration variations on the size and morphology of MgAl LDH nanoparticles. The aqueous precursor solution of Mg and Al chlorides ($Mg/Al = 2$) and the alkaline solution of NaOH and Na_2CO_3 were pumped with a peristaltic pump into the static spiral mixer. The precipitation started immediately in the mixer. For washing with the semi-continuous tubular centrifuge, the LDH suspension was injected with a given flow rate at the rotor bottom with a nozzle entering immediately the rotor accelerator and then accelerated to nearly full rotor speed

(25000 rpm). Inside the rotor, due to the high g-force, the liquid flows to the head and the particles are sedimented according to Stokes' law. The continuous flow setup thus conceived is able to ensure the steady-state synthesis of cleaned LDH nanoparticles immediately quenched. The feasibility of the process and particularly the constant quality of the products going out of the static mixer are based on the efficiency of the washing procedure. In a first part the authors carried out a comparative study of the integrated washing step using the semi-continuous tubular centrifuge above described and of a conventional lab-scale centrifuge-washing approach. In this latter case redispersions of the collected products were achieved in different amounts of water and from one to six times. The number of consecutive washings was more efficient than the absolute amount of water as revealed by three cleanness indicators (pH, conductivity, ratio between (003) peak of LDH and (002) peak of NaCl excess salt). Interestingly, by diluting four times the LDH suspension introduced in the semi-continuous tubular centrifuge, the cleanness of the product is rather similar to the best result obtained by the conventional approach. Besides, the remarkable efficiency of the washing step using the semi-continuous tubular centrifuge is proved by the dramatic decrease of the hydrodynamic diameter of the particles from 5 μm before washing (collected right after precipitation) to 50 nm after washing. This indeed reveals the redispersion into primary particles of the agglomerates resulting from the presence of salt after immediate coprecipitation and no washing. Following these preliminary studies a continuous flow process is available able to produce clean products with constant conditions that are immediately quenched. The next step of the approach was to study the influence of the salts and NaOH concentrations, i. e. of the supersaturation level on the size and morphology of the particles. At high supersaturation (high concentration of metal salts and NaOH) round particles of ~ 100 nm are observed by SEM; their precipitation is probably driven by isotropic growth. Addition of carbonate during precipitation leads to more spherically shaped particles due to improvement of stacking in the *c* direction.

Post-treatments at 80 °C for one week were performed on the as-precipitated LDH in order to establish to what extent their morphology influences that of the products obtained after recrystallization. The spherical shape of the particles obtained at high supersaturation changes to a morphology close to a platelet-like one. The particles obtained at low supersaturation maintain their platelet-like morphology when dissolved in the presence of carbonate, but show a pronounced change when no carbonate is added with perfect hexagonal platelets in the range of 100 – 200 nm and with a high shape ratio are then obtained. This behaviour confirms the role of carbonate in the stacking of the layers. Two extreme morphologies have thus been obtained: spherical nanoparticles of as-precipitated LDH at high supersaturation and hexagonal platelets with sharp edges at low supersaturation and after thermal treatment at 80 °C. This obviously opens the door to different types of applications. This publication then demonstrates that LDH particles can be prepared at the lab scale in one-go using a continuous flow process including a washing step in a separate semi-continuous tubular centrifuge. Moreover, it shows a great modulability of the morphology of the MgAl LDH through the supersaturation level and the composition of the alkaline solution of the as-prepared particles and also through their hydrothermal treatment.

2. 7. Synthesis using hydrothermal continuous flow reactors

H. Liang et al. developed a strategy using a high temperature high pressure hydrothermal continuous flow reactor (HCFR) [88] in order to control the supersaturation level during synthesis and thus the nanostructure morphology and the size of LDH nanoplates. The HCFR allows maintaining supersaturation at a constant low level in the reaction system and favours the growth of the LDH contrary to the goal generally targeted in all previous processes. Hydrothermal conditions enhance the precursor diffusion, which could be also beneficial for the growth of highly crystalline particles. H. Liang et al. also added an exfoliation step of the

obtained LDH in a polar organic solvent in order to reach the surface area necessary for developing catalytic applications. The study was devoted to the synthesis of NiCo LDH to obtain oxygen evolution reaction (OER) catalysts as inexpensive alternatives to the precious-metal containing catalysts generally used. It must be pointed out that in spite of the difficult control of the cobalt oxidation state, NiCo LDHs are widely studied due to their great application potential as catalysts for water oxidation and OER and also as supercapacitors. NiCo LDHs with different nanoarchitectures avoiding agglomeration of the particles have thus been prepared to enhance electrocatalytic performances [109, 110]. However, due to the superior electrochemical properties over nanostructures, great effort has been also conducted to prepare NiCo LDH nanosheets with porous nanostructures on conductive materials using electrodeposition methods [111-116] or hydrothermal co-deposition methods [117].

H. Liang et al. reported the synthesis of Ni^{II}Co^{III}-LDH directly in HCFR yielding dense and uniform thin nanoplates [88]. For practical use they were grown on a carbon paper support to be easily available in electrochemical water oxidation device. The HCFR is based on a reaction column (HPLC preparative column, 250 mm length, 13 mm inside diameter) placed in a tube furnace with temperature control. It is equipped of a back pressure regulator which allows adjusting the internal pressure of the reaction system. The precursor solution is introduced in the reactor with a HPLC pump (Figure 12). The mixed aqueous solution of nickel and cobalt nitrate salts and ammonia, of dark brown color indicating the oxidation of Co²⁺ to Co³⁺, was continuously flowed through the HCFR heated at 160 °C at 1 mL min⁻¹ and at a pressure of ~160 psi.

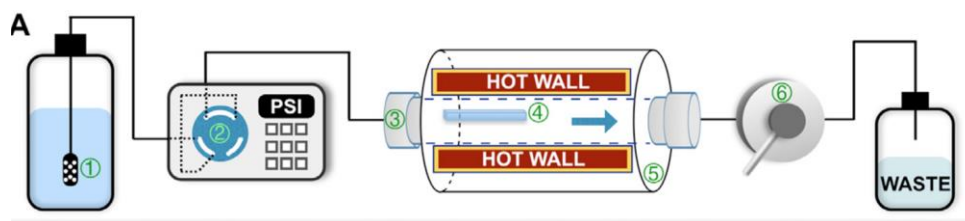


Figure 12 : Schematic of the HCFR (1. Reservoir; 2. HPLC pump; 3. Reaction column; 4. Substrate; 5. Tube furnace; and 6. Back pressure regulator) (Reproduced with permission from Ref. [88]).

Similar high density nanoplates were observed by SEM for the $\text{Ni}^{\text{II}}\text{Co}^{\text{III}}$ -LDH grown on the carbon paper support or collected from the suspension flowed through HCFR column with ~ 15 nm in thickness and $\sim 1\ \mu\text{m}$ length. They are covering all the support and form a highly open 3D hierarchical structure (Figure 13). The LDH phase in the particles was confirmed by XRD along with a minor $\beta\text{-Co}(\text{OH})_2$ phase. A sample prepared for comparison by static hydrothermal reaction (SHR) using the same conditions (precursor concentration and temperature) yields also ~ 90 nm thick hexagonal nanoplatelets coexisting with some small particles (Table 3, entry 7). The nanoplatelets are more disordered and aggregated and not covering the whole surface (Figure 13).

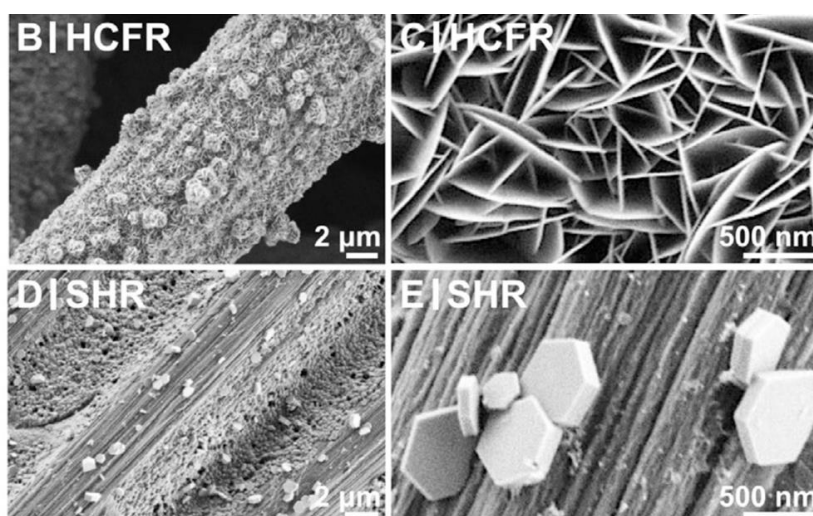


Figure 13 : SEM images of NiCo LDH nanostructures obtained from a HCFR reaction (B, C) and a SHR (D, E) (Reproduced with permission from Ref. [88]).

The HCFR leads to a better control of the morphology and size of the LDH particles. By immersion in formamide of the carbonate paper substrate covered with LDH nanoplatelets partial exfoliation is achieved as shown by the great decrease in intensity of the (003) diffraction peak in the XRD pattern. Exfoliation is not complete due to the interaction with the support. On contrary total exfoliation occurs for the free powder LDH. Exfoliation also reduces both the thickness of the nanoplates which varies between ~ 0.6 and ~ 8.8 nm and their lateral size to $\sim 80 - 100$ nm, exhibiting thus a high aspect ratio (Figure 14).

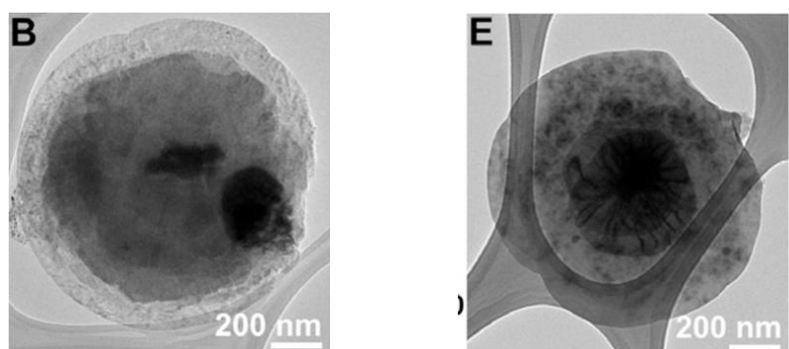


Figure 14 : TEM image of the as-synthesized NiCo LDH nanoplates on carbon paper grown via HCFR reaction (B) and after exfoliation (E) (Reproduced with permission from Ref. [88]).

The catalytic activity toward OER of the NiCo LDH nanoplates grown on carbon paper using HCFR is higher than that of nanoplates obtained by SHR in terms of lower onset overpotential and larger catalytic current density (Table 3, entry 7). This is due to the easier diffusion of ionic species and the higher accessibility to the active sites resulting from the largely open structure in the former samples. Furthermore, the catalytic activity is significantly enhanced after the exfoliation treatment. The reaction kinetics is more favorable and the number of low

coordination sites located along the edges which are more active for OER is increased due to the smaller size of the layers. The onset overpotential decreases and the current density increases for the OER making the activity of the exfoliated NiCo LDH nanosheets comparable to that of the best reported catalysts. Moreover, the XPS study reveals a change in the electronic structure of the exfoliated nanosheets which can also influence the catalytic activity.

The group of H. Liang also used the continuous flow reaction (CFR) at low supersaturation in order to elucidate the role of screw dislocations hypothesized to be the dominant factor in crystal growth of layered materials due to their high propensity to be formed [118]. The dislocations can play a major role on mechanical, thermal, electrical, optical, catalytic properties. The authors investigate the growth of ZnAl and CoAl LDHs on alumina-coated substrates by continuously flowing precursors at low concentration ($50 \mu\text{mol.L}^{-1} \text{Zn}(\text{NO}_3)_2$ and HMT; $0.5 \text{ mmol.L}^{-1} \text{CoCl}_2$ and urea) in the reactor heated at $50 \text{ }^\circ\text{C}$. The strategy is then to react metal cations, i. e. Zn^{2+} , Co^{2+} and Ni^{2+} on Al_2O_3 film as support maintaining supersaturation at a constant low level in order to obtain well-defined two dimensional nanoplates. The same syntheses, though at higher concentration of the precursors, were achieved in static conditions for comparison. In this latter case a dense film consisting of interpenetrated nanoplates growing perpendicularly to the substrate surface is formed as shown by SEM (Figure 15). For ZnAl LDH nanoflower morphologies similar to 3D assemblies of delaminated layers are obtained in static conditions, while large isolated nanoplates with well defined shapes are formed when the samples are prepared in CFR. SEM images of the latter show that ZnAl LDH nanoplates have diameters ranging from 10 to 20 μm and thicknesses of few hundred nm, while smaller platelets with diameters of few microns and thicknesses below 100 nm are observed in the case of CoAl LDH obtained in CFR (Table 3, entry 8).

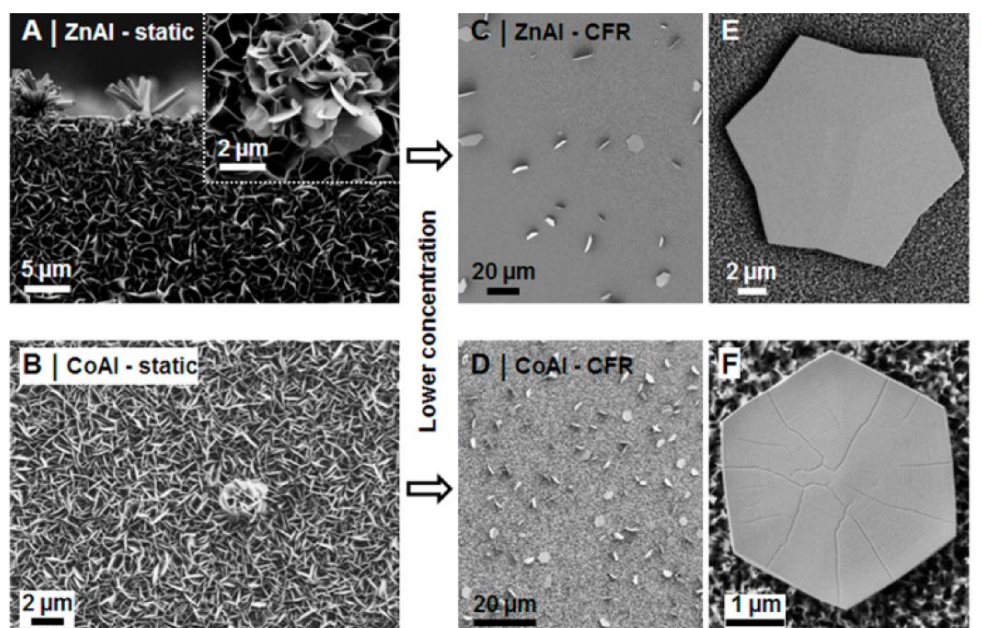


Figure 15: Structural characterization of ZnAl and CoAl LDHs grown on alumina-coated substrates in static and flow reactions. SEM images of large ensembles of ZnAl and CoAl LDHs grown in static conditions (A and B, respectively) and in the CFR (C and D, respectively), and the magnified SEM images of individual 2D LDH nanoplates from CFR growth (E and F, respectively) (Reproduced with permission from Ref. [118]).

Both LDHs show screw dislocation growth spirals clearly identified as spirals by AFM confirming the growth mechanism. However, slight differences are noted: dislocations are more complex with double ones of same directionality and multiple cores for ZnAl LDH nanoplates but single ones for CoAl LDH, both showing step heights consistent with that of one LDH layer (< 1 nm) (Figure 16).

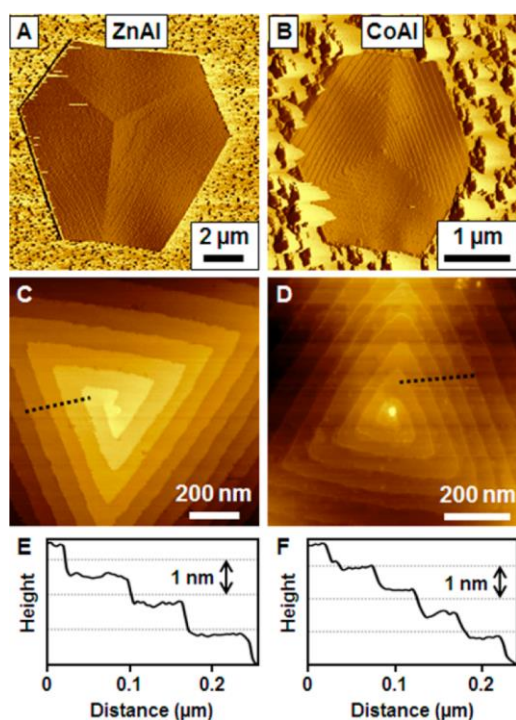


Figure 16: Tapping mode AFM images and step heights of ZnAl and CoAl LDHs nanoplates synthesized in the CFR on alumina-coated substrates. (A,B) Amplitude images of complete nanoplates, (C,D) topographic images of the dislocation cores and (E,F) their corresponding step height profiles from the black dotted lines in (C) and (D) for ZnAl (left panels) and CoAl LDHs (right panels), respectively (Reproduced with permission from Ref. [118]).

The use of CFR allows establishing the generality of the screw dislocation-driven crystal growth of LDHs, as spiral steps are also evidenced for ZnGa LDH nanoplates prepared in static conditions. Another approach using CFR was developed for the synthesis of ZnAl LDH starting from ZnO seeds previously synthesized and deposited on a clean silicon substrate. The seed-covered substrate is then introduced in the CFR through which Zn and Al nitrate salts and HMT are flowed at 80 °C to maintain a low supersaturation level by slowing down the HMT hydrolysis. Thin (< 100 nm) and sparse ZnAl LDH nanoplates are obtained exhibiting clear screw dislocations, which are multiple in the core and single on the edges (Figure 17). The same CFR synthesis performed without ZnO seeds did not yield products, thus emphasizing the

critical role of defective nucleation sites to enable crystal growth. The static growth of CoAl LDH was also proved to be driven by screw dislocation.

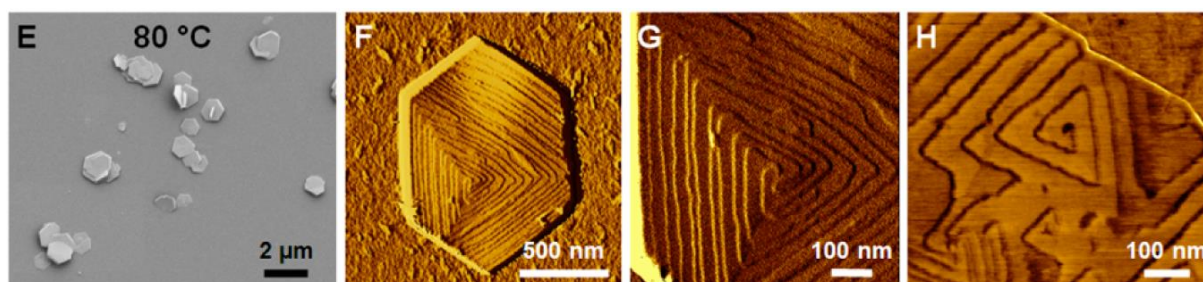


Figure 17: Tapping mode AFM images and step heights of ZnAl and CoAl LDHs nanoplates synthesized in the CFR on alumina-coated substrates. (A,B) Amplitude images of complete nanoplates, (C,D) topographic images of the dislocation cores and (E,F) their corresponding step height profiles from the black dotted lines in (C) and (D) for ZnAl (left panels) and CoAl LDHs (right panels), respectively (Reproduced with permission from Ref. [118]).

Different approaches were used in this study for the synthesis of ZnAl and CoAl LDH nanoplates, i. e. static conditions or CFR growth on alumina-coated substrate using in both cases Zn or Co salts; CFR growth using Zn or Co and Al salts in the presence of ZnO seeds, all at low supersaturation level. The nanoplates obtained confirm the generality of the dislocation-driven mechanism. Moreover, the supersaturation level can allow controlling the aspect ratio of the spiral nanoplates. Another aspect which must be pointed out is that the LDH phase is precipitated on an alumina substrate in continuous flow as it has been already demonstrated in conventional experiments by contacting aqueous divalent cation solutions and aluminium (oxyhydr)oxide in alkaline media [119-125].

3. Extension to the continuous production of functional LDHs and LDH-based composites

In spite of the great interest of functional LDH and LDH-based composites for several industrial applications, their synthesis has been still scarcely investigated through continuous flow methods. However, since 2015 functionalization of LDH with enzymes, surfactants or nanoparticles has been emerging [126-128]. Noteworthy, in these recent reports the biohybrids are likely formed by immobilization of the enzymes on the LDH nanoparticles, whereas the organic-LDH hybrids are obtained either by intercalation or by immobilization of surfactants on the surface. It must also be noticed that the microreactor technology has been privileged for the preparations since it is particularly adapted to *in situ* functionalization during LDH coprecipitation. LDH-based composites are increasingly developed because they allow combining the intrinsic properties of their building blocks and give rise to assemblies with original properties, particularly porosity, with better accessibility to the different active sites. They are indicated for applications requiring composite films such as corrosion protection materials. Continuous flow synthesis, particularly HCFR method, is well adapted to the direct growth of the composite film on the surface of a substrate and this was developed for the first time in 2017 [129]. The different studies achieved using continuous flow methods are presented in the following; they all include examples of application or investigation dealing with potential applications.

3. 1. Hybrid organic LDH

Great attention has been focused on polymer-LDH nanocomposites as flame retardant materials. This application has been recently reviewed in two publications. One of them focuses on the dispersion of the LDH in the polymer matrix, and the influence on the fire retardant

properties of the nanocomposites [43]. The other one concerns the flame retardant evaluation and mechanism as a function of the composition of the nanocomposites [52]. LDHs have several properties related to their chemical composition, layered structure and aspect ratio which make them very attractive as flame retardants and smoke inhibitors; among those properties are their endothermic decomposition and the formation of stable char. Moreover, intercalation of organic anions or coating with surfactants allow increasing the hydrophobic character of the LDHs which then become highly efficient nanofillers [51]. The endothermic decomposition of LDH induces release of H₂O and CO₂ in the case of CO₃²⁻ or organic intercalated anions, thus reducing or totally inhibiting combustion. Char produced acts as a thermal barrier on the polymer surface and suppresses the smoke production. These effects are improved when mixed oxides and spinel-like phase, e. g. MgAlO and MgAl₂O₄ are formed upon thermal decomposition of MgAl LDH above 500 °C because they act as thermal barriers. Therefore, heat absorption, dilution of the combustion gases and char formation account for the flame retardant ability of LDHs.

In order to improve the flame retardancy property of LDH, S. Elbasuney modified the particle surface with surfactants [126]. For the first time an integrated approach was followed going from the synthesis of MgAl LDH in a continuous flow, to functionalization in a separated step. Poly(ethylene-co-acrylic acid) (PEA) and dodecanedioic acid (DDA) as polymeric surfactant and organic ligand, respectively, were chosen to modify the surface properties from hydrophilic to hydrophobic. These modifications enhance the dispersion of the modified LDH in the polymer matrix and improve the flame retardant property. The continuous hydrothermal synthesis of the surface modified MgAl LDH was achieved with a counter-current flow reactor (Figure 18). A super-heated water solution of NaOH and NaNO₃ was injected down an inner nozzle pipe against an upper flow of the cold metal salt water solution (Mg/Al = 3) in a tubular reactor (total volume of the reactor is not indicated). LDH is obviously precipitated at the

interface of the up and down flows. The synthesized LDHs are post-treated for surface modification by injection of the surfactant (PEA in toluene or DDA in ethanol) in the flow stream going out of the reactor.

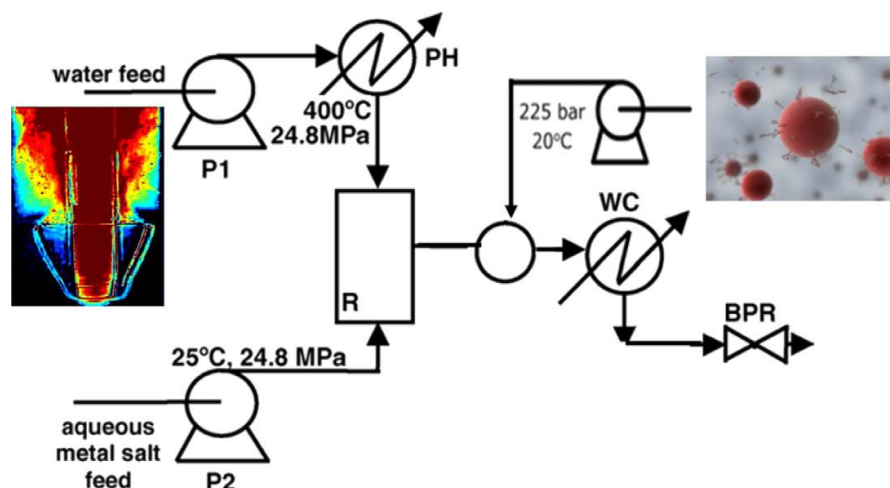


Figure 18: Flow diagram of the continuous hydrothermal synthesis system used for the instant production of LDH (P1, P2, and P3: HPLC pumps, PH: preheater, R: continuous reactor, E: capping point, WC: water cooling, BPR: back pressure regulator) (Reproduced with permission from Ref. [126]).

Highly hydrophobic PEA modified LDH particles remain in the organic phase separated from water, while DDA modified LDH particles flocculate in the mixture ethanol/water (Figure 19). These organic modified LDHs can then be integrated as a dry powder after separation and centrifugation or as colloidal nanoparticles in the polymeric matrix. Such integration of colloidal nanoparticles enhances dispersion because freeze drying and re-dispersion of aggregated dry particles into polymeric matrix can be suppressed [130].

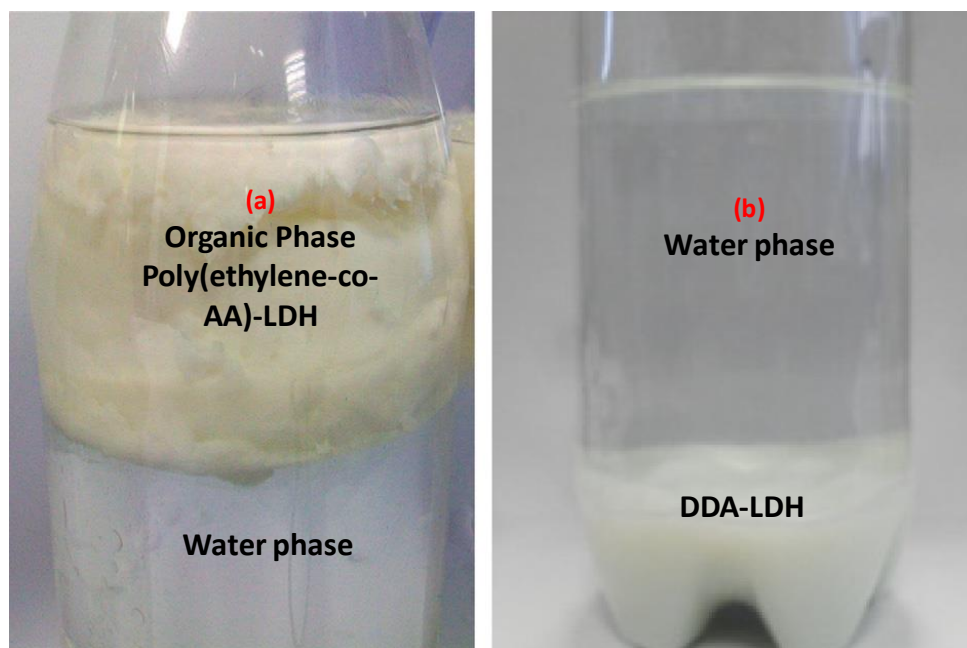


Figure 19: Harvested poly(ethylene-co-acrylic acid)-LDH (a), and flocculated DDA-LDH (b) (Reproduced with permission from Ref. [126]).

Well crystallized bare MgAl-CO₃ LDH nanoplatelets were obtained with an average size of 40 nm in colloidal suspension and slightly aggregated after freeze drying into particles of 50 nm average size. FTIR bands of the carboxylic group present in the region 1500 – 4000 cm⁻¹ in the organic modified LDHs compared with the uncoated MgAl LDH confirm adsorption of the surfactants onto the LDH nanoparticle surface. Loadings of PEA and DDA of 3 and 8 wt%, respectively, were determined by TG analysis. The heat sink property of the unmodified LDH was only evaluated through DSC and shows an endothermic decomposition at 345 °C with adsorption of 478.6 J.g⁻¹. This result and the decomposition into mixed oxides above 500 °C which are both well-known, suggest the potentiality of LDH as heat sink materials able to cool down the burning polymer surface and as protective layer against degradation of a polymer. However, no experiment has been achieved after dispersion of the modified LDH in polymer matrix in order to check their compatibility and the effectiveness of the heat sink property. Therefore, the main interest of the publication is to report for the first time functionalization of

LDH synthesized by continuous flow technology and modification of the surface property from hydrophilic to hydrophobic, opening the route for the large-scale production of LDH as nano-fillers.

3. 2. *Bio-hybrid and inorganic-LDH*

Several studies showed the interest of immobilizing heme proteins, particularly hemoglobin (Hb), on LDH or LDH-containing nanocomposite supports to fabricate biosensors based on the direct electrochemistry of redox protein. These bioelectrodes have low detection limit and very high sensitivity for the amperometric detection of H₂O₂ or high activity for the electrocatalytic reduction to trichloroacetic acid for example [131-134]. Among LDH matrices, the Fe-containing ones have a peculiar interest as they promote direct electron transfer between heme proteins and the underlying electrode, iron atoms acting as electron relays [131]. Preparation of such LDH nanohybrids in one pot using a continuous flow approach can lead to aqueous colloidal suspensions with controlled particle size and well organized assemblies of LDH platelets and proteins, which improve the properties of this latter.

This was the incitement of the work achieved by the group of Hou [127]. It follows their publication dealing with synthesis of LDH nanosheets by coprecipitation in continuous flow using a T-shaped microreactor previously described [86]. They further extended the approach to the preparation of bio-hybrid LDH through assembly of hemoglobin (Hb) and MgAl LDH nanosheets (denoted Hb-LDHNS) [127]. The biohybrids were directly coprecipitated using the T-shaped microreactor previously described [86] pumping simultaneously through a first microchannel the mixed Mg and Al nitrate salts dissolved in a aqueous solution of Hb and through a second microchannel a NaOH solution. The two flow rates are adjusted to maintain pH at ~ 9 (Figure 20).

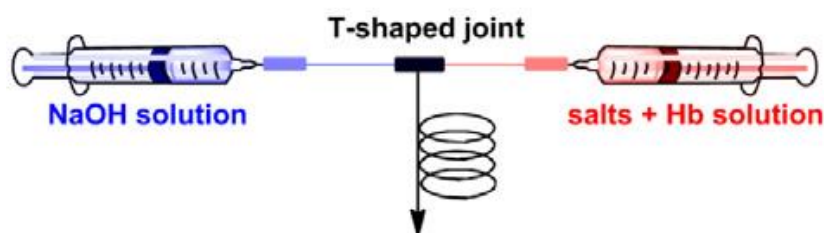


Figure 20: Schematic diagram of experimental setup of T-shaped microreactor for the synthesis of Hb/MgAl LDH bio-hybrids (Reproduced with permission from Ref. [127]).

The mixed metallic salts concentration in the Hb solution was varied between 6 and 48 mmol. L⁻¹. The collected suspension at the reactor outlet was aged for 24 h at room temperature under N₂, then centrifuged and washed with water. Semi-transparent gels were obtained (Biohybrids were respectively denoted as Hb-LDHNS_x with x = 6, 12, 24 and 48). Several physico-chemical characterizations accounted for the immobilization of Hb on the LDH nanosheets matrices. First, XRD patterns of the Hb/MgAl LDH bio-hybrids display the well defined reflections of LDH whose crystallinity increases with the metallic salt concentration in the initial Hb solution. However, LDH particles are less crystalline than the pristine MgAl LDH accounting for a turbostratic effect in the presence of Hb. Such effect is also noted on SEM images exhibiting cloud-like or sponge-shape morphology for low LDH concentration. Hb indeed acts as a templating agent for nucleation and growth of LDH crystals joined by the protein molecules resulting in dense particle networks or continuous sponge-like structures. At higher salt concentration, Hb has a lower influence on the morphology of the bio-hybrid, which appears as plate-like particles with a average size of 20 – 40 nm. The d₀₀₃ basal spacing is enhanced at lower metallic salt concentration (0.938 - 0.801 nm) in comparison to higher concentration corresponding to CO₃²⁻ intercalation (0.784 nm). This is consistent with an ultrafine assembly

of Hb and LDH nanosheets in the former case and adsorption of Hb on the nanosheet surface in the latter case. The Hb/MgAl LDH bio-hybrids prepared using the T-shaped microreactor then exhibit non hexagonal platelets uniformly dispersed with edge-to-edge interactions through Hb molecules. They greatly differ from those obtained by conventional coprecipitation in static conditions exhibiting large platelets of 80 – 200 nm with some aggregation (Table 3, entry 9). Interaction between Hb and LDH nanosheets was assessed by spectroscopy (FTIR, UV-vis and fluorescence). FTIR confirms that CO_3^{2-} is the compensating anion in the layer structure and that the immobilized Hb exhibits the vibrational bands from amide I and II of the polypeptide chain as the native enzyme. The immobilized Hb then maintains its helical structure, although with a slightly different peak shape, accounting for the interaction with the LDH nanosheets. UV- vis spectra show Soret absorption peaks at 402 - 406 nm in the bio-hybrids, similar to those of native Hb (Figure 21). This confirms that the immobilized enzymes keep their secondary structure and interact with the matrices as shown by weakening and widening of the absorption peaks. Moreover, the invariance of the absorption bands when the bio-hybrids are examined at 90 °C reveals that immobilization prevents denaturation of Hb by dissociation of the hemin groups. Finally, fluorescence spectra confirm these behaviors using the fluorescence of the tryptophan residues embedded in the hydrophobic areas near the heme group (Figure 22). The similar structure of the immobilized and of the native Hb is again confirmed. Furthermore, the enhancement of the fluorescence intensity indicates that these residues are located in a more hydrophilic environment. A slight difference is noted at high temperature as a function of the Hb loading. The secondary structure is maintained because Hb is better protected by the LDH nanosheets at lower than at higher loading. Therefore, from this wide set of characterizations one can conclude that the Hb molecules strongly interact with LDH nanosheet matrices and keep their native secondary structures.

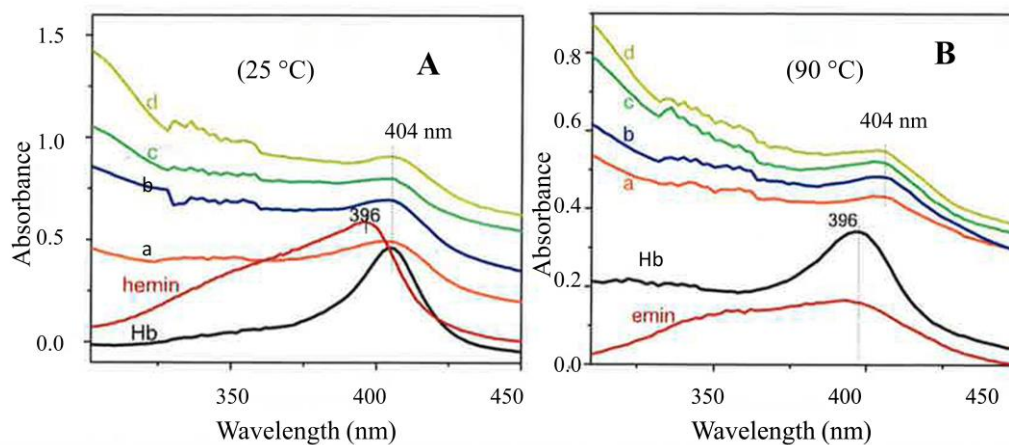


Figure 21: UV-vis spectra of Hb-LDHNS₆ (a), Hb-LDHNS₁₂ (b), Hb-LDHNS₂₄ (c), Hb-LDHNS₄₈ (d), Hb and hemin in aqueous solution at 25 °C (A) and 90 °C (B), respectively (Reproduced with permission from Ref. [127]).

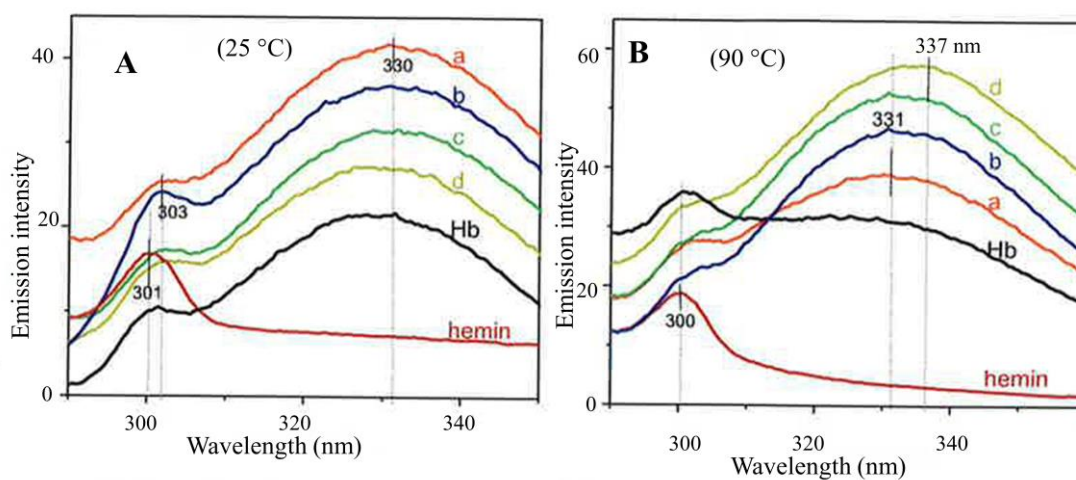


Figure 22: Fluorescence spectra of Hb-LDHNS₆ (a), Hb-LDHNS₁₂ (b), Hb-LDHNS₂₄ (c), Hb-LDHNS₄₈ (d), Hb and hemin in aqueous solution at 25 °C (A) and 90 °C (B), respectively (Reproduced with permission from Ref. [127]).

A remarkable benefit regarding the bio-hybrids synthesized in continuous flow is the higher Hb immobilization rate (90.5 - 95.8%) in comparison to those obtained by conventional coprecipitation (66.5%).

The catalytic activity of the bio-hybrids has been evaluated in the oxidative reaction of *o*-phenylenediamine (OPD) with H₂O₂ to form 2,3-diaminophenazine. At 25 °C the bioactivity, based on the same Hb amount (1 mg), of the bio-hybrids is lower than that of free Hb. At 90 °C, Hb is deactivated by more than 90%, while in contrast the bioactivity of the hybrids is improved increasing from 31 to 73.5% of the soluble Hb at 25 °C with the metal salts concentration. Moreover, they are more active than the biohybrid prepared by classical coprecipitation whose bioactivity is of 21.44%. The higher activity of Hb-LDHNS₁ and Hb-LDHNS₁₂ of 73.5 and 68.35%, respectively (Table 3, entry 9), shows that the ultrafine assembling proved by XRD and SEM provides a better protection for Hb immobilized on the LDH nanosheets than when adsorbed on the surface. The bio-hybrids can also be reused at least four times with less than 20% deactivation. All the characteristics of the Hb/MgAl LDH bio-hybrids make them very promising for industrial applications particularly as their synthesis can be scaled-up by microreactor technology.

O. Pascu et al. have achieved the one-pot synthesis in a continuous hydrothermal multi-step process of functional LDHs intercalated by large organic species like dodecyl sulfate (DS), with immobilized enzymes (i. e. transketolase (TK)) and deposited metal/oxide nanocrystals (Pd or Ru NCs). Thus they obtained organic-hybrids, bio-hybrid and inorganic LDH in a highly versatile method [128]. The process uses a configured set-up directly inspired from a supercritical microfluidic co-flow system previously used for the synthesis of hybrid ZnO or Pd nanocrystals [135, 136]. Contrary to the previous continuous flow synthesis of LDH based on microreactor technology using T-shaped microreactors, the set-up is based on a coaxial flowing microsystem made of two capillaries (Figure 23). Into the inner tube ($\phi = 0.75$ mm)

was injected the room temperature aqueous solution of M^{2+} (Mg^{2+} , Ni^{2+} or Zn^{2+}) and Al^{3+} nitrate salt solution ($[M^{2+} + Al^{3+}] = 3.3 \cdot 10^{-2} \text{ mol.L}^{-1}$; M^{2+}/Al^{3+} molar ratio of 2) with a high pressure pump at a given flow rate and 25 MPa. In the external tube (length: 30 cm; $\phi = 2.1 \text{ mm}$) was injected the preheated base solution ($NaOH + Na_2CO_3$) at a double flow rate compared to that of the cationic salts solution and at 25 MPa. The functionalizing reagents (DS, TK, Pd, Ru) were added in the precursor solution. The tubular reactor is put inside an oil bath to regulate the temperature. Nucleation of the LDH particles starts at the beginning of the tubular reactor when the salt and base solutions start to mix. Crystal growth occurs along the whole reactor length. Temperature and flow rates were adjusted for residence times in the range 5 - 10 s at a pressure of 20 MPa. At the end of reaction the precipitated LDH is recovered in the outlet solution.

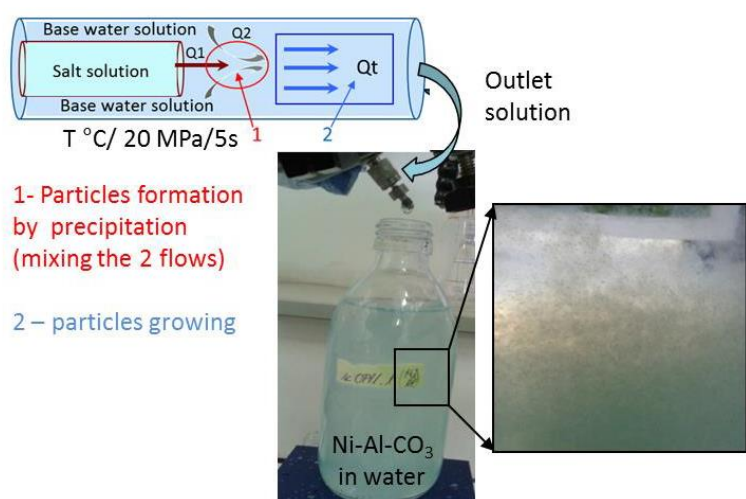


Figure 23: Sketch of the continuous hydrothermal synthesis approach for the synthesis in one-pot of functionalized LDHs (Reproduced with permission from Ref. [128]).

This approach allows carrying out synthesis of pristine $MgAl-CO_3$, $NiAl-CO_3$ and $ZnAl-CO_3$ LDH, exhibiting platelets of rounded shapes with diameters and thicknesses determined from XRD patterns in the range 10 - 23 nm and 5.6 - 17.5 nm, respectively. $NiAl-$ $MgAl-$ and $ZnAl-CO_3$ samples contain 7, 15 and 23 stacked layers, respectively. Comparison of particle

diameters obtained from XRD and TEM analysis allows concluding for a monocrystallinity of NiAl-CO₃ LDH, polycrystallinity of MgAl-CO₃ LDH and presence of several coherent domains in the same platelets for ZnAl-CO₃ LDH. The different sorts of functional LDH were prepared following the same previous procedure but adding the functionalizing reagent in the precursor solution. Their main characteristics can be further described.

The hybrid LDHs fully intercalated with DS show enhancement of the basal spacing to 2.7 nm suggesting interdigitated bilayer arrangement of the anionic species, whereas the structures are almost similar to that of the pristine LDH. On the contrary the morphology exhibits hydrophobic characteristics with sticky particles in the case of MgAl-DS LDH and, surprisingly, rounded shaped pellets within an organic network of the DS molecules in the case of NiAl-DS LDH (Figures 24 and 25). The preparation of bio-hybrid LDH with 96% immobilization of TK, which is not intercalated due to its large size, required an optimization of the introduction procedure in the reaction media. Indeed aggregation of the pellets which occurs when growth is achieved in the presence of protein must be avoided [137]. TK was introduced downstream the initial mixing point where LDH starts forming in the reactor, this allows maintaining pH > 7 which is optimal for adsorption. Materials obtained by functionalizing MgAl LDH with Pd(NO₃)₃ and RuCl₃ precursors were designated inorganic LDHs. This functionalization leads to the formation of small NCs on the LDH surface (Pd and Ru NCs ≈ 2 and 1 nm, respectively) instead of isomorphic substitution of Mg²⁺ by Pd²⁺ or Ru³⁺ due to the too large ionic radius of the precious metal cations. Indeed the structural parameters remain similar to that of pristine MgAl-CO₃ LDH after addition of the Pd or Ru precursors. However, partial substitution of Ni²⁺ by Ru³⁺ is achieved in NiAl-CO₃ LDH. Functionalization induces morphological changes with sticky and rounded shaped pellets, respectively, observed for DS-containing MgAl and NiAl LDHs as previously underlined, pellets aggregation for TK-

LDHs and less aggregated inorganic LDH particles compared to the organic ones (Figure 24 and 25).

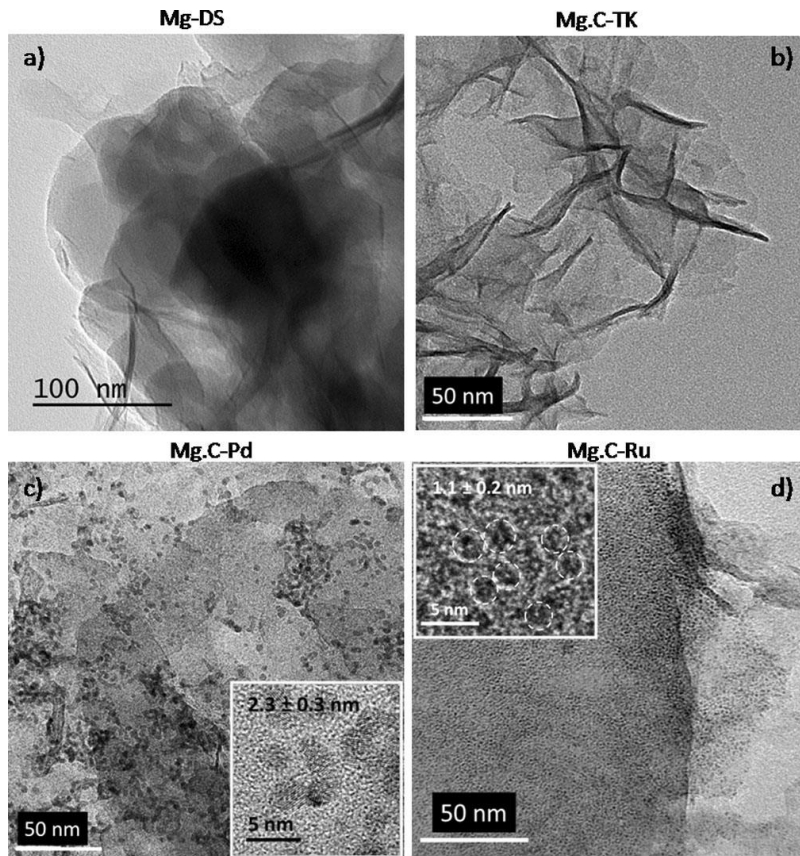


Figure 24: TEM images of functional MgAl-CO₃ LDH materials using: dodecyl sulfate DS (a), enzyme TK (b) and Pd (c) and Ru (d) NPs as functional agents (Reproduced with permission from Ref. [128]).

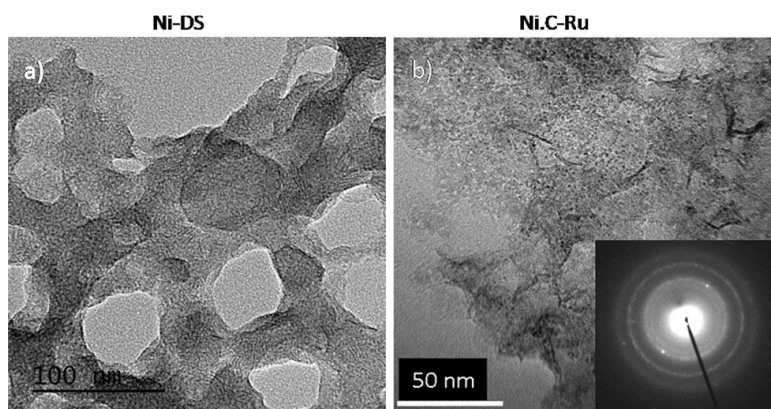


Figure 25: TEM images of functional NiAl-CO₃ LDH materials with dodecyl sulfate DS (a), Ru NPs (b) (Reproduced with permission from Ref. [128]).

Both bio-hybrid and inorganic LDHs obtained by the continuous flow method show interesting catalytic properties. TK maintains at least half of its activity once immobilized on LDH support and the Pd- and Ru-containing MgAl LDH catalysts lead to unexpected reactivity and selectivity in cinnamaldehyde hydrogenation reaction. Complete conversion of *trans*-cinnamaldehyde to 3-phenylpropionaldehyde in 12 hours in 0.1 MPa hydrogen at RT was reached with MgAl-Pd-LDH (5 mg). With MgAl-Ru-LDH contrary to the expected C=O bond reduction, 43 - 46% yield in 3-phenylpropionaldehyde was obtained after 12 hours in 8 MPa of hydrogen.

3.3 Synthesis of LDH-based composites

A wide variety of composites have been conceived using as building blocks LDH nanosheets of different compositions and metal oxides [138, 139], metal phosphides and sulfides [140-142], polyoxometallates [143], zero-three dimensional carbon materials [144-147] polymers [53]. Graphene-LDH hybrids have received much attention due to the 2D structural compatibility of the monolayer sheets of graphene and of the LDH brucite-like layer building blocks. The hierarchical composites allow combining electrical conductivity and mechanical strength properties of graphene with the chemical reactivity of LDH [144]. Graphene/LDH nanocomposites have been studied as flame retardants [148-150] adsorbents for wastewater treatments [151-153], catalysts [154], nanofillers for polymer composites [155], sensors for medical applications [156, 157], CO₂ adsorbents [158, 159] and in a wide extent as supercapacitors of high performances [146, 160-169]. Several methods for assembling the building blocks into the hierarchical graphene/LDH composite structures have been employed

[147]. The most common is the coprecipitation and growth of LDH phases on graphene oxide (GO) supports under hydrothermal or microwave-assisted reflux methods [161-166, 170]. Hybrid films were also prepared by hydrogen-bonding layer-by-layer self-assembly method [155, 171]. LDH films are developed as corrosion protection for metals and alloys. However, they suffer several drawbacks, particularly when Cl^- are the compensating anions and when they coexist with adsorbed water. This latter enhances diffusion of oxygen and Cl^- leading to defective structured films. Graphene and graphene oxide (GO) grafted with polymers (polyaniline, polystyrene) exhibit high corrosion protection performance but are not easily synthesized. In this context, reduced graphene (RGO)/LDH composite films are very attractive as corrosion protection materials. They can decrease water diffusion which is damageable for LDH due to the barrier property of RGO and improve the corrosion protection ability of the films.

X. Luo et al. [129] have developed a hydrothermal continuous flow method to prepare RGO/ZnAl LDH composite film on the surface of an Al alloy. The HCFR setup quite similar to that described in the work of H. Liang et al [88] (Figure 12) is constituted of a reservoir containing the precursor solution provided by a HPLC pump into a Teflon-lined 316 stainless steel reaction column placed in a tubular furnace connected to a pressure regulator. In a typical experiment a precursor solution (160 mL) containing Zn and Al nitrate salts ($\text{Zn/Al} = 6$) (0.44 mol.L^{-1}), NH_4NO_3 (0.88 mol.L^{-1}) and NH_4OH (1%, w/w), in required amounts to have pH 5.6, were mixed with 10 mL of RGO dispersion ($0.5 - 2 \text{ mg.L}^{-1}$) obtained from preoxidized graphite using a modified Hummers method [172] and put into the reservoir for continuous flow reaction. Formation of the RGO/ZnAl-LDH film-coated Al alloys proceeds in two steps. First nucleation of ZnAl LDH was achieved putting the pre-cleaned Al alloy substrate into the center of the reactor with an amount (50 mL) of the previous precursor solution at $130 \text{ }^\circ\text{C}$ for 45 min in order to allow seed growing. In a second step the precursor solution was flowed (0.5 mL.min^{-1}

¹) through the reactor at $P = 90$ psi and 80 °C for 2 h. RGO/ZnAl-LDH-t1(t2 or t3) (t1, t2 and t3 corresponding to RGO dispersion of $5 \cdot 10^{-4}$, $1 \cdot 10^{-3}$ and $2 \cdot 10^{-3}$ mg.mL⁻¹, respectively) were thus obtained (Figure 26). The successful synthesis of RGO/ZnAl-LDH composites by the hydrothermal continuous flow method is well evidenced. Indeed the materials exhibit the characteristic XRD peaks of ZnAl LDH. Moreover, the presence of both RGO and LDH building blocks is confirmed by FT-IR, Raman and XPS spectroscopies. FT-IR spectra of the RGO/ZnAl LDH films reveal the presence of RGO, particularly with the increase in intensity of the C=C/C-C stretching vibration band at 1622 cm⁻¹ with the RGO content. Metal-oxygen and metal-hydroxyl stretching vibrations in the LDH lattice are present below 1000 cm⁻¹ (Figure 26). Typical Raman peaks of RGO (D- and G-bands at 1346.8 and 1576.4 cm⁻¹, respectively) and of LDH (598.1 and 1068.3 cm⁻¹) are also observed.

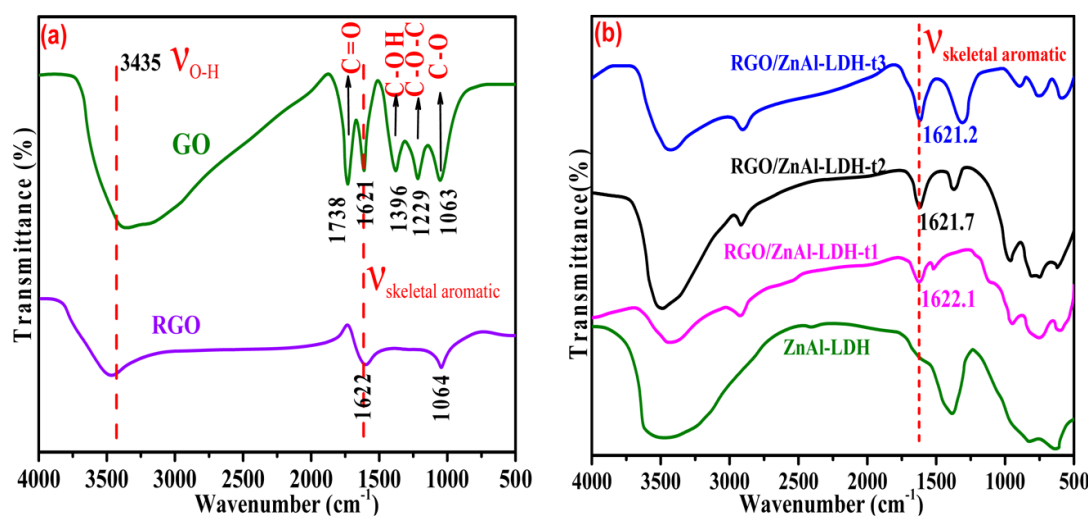


Figure 26: FT-IR spectra (a) of GO and RGO and (b) of ZnAl-LDH film, RGO/ZnAl-LDH-t1 film, RGO/ZnAl-LDH-t2 film, and RGO/ZnAl-LDH-t3 film (Reproduced with permission from Ref. [129]).

Consistently, in the XPS spectra the increase in relative intensity of the C 1s peak with the RGO loading shows that more RGO nanosheets are incorporated in the composite. SEM and TEM

images of the RGO/ZnAl LDH films of $\sim 1.8 \mu\text{m}$ thickness show that more compact RGO/ZnAl LDH is grown on the Al support as the RGO loading increases compared with the ZnAl LDH film and it is clearly embedded in the ZnAl LDH layers (Figure 27).

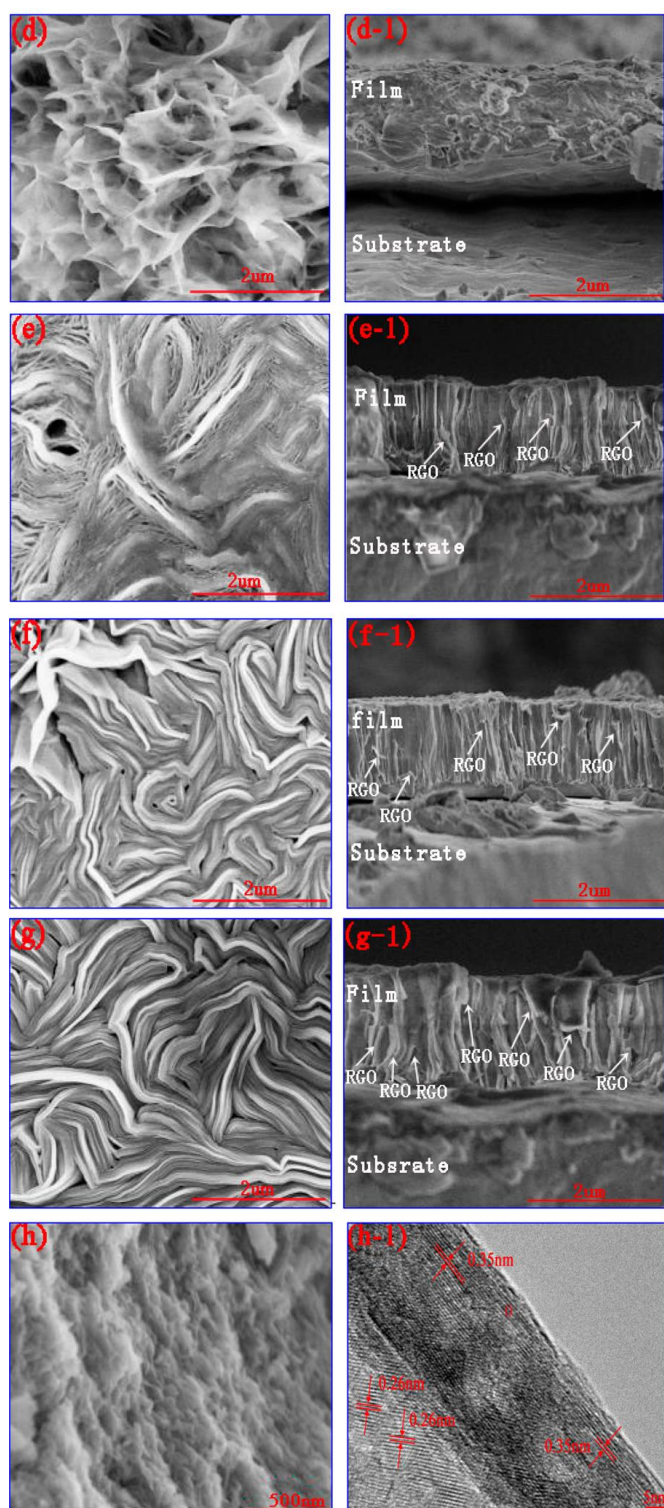


Figure 27: SEM images of (d) ZnAl LDH film, (e) RGO/ZnAl-LDH-t1 film, (f) RGO/ZnAl-LDH-t2 film, and (g) RGO/ZnAl-LDH-t3 film. Images in panels d-1, e-1, f-1, and g-1 correspond to the cross-sectional views of the four films. SEM (h) and HRTEM (h-1) images of the RGO/ZnAl-LDH composite scraped from the RGO/ZnAl-LDH-t2 film (Reproduced with permission from Ref. [129]).

The RGO/ZnAl LDH composites are expected to provide efficient barrier effect. Potentiodynamic polarization measurements show that, after 0.5 day of immersion in 3.5 wt% NaCl solution, corrosion protection of the Al alloy support is improved with the RGO/ZnAl-LDH films in comparison to a ZnAl-LDH film which yet acts as a physical barrier for bare Al alloy against aggressive medium. After 7 days of immersion, the ZnAl LDH film is degraded and its protection efficiency drops due to diffusion into the film/Al interface of the Cl^- compensating anions, whereas RGO/ZnAl LDH films still provide good corrosion protection to the Al alloy. This is attributed to the presence of RGO in the composites. The higher corrosion protection is confirmed when soaking the RGO/ZnAl LDH films in a higher concentration of Cl^- corrosive species (5.0 wt% NaCl) for 0.5 and 7 days. RGO acts as a physical barrier decreasing diffusion of H_2O , O_2 and Cl^- . XRD patterns of RGO/ZnAl LDH film-coated and ZnAl LDH film-coated samples immersed in a 3.5 wt% NaCl solution reveal that in all cases the LDH phase is intercalated with Cl^- . However, EDX spectra in the cross-section of the films reveal that Cl^- ions diffuse into the film/alloy interface in the GO-free film, while in contrast it is not detected at the interface in the case of the RGO/ZnAl LDH film in agreement with the barrier property of RGO for Cl^- . Last confirmation of this barrier property is provided by the higher rejection performance toward NaCl of the RGO/ZnAl LDH membrane compared to the ZnAl LDH membrane, which increases with the RGO loading. These results obviously led the authors to suggest a mechanism accounting for superior corrosion protection performance of the RGO/ZnAl LDH composite film compared to the ZnAl LDH film based on a synergetic effect between RGO and the LDH layer. The disordered arrangement of RGO in the RGO/ZnAl LDH film and the resulting tortuosity decrease the diffusion of O_2 and H_2O . This is reinforced by the hydrophobic character of RGO preventing H_2O to act as a conducting path for O_2 and Cl^- diffusion. Cl^- rejection which is essential against corrosion is attributed to the electrostatic

repulsion of Cl^- and negatively charged oxygen-containing functional groups at the edge of RGO. Therefore, in the RGO/ZnAl LDH composite, RGO can be considered as the key component that improves the anticorrosion properties through several contributions, i. e. antipenetration, hydrophobicity, tortuosity of the diffusion pathway and electrostatic repulsion as illustrated on Figure 28.

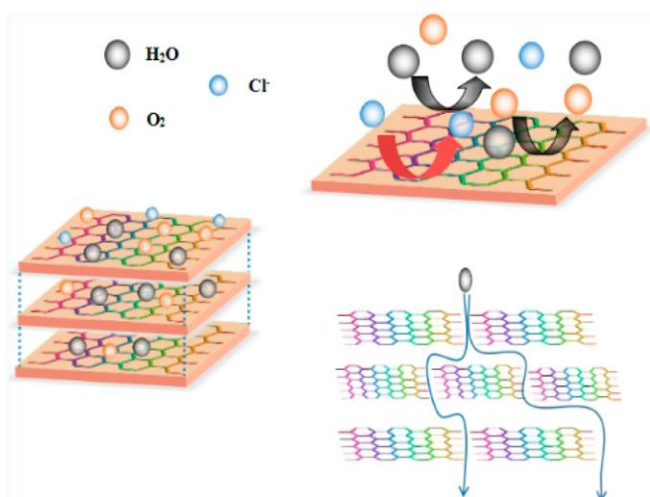


Figure 28: Mechanistic model for corrosion protection offered by the RGO/ZnAl-LDH-ts ($s = 1, 2, 3$) films (Reproduced with permission from Ref. [129]).

4. Concluding remarks and perspectives

We have reviewed the results concerning the different preparation processes of LDHs and LDH-based hybrids and composites since the pioneering work which uses a continuous coprecipitation method under steady-state conditions in a laboratory cylindrical tank reactor. They emphasize the versatility of the approaches implemented and the characteristics of the materials obtained.

The approaches first greatly differ by the setup employed, particularly the wide variety of reactors, going from cylindrical tank of large volume (230 mL) with magnetic stirring, to a precipitation chamber of reduced volume (6 mL) equipped with high speed disperser, counter-

current and parallel flow cylindrical reactors, meso-scale flow reactor and micromixer with capillary volume ($4 \cdot 10^{-2}$ mL) with two colliding flows as increasingly used nowadays in microfluidic approaches. The successive use of these different reactors allows to dramatically decrease the reaction volume and increase the mixing efficiency.

The continuous flow methods considered in this review allow obtaining a wide variety of pristine LDHs going from colloidal suspensions of individual nanosheets to exfoliated LDHs and nanoplatelets of several tens of stacked layers and of 1 - 2 μm lateral size. It must be emphasized that very different textural, morphological and structural features are also obtained. Singular properties have been indeed reached in the ILDP method at very short residence times: LDH particles composed of uniformly sized and tightly packed crystallites exhibiting no surface area and porosity. Thin LDH nanoplates have been otherwise directly precipitated from metal salts and ammonia solution on carbon paper or from divalent metal cation and alkaline solutions on an alumina substrate. This shows the great adaptability of the continuous flow methods to the preparation of different types of LDH-containing materials, including the functional LDH and LDH-based composites. These features open interesting outlooks because all the application fields of LDH are concerned and can be contemplated through preparations in continuous flow methods. In the different processes implemented, short contact times of the precursor solutions and controlled residence times ranging from $1 \cdot 10^{-3}$ to 1800 s of the mixed solutions in the reactors, as well as quasi constant high supersaturation rates participate to favor nucleation and to greatly reduce growth of the particles. Experiments with T-shape micromixer at very short residence time (Table 1, entry 8) and the so-called “flash precipitation” with residence time of 1 s carried out in the ILDP method (Table 1, entry 2) reveal that nucleation of well crystallized LDH is “extraordinary fast” as pointed out by M. Ren et al. [68]. In the latter case where growing is almost avoided, tightly packed colloid-sized nucleating particles are obtained. On the other hand, large hexagonal platelets can be obtained at long residence

time and low supersaturation as shown for NiCo and ZnAl LDH using the HCFR method (Table 2, entries 10 and 11). It is worth noting that, excepted in the experiment with the static mixer coupled to a tubular centrifuge (Table 1 entry 8) and that with the two-step process involving coprecipitation in a meso-scale reactor followed by aging in a thermostated beaker (Table 1, entry 5), washing steps were not performed in any experiment. The absence of these steps increases agglomeration, particularly due to the presence of electrolytes acting as aggregating agents [70]. Indeed in most cases agglomerates of primary crystallites have been clearly evidenced by microscopy analysis.

Regarding the morphological characteristics of the LDH prepared with the different approaches, an interesting comparison can be done between D_{003} and lateral dimensions of the samples reported in Table 2. Obviously, the most largely studied composition are MgAl LDH which have been obtained using, i. e. turbulent regime with co-precipitation chamber (Table 1, entry 2), mixing of counter-current flows in a continuous nozzle reactor (Table 1, entry 3) and simultaneous mixing and segmentation of flows in T-shaped microreactor (Table 1, entries 6, 7, 9). Dimensions in the (003) direction, related to the number of stacked layers, are always by far lower than those in the lateral directions showing high aspect ratios of the particles. A three times increase is noted for the dimension in the c direction, ranging from 4 to 12 nm, which represents about 5 to 12 stacked layers, while variation is dramatically larger in the ab plane going from less than 10 nm to about 17 μm . Remarkably, naked nanosheets were obtained with the T-type micromixer (Table 2, entry 7) and this can be assigned to the use of ammonia instead of mixed NaOH and Na_2CO_3 as the alkaline precipitating solution. This confirms that the presence of CO_3^{2-} in reaction media allows improving the stacking of the layers in the c direction and the structural order [173, 174]. Results reported in Table 2, entries 2 and 9, show that similar dimensions are obtained in the stacking direction in spite of a very large increase of the residence time from 1×10^{-3} to 12 s. On the contrary, an important increase is observed

in the lateral dimension as a function of the residence time which accounts for growing of the individual crystals within the reactor, but also for intergrowth of the crystals and development of edge-to-face aggregation [81]. Very large lateral dimensions observed with cross micromixer (Table 2, entry 6) must be assigned both to moderate Reynolds numbers and to high supersaturation level which gives rise to very small particles which have strong tendency to form agglomerates. As expected pronounced agglomeration occurs due to the post aging treatment in the two-step process of coprecipitation using a meso-scale reactor (Table 2, entry 5). Aspect ratios vary from about 2 to more than 100 depending on the process. Moreover, as aspect ratios can also be varied within a same process through the experimental parameters, such as residence time or stirring rate (Table 2, entry 2), the continuous flow methods offer great versatility to adjust this important property.

It is worth emphasizing the possibility to prepare naked LDH nanosheets using a continuous flow process with T-shaped micromixer as shown by X. Pang et al. [86]. Preparation of naked LDH nanosheets has been also later carried out by the same group using the PWD route in a beaker under magnetic stirring [108]. This allows comparing the morphology of the nanosheets obtained with both procedures, particularly because the concentration of the solutions are the same ($[Mg^{2+} + Al^{3+}] = 0.3 \text{ mol.L}^{-1}$ and $Mg/Al = 2$) (Table 3, entry 6). Closer concentration of LDH phase in the range 7 - 8.5% was obtained from the co-precipitated gel centrifuged and water-washed. Differences observed in lateral dimensions of $\sim 80 \text{ nm}$ and $15 - 30 \text{ nm}$ with the beaker reactor in the PWD method and the T-shaped micromixer, respectively, for the nanosheets with 1 - 2 brucite-like layers thickness are assignable to the preparation method. Growing of the LDH particles is indeed more largely reduced in the T-shaped micromixer. It is consistent with the addition time of the solutions of $\sim 10 \text{ min}$ in the beaker while the residence time is estimated at 12.10^{-3} s in the T-shaped micromixer.

For ZnAl LDH samples the D_{003} and lateral dimensions of those prepared with a tank (Table 2, entry 1) or a column reactor (Table 2, entry 11) are by far higher in the latter case, which is consistent with the very low supersaturation level obtained with HMT as alkaline agent. Aspect ratios are in the range from 2 to 4, but dimensions in the c direction and (a, b) planes are higher than for MgAl LDH as generally observed also for batch or semi-batch synthesis [175]. Very similar results were obtained regarding hydrocalumite samples, i. e. CaAl LDH, in the two studies using a counter-current flow reactor (Table 2, entries 3 and 4); they show the reproducibility of the preparation and they confirm that particles are larger in both c direction and (a, b) planes in the case of hydrocalumite compared to hydrotalcite when synthesized in similar conditions (Table 2 entry 3).

The available comparisons of the properties and activities in different applications of the LDHs prepared using either continuous-flow or static methods have been summarized in Table 3. They show that particles of lower size with a better control of the morphology are generally obtained in continuous-flow in comparison to batch experiments. The reverse is observed when the comparison is done with rapid synthesis in colloid mills because the aging time is greatly reduced. Only two examples of applications are reported but both confirm an improvement of the activity for the samples prepared in continuous-flow.

Productivity is a fundamental feature of intensified methods in industrial practice. In several previous studies comparisons have been achieved between productivities in continuous flow processes and in co-precipitations in batch reactor vessels. Higher productivities were always obtained in the former procedures. Chang et al. compared the results obtained with reactors of similar volumes; they reported productivities about 3 to 8 times higher in continuous flow than with the traditional batch method [80]. Dramatically higher differences are reported using the precipitation chamber (6 mL) in the ILDP method and a T-type microreactor [81, 85] with, in both cases, productivities three orders of magnitude higher than in static conditions.

Productivity is several tons of LDH per hour and cubic meter of reactor in the ILDP method and 10^3 g per hour and cubic meter with the T-shaped micromixer instead of 0.3 g LDH per hour and cubic meter in stirred batch (Table 3, entries 1 and 4). It must be emphasized that scaling the synthesis of LDH at an industrial scale using a T-shape micromixer can be difficult and that the results obtained with a meso-scale reactor (Table 1 and 2, entries 5) offer an interesting alternative provided that the operating conditions will be carefully chosen.

Another important aspect for industrial practice concerns the concentration of the solutions usable with the different types of reactors. The highest metal salt concentrations which were reported, in the range 0.1 - 1 mol.L⁻¹, concerned the ILDP method with the precipitation chamber efficiently stirred, and the experiments involving counter-current flow reactors. Lower metal salt concentrations were generally used with the micromixers probably to prevent clogging of the channels. However, this drawback is overcome by segmenting the reactant streams introduced in the channel using simultaneous injection of air. This allows improving mixing and reducing axial dispersion [6, 85].

Narrow LDH particle size distribution has been obtained by the group of Duan and Evans [72] using a method involving firstly a nucleation step in a colloid mill where rapid mixing of the precursor solutions (2 min) occurs under a highly turbulent regime, followed by a separate aging step at 130 °C for 13 h. Well crystallized hexagonal Mg-Al LDH particles (Mg/Al = 3) with $D_{003} = 21.8$ nm which represent ~ 28 stacked layers and lateral dimensions in the range of 60 - 80 nm were obtained. These characteristics can be interestingly compared with those of the MgAl LDH prepared in continuous flow with a T-shaped micromixer using also a mixture of NaOH and Na₂CO₃ as alkaline solution where nucleation was very fast ($1.3 \cdot 10^{-3}$ s) and hydrothermal treatment achieved at 150 °C for 2 h (Table 2 entry 9). Particles of ca. 20 - 100 nm and regular hexagonal plate-like morphology grew to larger sizes from ca. 50 - 150 nm after aging. The particle size distribution after aging is then larger than the one of samples

coprecipitated in the colloid mill. This accounts for the dissolution-recrystallization phenomena occurring during aging of the particles when obtained from continuous flow experiments, which are avoided in the separated nucleation-aging method due to the intermediate washings (Table 3, entry 6). These results emphasized the very relevant approach initiated in the work of Fleger et al. where coprecipitation in continuous flow was followed by an immediate cleaning process, although further developments are necessary to adapt the process to reactors other than static mixer [87]. LDH nanohybrids containing large organic molecules able to improve the hydrophobic character of the particles are widely studied and DS has been in most cases used as a model guest species. MgAl LDH nano-hybrids intercalated with DS anions have been prepared using the continuous, high-pressure, co-flow system (Tables 1 and 2, entries 14) and by co-assembly of the naked nanosheets obtained using a T-type micromixer and DS anions (Tables 1 and 2, entries 7); similar crystallinities were obtained in both cases and d_{003} values of 2.70 nm with the co-flow system and 2.56 nm with the T-type reactor were determined, suggesting interdigitated bilayer arrangement of the anions between the brucite-like layers. However, the similar structural and morphological characteristics make more attractive the one-pot process using the co-flow system rather than the co-assembly achieved in two or several steps. Modification from hydrophilic to hydrophobic of the LDH surface property has also been achieved by S. Elbasuney [126] with other types of surfactants (PEA and DDA) via post synthesis treatment of LDH obtained in continuous flow (Tables 1 and 2, entries 12). The modified LDH particles can be easily recovered from an organic phase and become highly compatible for example with hosting polymers when they are employed as nanofillers for flame retardancy.

It is almost as challenging to obtain LDH particles with controlled size and morphology or LDH nanosheets as LDH-based hybrids and nanocomposites through continuous flow methods. The most relevant results reported in this review on LDH-based hybrids and nanocomposites must

be an incitement in a near future toward the development of their large-scale preparation with constant quality and properties. Indeed, considering the potential of these materials for applications in fields as diverse as drug delivery, nanofillers for polymers, catalysts and photocatalysts, sensors, water remediation, energy storage and so on, continuous flow methods of synthesis will be particularly useful for industrial developments. It is particularly the case when functionalization is achieved by intercalation of anionic species during coprecipitation in a bottom-up approach. The continuous flow methods are indeed not adapted to intercalation methods such as anionic exchange or reconstruction, which are the two conventional well known routes to intercalate guest species into host LDH structures. Production in large amounts of drug/LDH hybrids by continuous flow method of synthesis appears now as one of the most possible developments. Many drugs are chemically and thermally stable enough to be successfully intercalated during coprecipitation in continuous flow method.

Preparation of multicomponent assemblies by continuous flow methods remains still very challenging. However, preparation of hierarchical systems involving a magnetic core and a shell of LDH offers interesting possibilities for catalytic applications, drug delivery and adsorption. In the case of catalysts, they are magnetically separable and then more easily recyclable. Concerning drug delivery vectors, LDH shell exchanged with anionic drug can reasonably be contemplated. Such hierarchical materials elaborated through continuous flow methods will probably be hardly obtained in a one-step process. The magnetic core should be previously synthesized; further continuous flow synthesis of the LDH phase in the presence of the magnetic phase could then be performed. Optimization of the process, particularly the type of reactor, will be the key point that will need deep investigations. Extending these approaches to the preparation of nanocomposites involving LDHs and carbon supports (carbon nanofibers, carbon nanotubes, graphene oxide) can be also reasonably considered.

A promising field of application of the continuous flow methods is that of the LDH/polymer composites. The possibility to obtain LDH nanosheets by continuous flow method and then to optimize the interfacial contact between the nanofiller and the polymer offers interesting outlooks which should be considered. It is another case where a multistep process must be considered, the continuous flow production of the LDH being the initial one.

Production in large scale through continuous flow methods can be an exciting outlook in catalysis, regarding the challenging problem of replacement of rare or noble metal cations with cheaper and abundant transition metal cations. From an economical point of view, production of LDH precursors, particularly LDH containing transition metal cations, can allow the use of larger amounts of less efficient catalysts than noble metal-containing catalysts. They LDHs would be prepared at a lower cost with high reproducibility by the continuous flow methods. The variety of multicationic LDHs obtained through the two-step coprecipitation and aging process or with a micromixer (Table 1, entries 5 and 9) show that the continuous flow methods are adapted to the synthesis of the required materials.

A variety of reactor designs are available to achieve the continuous flow synthesis; and the right reactor should be chosen as a function of the targeted material. Recent reports dealing with the continuous production of materials such as MOFs, functional mesoporous silica nanofibers or biomaterials using microfluidic technology generally emphasize the difficulty to realize large scale fabrication [3, 176-180]. On the other hand, aluminophosphates or zeolites are produced in large scale in continuous flow using tubular reactors with an accurate control of the synthesis parameters [98, 181-183]. Then if one considers that the industrial applications involving LDH-based hybrids or nanocomposites generally yield lower quantity of products of higher added value than those involving bare LDH particles, microfluidic technology could be more adapted in the former case and tubular reactors in the latter.

The examples of preparation by continuous flow methods of dense and uniform thin nanoplates of NiCo LDH on carbon paper support [88], of ZnAl and CoAl LDHs on alumina-coated substrates [118] and of graphene/LDH composite film on aluminium alloy [129] reported in this review show that different shaping of LDH-based materials can be achieved. This is of high interest for further developments and it is probably one of the most promising tracks to develop. All the aspects already discussed are summarized in Figure 1 showing the achievements already obtained for the preparation of a wide variety of LDHs and LDH-based materials through the careful choice of the reactor design and of a set of operating conditions which can also allow choosing the adapted continuous flow methods for further LDH scaling.

A next challenge would be to develop a continuous flow process including coprecipitation, washing and aging steps in a same integrated setup and future developments should focus on this goal.

References

- [1] J.A. Darr, J. Zhang, N.M. Makwana and X. Weng, Continuous Hydrothermal Synthesis of Inorganic Nanoparticles: Applications and Future Directions, *Chemical Reviews*, 117 (2017) 11125-11238.
- [2] A.S.M. Peter W. Dunne, Chris L. Starkey, Tom A. Huddle, Ed H. Lester, Continuous-flow hydrothermal synthesis for the production of inorganic nanomaterials, *Phil. Trans. R. Soc. A*, (2015).
- [3] J. Ren, X. Dyosiba, N.M. Musyoka, H.W. Langmi, M. Mathe and S. Liao, Review on the current practices and efforts towards pilot-scale production of metal-organic frameworks (MOFs), *Coordination Chemistry Reviews*, 352 (2017) 187-219.
- [4] J. Ma, Y. Wang and J. Liu, Biomaterials Meet Microfluidics: From Synthesis Technologies to Biological Applications, *Micromachines*, 8 (2017) 255.

- [5] S. Marre and K.F. Jensen, Synthesis of micro and nanostructures in microfluidic systems, *Chemical Society Reviews*, 39 (2010) 1183-1202.
- [6] C.-X. Zhao, L. He, S.Z. Qiao and A.P.J. Middelberg, Nanoparticle synthesis in microreactors, *Chemical Engineering Science*, 66 (2011) 1463-1479.
- [7] X. Yao, Y. Zhang, L. Du, J. Liu and J. Yao, Review of the applications of microreactors, *Renewable and Sustainable Energy Reviews*, 47 (2015) 519-539.
- [8] F. Cavani, F. Trifiro and A. Vaccari, Hydrotalcite-type anionic clays: Preparation, properties and applications, *Catal Today*, 11 (1991) 173-301.
- [9] A. Vaccari, Layered double hydroxides: present and future: V. Rives (Ed.), Nova Science Publishers, Inc., New York, 2001, IX+439 pp., ISBN 1-59033-060-9, *Applied Clay Science*, 22 (2002) 75-76.
- [10] J.L.R.a.J.E.I. Carlos J. Serna, Crystal-Chemical Study of Layered $[Al_2Li(OH)_6]^{+X-} \cdot nH_2O$, *Clay Clay Miner*, 30 (1982) 180-184.
- [11] S. Velu, D.P. Sabde, N. Shah and S. Sivasanker, New Hydrotalcite-like Anionic Clays Containing Zr^{4+} in the Layers: Synthesis and Physicochemical Properties, *Chem Mater*, 10 (1998) 3451-3458.
- [12] D. Tichit, N. Das, B. Coq and R. Durand, Preparation of Zr-Containing Layered Double Hydroxides and Characterization of the Acido-Basic Properties of Their Mixed Oxides, *Chem Mater*, 14 (2002) 1530-1538.
- [13] K. Rozov, H. Curtius and D. Bosbach, Preparation, characterization and thermodynamic properties of Zr-containing Cl-bearing layered double hydroxides (LDHs), in: *Radiochimica Acta*, Vol 103, 2015, pp. 369.
- [14] J. Poonosamy, F. Brandt, M. Stekiel, P. Kegler, M. Klinkenberg, B. Winkler, V. Vinograd, D. Bosbach and G. Deissmann, Zr-containing layered double hydroxides: Synthesis,

characterization, and evaluation of thermodynamic properties, *Applied Clay Science*, 151 (2018) 54-65.

[15] S. Velu, K. Suzuki, M.P. Kapoor, S. Tomura, F. Ohashi and T. Osaki, Effect of Sn Incorporation on the Thermal Transformation and Reducibility of M(II)Al-Layered Double Hydroxides [M(II) = Ni or Co], *Chem Mater*, 12 (2000) 719-730.

[16] S. Velu, K. Suzuki, M. Okazaki, T. Osaki, S. Tomura and F. Ohashi, Synthesis of New Sn-Incorporated Layered Double Hydroxides and Their Thermal Evolution to Mixed Oxides, *Chem Mater*, 11 (1999) 2163-2172.

[17] M. Intissar, S. Holler, F. Malherbe, J.-P. Besse and F. Leroux, Incorporation of Ti⁴⁺ into layered double hydroxide sheets? The response by X-ray diffraction and absorption study, *Journal of Physics and Chemistry of Solids*, 65 (2004) 453-457.

[18] C.G. Silva, Y. Bouzidi, V. Fornés and H. García, Layered Double Hydroxides as Highly Efficient Photocatalysts for Visible Light Oxygen Generation from Water, *J Am Chem Soc*, 131 (2009) 13833-13839.

[19] B. Li, Y. Zhao, S. Zhang, W. Gao and M. Wei, Visible-Light-Responsive Photocatalysts toward Water Oxidation Based on NiTi-Layered Double Hydroxide/Reduced Graphene Oxide Composite Materials, *ACS Applied Materials & Interfaces*, 5 (2013) 10233-10239.

[20] D. Wang, N. Ge, S. Qian, J. Li, Y. Qiao and X. Liu, Selenium doped Ni-Ti layered double hydroxide (Ni-Ti LDH) films with selective inhibition effect to cancer cells and bacteria, *RSC Advances*, 5 (2015) 106848-106859.

[21] R. Bîrjega, O.D. Pavel, G. Costentin, M. Che and E. Angelescu, Rare-earth elements modified hydrotalcites and corresponding mesoporous mixed oxides as basic solid catalysts, *Applied Catalysis A: General*, 288 (2005) 185-193.

- [22] E. Angelescu, O.D. Pavel, M. Che, R. Bîrjega and G. Constantin, Cyanoethylation of ethanol on Mg–Al hydrotalcites promoted by Y^{3+} and La^{3+} , *Catalysis Communications*, 5 (2004) 647-651.
- [23] M. Intissar, J.-C. Jumas, J.-P. Besse and F. Leroux, Reinvestigation of the Layered Double Hydroxide Containing Tetravalent Cations: Unambiguous Response Provided by XAS and Mössbauer Spectroscopies, *Chem Mater*, 15 (2003) 4625-4632.
- [24] S. Miyata and T. Kumura, SYNTHESIS OF NEW HYDROTALCITE-LIKE COMPOUNDS AND THEIR PHYSICO-CHEMICAL PROPERTIES, *Chemistry Letters*, 2 (1973) 843-848.
- [25] H. Tagaya, S. Sato, H. Morioka, J. Kadokawa, M. Karasu and K. Chiba, Preferential intercalation of isomers of naphthalenecarboxylate ions into the interlayer of layered double hydroxides, *Chem Mater*, 5 (1993) 1431-1433.
- [26] S. P. Newman and W. Jones, Synthesis, characterization and applications of layered double hydroxides containing organic guests, *New Journal of Chemistry*, 22 (1998) 105-115.
- [27] T. Kameda, H. Takeuchi and T. Yoshioka, Hybrid inorganic/organic composites of Mg–Al layered double hydroxides intercalated with citrate, malate, and tartrate prepared by co-precipitation, *Mater Res Bull*, 44 (2009) 840-845.
- [28] T. Kwon and T.J. Pinnavaia, Pillaring of a layered double hydroxide by polyoxometalates with Keggin-ion structures, *Chem Mater*, 1 (1989) 381-383.
- [29] S.K. Yun and T.J. Pinnavaia, Layered Double Hydroxides Intercalated by Polyoxometalate Anions with Keggin (α -H₂W₁₂O₄₀6⁻), Dawson (α -P₂W₁₈O₆₂6⁻), and Finke (Co₄(H₂O)₂(PW₉O₃₄)₂10⁻) Structures, *Inorg Chem*, 35 (1996) 6853-6860.
- [30] V. Rives and M.a. Angeles Ulibarri, Layered double hydroxides (LDH) intercalated with metal coordination compounds and oxometalates, *Coordination Chemistry Reviews*, 181 (1999) 61-120.

- [31] F. Kooli, W. Jones, V. Rives and M.A. Ulibarri, An alternative route to polyoxometalate-exchanged layered double hydroxides: the use of ultrasound, *J Mater Sci Lett*, 16 (1997) 27-29.
- [32] F. Leroux and C. Taviot-Gueho, Fine tuning between organic and inorganic host structure: new trends in layered double hydroxide hybrid assemblies, *J Mater Chem*, 15 (2005) 3628-3642.
- [33] C. Roland-Swanson, J.-P. Besse and F. Leroux, Polymerization of Sulfopropyl Methacrylate, a Surface Active Monomer, within Layered Double Hydroxide, *Chem Mater*, 16 (2004) 5512-5517.
- [34] C. Vaysse, L. Guerlou-Demourgues, E. Duguet and C. Delmas, Acrylate Intercalation and in Situ Polymerization in Iron-, Cobalt-, or Manganese-Substituted Nickel Hydroxides, *Inorg Chem*, 42 (2003) 4559-4567.
- [35] Q. Wang, X. Zhang, C.J. Wang, J. Zhu, Z. Guo and D. O'Hare, Polypropylene/layered double hydroxide nanocomposites, *J Mater Chem*, 22 (2012) 19113-19121.
- [36] M. Jobbágy and A.E. Regazzoni, Anion-Exchange Equilibrium and Phase Segregation in Hydrotalcite Systems: Intercalation of Hexacyanoferrate(III) Ions, *The Journal of Physical Chemistry B*, 109 (2005) 389-393.
- [37] E. Coronado, C. Martí-Gastaldo, E.n. Navarro-Moratalla and A. Ribera, Confined Growth of Cyanide-Based Magnets in Two Dimensions, *Inorg Chem*, 49 (2010) 1313-1315.
- [38] G.r. Layrac, D. Tichit, J. Larionova, Y. Guari and C. Guérin, Controlled Growth of Cyano-Bridged Coordination Polymers into Layered Double Hydroxides, *The Journal of Physical Chemistry C*, 115 (2011) 3263-3271.
- [39] A.I. Khan, L. Lei, A.J. Norquist and D. O'Hare, Intercalation and controlled release of pharmaceutically active compounds from a layered double hydroxide, *Chem Commun*, (2001) 2342-2343.

- [40] V. Rives, M. del Arco and C. Martín, Intercalation of drugs in layered double hydroxides and their controlled release: A review, *Applied Clay Science*, 88 (2014) 239-269.
- [41] V. Rives, M. del Arco and C. Martín, Layered double hydroxides as drug carriers and for controlled release of non-steroidal antiinflammatory drugs (NSAIDs): A review, *J. Control. Release*, 169 (2013) 28-39.
- [42] G. Darmograi, B. Prelot, G. Layrac, D. Tichit, G. Martin-Gassin, F. Salles and J. Zajac, Study of Adsorption and Intercalation of Orange-Type Dyes into Mg–Al Layered Double Hydroxide, *The Journal of Physical Chemistry C*, 119 (2015) 23388-23397.
- [43] Z. Matusinovic and C.A. Wilkie, Fire retardancy and morphology of layered double hydroxide nanocomposites: a review, *J Mater Chem*, 22 (2012) 18701-18704.
- [44] S. Abello, F. Medina, D. Tichit, J. Perez-Ramirez, Y. Cesteros, P. Salagre and J.E. Sueiras, Nanoplatelet-based reconstructed hydrotalcites: towards more efficient solid base catalysts in aldol condensations, *Chem Commun*, (2005) 1453-1455.
- [45] J.C.A.A. Roelofs, D.J. Lensveld, A.J. van Dillen and K.P. de Jong, On the Structure of Activated Hydrotalcites as Solid Base Catalysts for Liquid-Phase Aldol Condensation, *J Catal*, 203 (2001) 184-191.
- [46] X. Lei, W. Lu, Q. Peng, H. Li, T. Chen, S. Xu and F. Zhang, Activated MgAl-layered double hydroxide as solid base catalysts for the conversion of fatty acid methyl esters to monoethanolamides, *Applied Catalysis A: General*, 399 (2011) 87-92.
- [47] V. Ambrogi, G. Fardella, G. Grandolini and L. Perioli, Intercalation compounds of hydrotalcite-like anionic clays with antiinflammatory agents — I. Intercalation and in vitro release of ibuprofen, *Int J Pharm*, 220 (2001) 23-32.
- [48] P. Gunawan and R. Xu, Direct control of drug release behavior from layered double hydroxides through particle interactions, *Journal of Pharmaceutical Sciences*, 97 (2008) 4367-4378.

- [49] J.-M. Oh, S.-H. Hwang and J.-H. Choy, The effect of synthetic conditions on tailoring the size of hydrotalcite particles, *Solid State Ionics*, 151 (2002) 285-291.
- [50] H. Dong, M. Chen, S. Rahman, H.S. Parekh, H.M. Cooper and Z.P. Xu, Engineering small MgAl-layered double hydroxide nanoparticles for enhanced gene delivery, *Applied Clay Science*, 100 (2014) 66-75.
- [51] F. Leroux and J.-P. Besse, Polymer Interleaved Layered Double Hydroxide: A New Emerging Class of Nanocomposites, *Chem Mater*, 13 (2001) 3507-3515.
- [52] Y. Gao, J. Wu, Q. Wang, C.A. Wilkie and D. O'Hare, Flame retardant polymer/layered double hydroxide nanocomposites, *Journal of Materials Chemistry A*, 2 (2014) 10996-11016.
- [53] C. Taviot-Guého, V. Prévot, C. Forano, G. Renaudin, C. Mousty and F. Leroux, Tailoring Hybrid Layered Double Hydroxides for the Development of Innovative Applications, *Advanced Functional Materials*, 28 (2017) 1703868.
- [54] Y. Kuthati, R.K. Kankala and C.-H. Lee, Layered double hydroxide nanoparticles for biomedical applications: Current status and recent prospects, *Applied Clay Science*, 112-113 (2015) 100-116.
- [55] G. Mishra, B. Dash and S. Pandey, Layered double hydroxides: A brief review from fundamentals to application as evolving biomaterials, *Applied Clay Science*, 153 (2018) 172-186.
- [56] A.N. Ay, B. Zumreoglu-Karan, A. Temel and V. Rives, Bioinorganic magnetic core-shell nanocomposites carrying antiarthritic agents: intercalation of ibuprofen and glucuronic acid into Mg-Al-layered double hydroxides supported on magnesium ferrite, *Inorg Chem*, 48 (2009) 8871-8877.
- [57] J. Wang, R. Zhu, B. Gao, B. Wu, K. Li, X. Sun, H. Liu and S. Wang, The enhanced immune response of hepatitis B virus DNA vaccine using SiO₂@LDH nanoparticles as an adjuvant, *Biomaterials*, 35 (2014) 466-478.

- [58] H. Zhang, D. Pan and X. Duan, Synthesis, Characterization, and Magnetically Controlled Release Behavior of Novel Core–Shell Structural Magnetic Ibuprofen-Intercalated LDH Nanohybrids, *The Journal of Physical Chemistry C*, 113 (2009) 12140-12148.
- [59] Z. Rezvani and M. Sarkarat, Synthesis and Characterization of Magnetic Composites: Intercalation of Naproxen into Mg-Al Layered Double Hydroxides Coated on Fe₃O₄, *Zeitschrift für anorganische und allgemeine Chemie*, 638 (2012) 874-880.
- [60] Z. Yang, F. Wang, C. Zhang, G. Zeng, X. Tan, Z. Yu, Y. Zhong, H. Wang and F. Cui, Utilization of LDH-based materials as potential adsorbents and photocatalysts for the decontamination of dyes wastewater: a review, *RSC Advances*, 6 (2016) 79415-79436.
- [61] M. Zubair, M. Daud, G. McKay, F. Shehzad and M.A. Al-Harhi, Recent progress in layered double hydroxides (LDH)-containing hybrids as adsorbents for water remediation, *Applied Clay Science*, 143 (2017) 279-292.
- [62] C. Chen, P. Gunawan and R. Xu, Self-assembled Fe₃O₄-layered double hydroxide colloidal nanohybrids with excellent performance for treatment of organic dyes in water, *J Mater Chem*, 21 (2011) 1218-1225.
- [63] D.P. Debecker, E.M. Gaigneaux and G. Busca, Exploring, Tuning, and Exploiting the Basicity of Hydrotalcites for Applications in Heterogeneous Catalysis, *Chem-Eur J*, 15 (2009) 3920-3935.
- [64] Z.P. Xu, J. Zhang, M.O. Adebajo, H. Zhang and C. Zhou, Catalytic applications of layered double hydroxides and derivatives, *Applied Clay Science*, 53 (2011) 139-150.
- [65] S. He, Z. An, M. Wei, D.G. Evans and X. Duan, Layered double hydroxide-based catalysts: nanostructure design and catalytic performance, *Chem Commun*, 49 (2013) 5912-5920.

- [66] G. Fan, F. Li, D.G. Evans and X. Duan, Catalytic applications of layered double hydroxides: recent advances and perspectives, *Chemical Society Reviews*, 43 (2014) 7040-7066.
- [67] S. Abello, S. Mitchell, M. Santiago, G. Stoica and J. Perez-Ramirez, Perturbing the properties of layered double hydroxides by continuous coprecipitation with short residence time, *J Mater Chem*, 20 (2010) 5878-5887.
- [68] M. Ren, M. Yang, G. Chen and Q. Yuan, High-Throughput Preparation of Monodispersed Layered Double Hydroxides via Microreaction Technology, *Journal of Flow Chemistry*, 4 (2014) 164-167.
- [69] Z. Chang, C. Wu, S. Song, Y. Kuang, X. Lei, L. Wang and X. Sun, Synthesis Mechanism Study of Layered Double Hydroxides Based on Nanoseparation, *Inorg Chem*, 52 (2013) 8694-8698.
- [70] M. Pavlovic, P. Rouster, T. Oncsik and I. Szilagy, Tuning Colloidal Stability of Layered Double Hydroxides: From Monovalent Ions to Polyelectrolytes, *ChemPlusChem*, 82 (2017) 121-131.
- [71] L. Albiston, K.R. Franklin, E. Lee and J.B.A.F. Smeulders, Rheology and microstructure of aqueous layered double hydroxide dispersions, *J Mater Chem*, 6 (1996) 871-877.
- [72] Y. Zhao, F. Li, R. Zhang, D.G. Evans and X. Duan, Preparation of Layered Double-Hydroxide Nanomaterials with a Uniform Crystallite Size Using a New Method Involving Separate Nucleation and Aging Steps, *Chem Mater*, 14 (2002) 4286-4291.
- [73] M. Adachi-Pagano, C. Forano and J.-P. Besse, Synthesis of Al-rich hydrotalcite-like compounds by using the urea hydrolysis reaction—control of size and morphology, *J Mater Chem*, 13 (2003) 1988-1993.
- [74] J. Qu, Q. Zhang, X. Li, X. He and S. Song, Mechanochemical approaches to synthesize layered double hydroxides: a review, *Applied Clay Science*, 119 (2016) 185-192.

- [75] S. Miyata, Physicochemical properties of synthetic hydrotalcites in relation to composition, *Clay Clay Miner*, 28 (1980) 50-56.
- [76] K. Takehira, Recent development of layered double hydroxide-derived catalysts –Rehydration, reconstitution, and supporting, aiming at commercial application–, *Applied Clay Science*, 136 (2017) 112-141.
- [77] R.M.M. Santos, J. Tronto, V. Briois and C.V. Santilli, Thermal decomposition and recovery properties of ZnAl–CO₃ layered double hydroxide for anionic dye adsorption: insight into the aggregative nucleation and growth mechanism of the LDH memory effect, *Journal of Materials Chemistry A*, 5 (2017) 9998-10009.
- [78] Q. Wang and D. O'Hare, Recent Advances in the Synthesis and Application of Layered Double Hydroxide (LDH) Nanosheets, *Chemical Reviews*, 112 (2012) 4124-4155.
- [79] G. Layrac, M. Destarac, C. Gérardin and D. Tichit, Highly Stable Layered Double Hydroxide Colloids: A Direct Aqueous Synthesis Route from Hybrid Polyion Complex Micelles, *Langmuir*, 30 (2014) 9663-9671.
- [80] Z. Chang, D.G. Evans, X. Duan, C. Vial, J. Ghanbaja, V. Prevot, M. de Roy and C. Forano, Synthesis of [Zn–Al–CO₃] layered double hydroxides by a coprecipitation method under steady-state conditions, *J Solid State Chem*, 178 (2005) 2766-2777.
- [81] S. Abelló and J. Pérez-Ramírez, Tuning Nanomaterials' Characteristics by a Miniaturized In-Line Dispersion–Precipitation Method: Application to Hydrotalcite Synthesis, *Adv Mater*, 18 (2006) 2436-2439.
- [82] Q. Wang, S.V.Y. Tang, E. Lester and D. O'Hare, Synthesis of ultrafine layered double hydroxide (LDHs) nanoplates using a continuous-flow hydrothermal reactor, *Nanoscale*, 5 (2013) 114-117.

- [83] I. Clark, P.W. Dunne, R.L. Gomes and E. Lester, Continuous hydrothermal synthesis of Ca₂Al-NO₃ layered double hydroxides: The impact of reactor temperature, pressure and NaOH concentration on crystal characteristics, *J Colloid Interface Sci*, 504 (2017) 492-499.
- [84] P. Yaseneva, N. An, M. Finn, N. Tidemann, N. Jose, A. Voutchkova-Kostal and A. Lapkin, Continuous synthesis of doped layered double hydroxides in a meso-scale flow reactor, *Chemical Engineering Journal*, 360 (2019) 190-199.
- [85] V.S. Shirure, B.P. Nikhade and V.G. Pangarkar, Intensification of Precipitation Using Narrow Channel Reactors: Case Study of Hydrotalcite Precipitation, *Ind Eng Chem Res*, 46 (2007) 3086-3094.
- [86] X. Pang, M. Sun, X. Ma and W. Hou, Synthesis of layered double hydroxide nanosheets by coprecipitation using a T-type microchannel reactor, *J Solid State Chem*, 210 (2014) 111-115.
- [87] A. Flegler, M. Schneider, J. Prieschl, R. Stevens, T. Vinnay and K. Mandel, Continuous flow synthesis and cleaning of nano layered double hydroxides and the potential of the route to adjust round or platelet nanoparticle morphology, *RSC Advances*, 6 (2016) 57236-57244.
- [88] H. Liang, F. Meng, M. Cabán-Acevedo, L. Li, A. Forticaux, L. Xiu, Z. Wang and S. Jin, Hydrothermal Continuous Flow Synthesis and Exfoliation of NiCo Layered Double Hydroxide Nanosheets for Enhanced Oxygen Evolution Catalysis, *Nano Lett*, 15 (2015) 1421-1427.
- [89] M. Yang, E. Tuckley, J.-C. Buffet and D. O'Hare, Rapid, efficient phase pure synthesis of Ca₂AlNO₃ layered double hydroxide, *Journal of Materials Chemistry A*, 4 (2016) 500-504.
- [90] Y. Chen, Y. Su, F. Jiao and G. Chen, A simple and efficient synthesis protocol for sulfonation of nitrobenzene under solvent-free conditions via a microreactor, *RSC Advances*, 2 (2012) 5637-5644.
- [91] Y. Zhao, C. Yao, G. Chen and Q. Yuan, Highly efficient synthesis of cyclic carbonate with CO₂ catalyzed by ionic liquid in a microreactor, *Green Chemistry*, 15 (2013) 446-452.

- [92] G. Trippa and R.J.J. Jachuck, Process Intensification: Precipitation of Calcium Carbonate Using Narrow Channel Reactors, *Chemical Engineering Research and Design*, 81 (2003) 766-772.
- [93] V.S. Shirure, A.S. Pore and V.G. Pangarkar, Intensification of Precipitation Using Narrow Channel Reactors: Magnesium Hydroxide Precipitation, *Ind Eng Chem Res*, 44 (2005) 5500-5507.
- [94] H. Wu, C. Wang, C. Zeng and L. Zhang, Preparation of Barium Sulfate Nanoparticles in an Interdigital Channel Configuration Micromixer SIMM-V2, *Ind Eng Chem Res*, 52 (2013) 5313-5320.
- [95] F. Castro, S. Kuhn, K. Jensen, A. Ferreira, F. Rocha, A. Vicente and J.A. Teixeira, Process intensification and optimization for hydroxyapatite nanoparticles production, *Chemical Engineering Science*, 100 (2013) 352-359.
- [96] F. Castro, S. Kuhn, K. Jensen, A. Ferreira, F. Rocha, A. Vicente and J.A. Teixeira, Continuous-flow precipitation of hydroxyapatite in ultrasonic microsystems, *Chemical Engineering Journal*, 215-216 (2013) 979-987.
- [97] J. Ju, C. Zeng, L. Zhang and N. Xu, Continuous synthesis of zeolite NaA in a microchannel reactor, *Chemical Engineering Journal*, 116 (2006) 115-121.
- [98] Z. Liu, T. Wakihara, D. Nishioka, K. Oshima, T. Takewaki and T. Okubo, Ultrafast Continuous-Flow Synthesis of Crystalline Microporous Aluminophosphate AlPO₄-5, *Chem Mater*, 26 (2014) 2327-2331.
- [99] J. Zhang, C. Gong, X. Zeng and J. Xie, Continuous flow chemistry: New strategies for preparative inorganic chemistry, *Coordination Chemistry Reviews*, 324 (2016) 39-53.
- [100] J. Wagner, T.R. Tshikhudo and J.M. Köhler, Microfluidic generation of metal nanoparticles by borohydride reduction, *Chemical Engineering Journal*, 135 (2008) S104-S109.

- [101] L. Xu, C. Srinivasakannan, J. Peng, D. Zhang and G. Chen, Synthesis of nickel nanoparticles by aqueous reduction in continuous flow microreactor, *Chemical Engineering and Processing: Process Intensification*, 93 (2015) 44-49.
- [102] S. Sharada, P.L. Suryawanshi, R. Kumar P, S.P. Gumfekar, T.B. Narsaiah and S.H. Sonawane, Synthesis of palladium nanoparticles using continuous flow microreactor, *Colloids and Surfaces A: Physicochemical and Engineering Aspects*, 498 (2016) 297-304.
- [103] L. Xu, J. Peng, C. Srinivasakannan, G. Chen and A.Q. Shen, Synthesis of copper nanocolloids using a continuous flow based microreactor, *Applied Surface Science*, 355 (2015) 1-6.
- [104] L. Xu, C. Srinivasakannan, J. Peng, L. Zhang and D. Zhang, Synthesis of Cu-CuO nanocomposite in microreactor and its application to photocatalytic degradation, *J Alloy Compd*, 695 (2017) 263-269.
- [105] J. Aubin, M. Ferrando and V. Jiricny, Current methods for characterising mixing and flow in microchannels, *Chemical Engineering Science*, 65 (2010) 2065-2093.
- [106] T. Hibino and M. Kobayashi, Delamination of layered double hydroxides in water, *J Mater Chem*, 15 (2005) 653-656.
- [107] C.A. Antonyraj, P. Koilraj and S. Kannan, Synthesis of delaminated LDH: A facile two step approach, *Chem Commun*, 46 (2010) 1902-1904.
- [108] Y. Zhang, H. Li, N. Du, R. Zhang and W. Hou, Large-scale aqueous synthesis of layered double hydroxide single-layer nanosheets, *Colloids and Surfaces A: Physicochemical and Engineering Aspects*, 501 (2016) 49-54.
- [109] J.Z. Changshui Wang, Caiyan Shi, Dandan Cai, Facile Synthesis of Ni-Co LDH Nanocages with Improved Electrocatalytic Activity for Water Oxidation Reaction, *Int. J. Electrochem. Sci.*, 12 (2017) 10003-10014.

- [110] X. Bai, Q. Liu, H. Zhang, J. Liu, Z. Li, X. Jing, Y. Yuan, L. Liu and J. Wang, Nickel-Cobalt Layered Double Hydroxide Nanowires on Three Dimensional Graphene Nickel Foam for High Performance Asymmetric Supercapacitors, *Electrochim Acta*, 215 (2016) 492-499.
- [111] L. Jiang, Y. Sui, J. Qi, Y. Chang, Y. He, Q. Meng, F. Wei, Z. Sun and Y. Jin, Hierarchical Ni-Co layered double hydroxide nanosheets on functionalized 3D-RGO films for high energy density asymmetric supercapacitor, *Applied Surface Science*, 426 (2017) 148-159.
- [112] H. Li, F. Musharavati, E. Zalenezhad, X. Chen, K.N. Hui and K.S. Hui, Electrodeposited NiCo layered double hydroxides on titanium carbide as a binder-free electrode for supercapacitors, *Electrochim Acta*, 261 (2018) 178-187.
- [113] S.B. Kulkarni, A.D. Jagadale, V.S. Kumbhar, R.N. Bulakhe, S.S. Joshi and C.D. Lokhande, Potentiodynamic deposition of composition influenced $\text{Co}_{1-x}\text{Ni}_x$ LDHs thin film electrode for redox supercapacitors, *International Journal of Hydrogen Energy*, 38 (2013) 4046-4053.
- [114] M. Wei, Q. Huang, Y. Zhou, Z. Peng and W. Chu, Ultrathin nanosheets of cobalt-nickel hydroxides hetero-structure via electrodeposition and precursor adjustment with excellent performance for supercapacitor, *Journal of Energy Chemistry*, 27 (2018) 591-599.
- [115] Y. Liu, X. Teng, Y. Mi and Z. Chen, A new architecture design of Ni-Co LDH-based pseudocapacitors, *Journal of Materials Chemistry A*, 5 (2017) 24407-24415.
- [116] S. Shahrokhian, S. Rahimi and R. Mohammadi, Nickel-cobalt layered double hydroxide ultrathin nanosheets coated on reduced graphene oxide nanosheets/nickel foam for high performance asymmetric supercapacitors, *International Journal of Hydrogen Energy*, 43 (2018) 2256-2267.
- [117] H. Chen, L. Hu, M. Chen, Y. Yan and L. Wu, Nickel-Cobalt Layered Double Hydroxide Nanosheets for High-performance Supercapacitor Electrode Materials, *Advanced Functional Materials*, 24 (2013) 934-942.

- [118] A. Forticaux, L. Dang, H. Liang and S. Jin, Controlled Synthesis of Layered Double Hydroxide Nanoplates Driven by Screw Dislocations, *Nano Lett*, 15 (2015) 3403-3409.
- [119] J.L. Paulhiac and O. Clause, Surface coprecipitation of cobalt(II), nickel(II), or zinc(II) with aluminum(III) ions during impregnation of γ -alumina at neutral pH, *J Am Chem Soc*, 115 (1993) 11602-11603.
- [120] J.-B. d'Espinose de la Caillerie, M. Kermarec and O. Clause, Impregnation of γ -Alumina with Ni(II) or Co(II) Ions at Neutral pH: Hydrotalcite-Type Coprecipitate Formation and Characterization, *J Am Chem Soc*, 117 (1995) 11471-11481.
- [121] H. Hur and R.J. Reeder, Formation of CoAl layered double hydroxide on the boehmite surface and its role in tungstate sorption, *Journal of Environmental Sciences*, 65 (2018) 103-115.
- [122] F. Hayashi, A. Shirasaki, H. Wagata, H. Kamikawa, Y. Aoki, S. Oishi and K. Teshima, Flux-Assisted Fabrication of Vertically Aligned Layered Double Hydroxide Plates on in Situ Formed Alumina Particles, *Crystal Growth & Design*, 15 (2015) 732-736.
- [123] W. Li, K.J.T. Livi, W. Xu, M.G. Siebecker, Y. Wang, B.L. Phillips and D.L. Sparks, Formation of Crystalline Zn–Al Layered Double Hydroxide Precipitates on γ -Alumina: The Role of Mineral Dissolution, *Environ Sci Technol*, 46 (2012) 11670-11677.
- [124] A.M. Scheidegger, G.M. Lamble and D.L. Sparks, Spectroscopic Evidence for the Formation of Mixed-Cation Hydroxide Phases upon Metal Sorption on Clays and Aluminum Oxides, *J Colloid Interface Sci*, 186 (1997) 118-128.
- [125] S.N. Towle, J.R. Bargar, G.E. Brown and G.A. Parks, Surface Precipitation of Co(II)(aq) on Al₂O₃, *J Colloid Interface Sci*, 187 (1997) 62-82.
- [126] S. Elbasuney, Surface engineering of layered double hydroxide (LDH) nanoparticles for polymer flame retardancy, *Powder Technol.*, 277 (2015) 63-73.

- [127] T. Zhan, Y. Song, Q. Yang and W. Hou, Structure and catalytic activity of hemoglobin assembled with layered double hydroxide nanosheets by coprecipitation using a T-shaped microreactor, *Chemical Engineering Journal*, 306 (2016) 1143-1150.
- [128] O. Pascu, S. Marre, B. Cacciuttolo, G. Ali, L. Hecquet, M. Pucheault, V. Prevot and C. Aymonier, Instant One-Pot Preparation of Functional Layered Double Hydroxides (LDHs) via a Continuous Hydrothermal Approach, *ChemNanoMat*, 3 (2017) 614-619.
- [129] X. Luo, S. Yuan, X. Pan, C. Zhang, S. Du and Y. Liu, Synthesis and Enhanced Corrosion Protection Performance of Reduced Graphene Oxide Nanosheet/ZnAl Layered Double Hydroxide Composite Films by Hydrothermal Continuous Flow Method, *ACS Applied Materials & Interfaces*, 9 (2017) 18263-18275.
- [130] S. Elbasuney, Dispersion characteristics of dry and colloidal nano-titania into epoxy resin, *Powder Technol.*, 268 (2014) 158-164.
- [131] M. Li, H. Ji, Y. Wang, L. Liu and F. Gao, MgFe-layered double hydroxide modified electrodes for direct electron transfer of heme proteins, *Biosensors and Bioelectronics*, 38 (2012) 239-244.
- [132] K. Charradi, C. Forano, V. Prevot, D. Madern, A. Ben Haj Amara and C. Mousty, Characterization of Hemoglobin Immobilized in MgAl-Layered Double Hydroxides by the Coprecipitation Method, *Langmuir*, 26 (2010) 9997-10004.
- [133] W. Sun, Y. Guo, Y. Lu, A. Hu, F. Shi, T. Li and Z. Sun, Electrochemical biosensor based on graphene, Mg₂Al layered double hydroxide and hemoglobin composite, *Electrochim Acta*, 91 (2013) 130-136.
- [134] T. Zhan, X. Wang, Y. Zhang, Y. Song, X. Liu, J. Xu and W. Hou, Direct electrochemistry and electrocatalysis of hemoglobin immobilized in layered double hydroxides modified with amino functionalized ionic liquid through coprecipitation technique, *Sensors and Actuators B: Chemical*, 220 (2015) 1232-1240.

- [135] S. Marre, C. Aymonier, P. Subra and E. Mignard, Dripping to jetting transitions observed from supercritical fluid in liquid microflows, *Appl Phys Lett*, 95 (2009) 134105.
- [136] T. Gendrineau, S. Marre, M. Vaultier, M. Pucheault and C. Aymonier, Microfluidic Synthesis of Palladium Nanocrystals Assisted by Supercritical CO₂: Tailored Surface Properties for Applications in Boron Chemistry, *Angewandte Chemie International Edition*, 51 (2012) 8525-8528.
- [137] G. Ali, T. Moreau, C. Forano, C. Mousty, V. Prevot, F. Charmantray and L. Hecquet, Chiral Polyol Synthesis Catalyzed by a Thermostable Transketolase Immobilized on Layered Double Hydroxides in Ionic liquids, *ChemCatChem*, 7 (2015) 3163-3170.
- [138] X. Hao, Y. Zhang, Z. Diao, H. Chen, A. Zhang and Z. Wang, Engineering one-dimensional and two-dimensional birnessite manganese dioxides on nickel foam-supported cobalt–aluminum layered double hydroxides for advanced binder-free supercapacitors, *RSC Advances*, 4 (2014) 63901-63908.
- [139] H. Zhu, Q. Liu, Z. Li, J. Liu, X. Jing, H. Zhang and J. Wang, Synthesis of exfoliated titanium dioxide nanosheets/nickel–aluminum layered double hydroxide as a novel electrode for supercapacitors, *RSC Advances*, 5 (2015) 49204-49210.
- [140] S. Wang, Z. Huang, R. Li, X. Zheng, F. Lu and T. He, Template-assisted synthesis of NiP@CoAl-LDH nanotube arrays with superior electrochemical performance for supercapacitors, *Electrochim Acta*, 204 (2016) 160-168.
- [141] Z. Li, M. Chen, Q. Zhang, J. Qu, Z. Ai and Y. Li, Mechanochemical synthesis of ultrafine ZnS/Zn-Al layered double hydroxide heterojunction and their photocatalytic activities in dye degradation, *Applied Clay Science*, 144 (2017) 115-120.
- [142] Z. Li, Q. Zhang, X. He and M. Chen, Enhanced visible light photocatalytic activity of the mechanochemically prepared nanosized Zn_xCd_{1-x}S/Zn-Al layered double hydroxide precursor heterojunctions, *Applied Clay Science*, 151 (2018) 201-210.

- [143] H.N.M.a.Y.-F.S. Tengfei Li, Polyoxometalate (POM)-Layered Double Hydroxides (LDH) Composite Materials: Design and Catalytic Applications, *Catalysts*, 7(9) (2017) 260.
- [144] M. Daud, M.S. Kamal, F. Shehzad and M.A. Al-Harhi, Graphene/layered double hydroxides nanocomposites: A review of recent progress in synthesis and applications, *Carbon*, 104 (2016) 241-252.
- [145] Y. Cao, G. Li and X. Li, Graphene/layered double hydroxide nanocomposite: Properties, synthesis, and applications, *Chemical Engineering Journal*, 292 (2016) 207-223.
- [146] M. Zhao, Q. Zhao, B. Li, H. Xue, H. Pang and C. Chen, Recent progress in layered double hydroxide based materials for electrochemical capacitors: design, synthesis and performance, *Nanoscale*, 9 (2017) 15206-15225.
- [147] M.-Q. Zhao, Q. Zhang, J.-Q. Huang and F. Wei, Hierarchical Nanocomposites Derived from Nanocarbons and Layered Double Hydroxides - Properties, Synthesis, and Applications, *Advanced Functional Materials*, 22 (2012) 675-694.
- [148] N. Hong, L. Song, B. Wang, A.A. Stec, T.R. Hull, J. Zhan and Y. Hu, Co-precipitation synthesis of reduced graphene oxide/NiAl-layered double hydroxide hybrid and its application in flame retarding poly(methyl methacrylate), *Mater Res Bull*, 49 (2014) 657-664.
- [149] P.S. Khobragade, D.P. Hansora, J.B. Naik and A. Chatterjee, Flame retarding performance of elastomeric nanocomposites: A review, *Polymer Degradation and Stability*, 130 (2016) 194-244.
- [150] X. Wang, S. Zhou, W. Xing, B. Yu, X. Feng, L. Song and Y. Hu, Self-assembly of Ni-Fe layered double hydroxide/graphene hybrids for reducing fire hazard in epoxy composites, *Journal of Materials Chemistry A*, 1 (2013) 4383-4390.
- [151] T. Wen, X. Wu, X. Tan, X. Wang and A. Xu, One-Pot Synthesis of Water-Swellable Mg-Al Layered Double Hydroxides and Graphene Oxide Nanocomposites for Efficient

Removal of As(V) from Aqueous Solutions, *ACS Applied Materials & Interfaces*, 5 (2013) 3304-3311.

[152] L. Tan, Y. Wang, Q. Liu, J. Wang, X. Jing, L. Liu, J. Liu and D. Song, Enhanced adsorption of uranium (VI) using a three-dimensional layered double hydroxide/graphene hybrid material, *Chemical Engineering Journal*, 259 (2015) 752-760.

[153] Q. Fang and B. Chen, Self-assembly of graphene oxide aerogels by layered double hydroxides cross-linking and their application in water purification, *Journal of Materials Chemistry A*, 2 (2014) 8941-8951.

[154] M.G. Álvarez, D. Tichit, F. Medina and J. Llorca, Role of the synthesis route on the properties of hybrid LDH-graphene as basic catalysts, *Applied Surface Science*, 396 (2017) 821-831.

[155] D. Chen, X. Wang, T. Liu, X. Wang and J. Li, Electrically Conductive Poly(vinyl alcohol) Hybrid Films Containing Graphene and Layered Double Hydroxide Fabricated via Layer-by-Layer Self-Assembly, *ACS Applied Materials & Interfaces*, 2 (2010) 2005-2011.

[156] H. Li, J. Wen, R. Yu, J. Meng, C. Wang, C. Wang and S. Sun, Facile synthesis of a nanocomposite based on graphene and ZnAl layered double hydroxides as a portable shelf of a luminescent sensor for DNA detection, *RSC Advances*, 5 (2015) 9341-9347.

[157] M. Li, J.E. Zhu, L. Zhang, X. Chen, H. Zhang, F. Zhang, S. Xu and D.G. Evans, Facile synthesis of NiAl-layered double hydroxide/graphene hybrid with enhanced electrochemical properties for detection of dopamine, *Nanoscale*, 3 (2011) 4240-4246.

[158] J. Wang, X. Mei, L. Huang, Q. Zheng, Y. Qiao, K. Zang, S. Mao, R. Yang, Z. Zhang, Y. Gao, Z. Guo, Z. Huang and Q. Wang, Synthesis of layered double hydroxides/graphene oxide nanocomposite as a novel high-temperature CO₂ adsorbent, *Journal of Energy Chemistry*, 24 (2015) 127-137.

- [159] A. Garcia-Gallastegui, D. Iruretagoyena, V. Gouvea, M. Mokhtar, A.M. Asiri, S.N. Basahel, S.A. Al-Thabaiti, A.O. Alyoubi, D. Chadwick and M.S.P. Shaffer, Graphene Oxide as Support for Layered Double Hydroxides: Enhancing the CO₂ Adsorption Capacity, *Chem Mater*, 24 (2012) 4531-4539.
- [160] G.B.B. Varadwaj and V.O. Nyamori, Layered double hydroxide- and graphene-based hierarchical nanocomposites: Synthetic strategies and promising applications in energy conversion and conservation, *Nano Research*, 9 (2016) 3598-3621.
- [161] Y. Kim and S. Kim, Direct growth of cobalt aluminum double hydroxides on graphene nanosheets and the capacitive properties of the resulting composites, *Electrochim Acta*, 163 (2015) 252-259.
- [162] N. Yulian, L. Ruiyi, L. Zaijun, F. Yinjun and L. Junkang, High-performance supercapacitors materials prepared via in situ growth of NiAl-layered double hydroxide nanoflakes on well-activated graphene nanosheets, *Electrochim Acta*, 94 (2013) 360-366.
- [163] T. Yan, R. Li and Z. Li, Nickel–cobalt layered double hydroxide ultrathin nanoflakes decorated on graphene sheets with a 3D nanonetwork structure as supercapacitive materials, *Mater Res Bull*, 51 (2014) 97-104.
- [164] J. Fang, M. Li, Q. Li, W. Zhang, Q. Shou, F. Liu, X. Zhang and J. Cheng, Microwave-assisted synthesis of CoAl-layered double hydroxide/graphene oxide composite and its application in supercapacitors, *Electrochim Acta*, 85 (2012) 248-255.
- [165] S. Huang, G.-N. Zhu, C. Zhang, W.W. Tjiu, Y.-Y. Xia and T. Liu, Immobilization of Co–Al Layered Double Hydroxides on Graphene Oxide Nanosheets: Growth Mechanism and Supercapacitor Studies, *ACS Applied Materials & Interfaces*, 4 (2012) 2242-2249.
- [166] J. Xu, S. Gai, F. He, N. Niu, P. Gao, Y. Chen and P. Yang, A sandwich-type three-dimensional layered double hydroxide nanosheet array/graphene composite: fabrication and high supercapacitor performance, *Journal of Materials Chemistry A*, 2 (2014) 1022-1031.

- [167] R. Ma, X. Liu, J. Liang, Y. Bando and T. Sasaki, Molecular-Scale Heteroassembly of Redoxable Hydroxide Nanosheets and Conductive Graphene into Superlattice Composites for High-Performance Supercapacitors, *Adv Mater*, 26 (2014) 4173-4178.
- [168] W. Ma, R. Ma, C. Wang, J. Liang, X. Liu, K. Zhou and T. Sasaki, A Superlattice of Alternately Stacked Ni-Fe Hydroxide Nanosheets and Graphene for Efficient Splitting of Water, *ACS Nano*, 9 (2015) 1977-1984.
- [169] G.-Q.S.H.I. Hai-Yan Wang, Layered Double Hydroxide/Graphene Composites and Their Applications for Energy Storage and Conversion, *Acta Physico-Chimica Sinica*, 34 (2018) 22-35.
- [170] P.L. Sunil, R. Jean-Marie and D. Philippe, One-pot Microwave-assisted Synthesis of Graphene/Layered Double Hydroxide (LDH) Nanohybrids, *Nano-Micro Letters*, 7 (2015).
- [171] H. Li, G. Zhu, Z.-H. Liu, Z. Yang and Z. Wang, Fabrication of a hybrid graphene/layered double hydroxide material, *Carbon*, 48 (2010) 4391-4396.
- [172] W.S. Hummers and R.E. Offeman, Preparation of Graphitic Oxide, *J Am Chem Soc*, 80 (1958) 1339-1339.
- [173] A.V. Radha, P.V. Kamath and C. Shivakumara, Order and disorder among the layered double hydroxides: combined Rietveld and DIFFaX approach, *Acta Crystallographica Section B*, 63 (2007) 243-250.
- [174] B. Gregoire, E. Andre, C. Ruby and C. Carteret, Tuning and Investigating the Structure of MII-FeIII Layered Double Hydroxides (MII = NiII, CoII and MgII) in Relation to their Composition: From Synthesis to Anionic Exchange Properties, *Current Inorganic Chemistry*, 5 (2015) 169-183.
- [175] A.V. Radha and P.V. Kamath, Aging of trivalent metal hydroxide/oxide gels in divalent metal salt solutions: Mechanism of formation of layered double hydroxides (LDHs), *Bull. Mat. Sci.*, 26 (2003) 661-666.

- [176] Y. Wang, L. Li, L. Yan, L. Cao, P. Dai, X. Gu and X. Zhao, Continuous synthesis for zirconium metal-organic frameworks with high quality and productivity via microdroplet flow reaction, *Chinese Chemical Letters*, 29 (2018) 849-853.
- [177] Y. Wang, L. Li, L. Yan, X. Gu, P. Dai, D. Liu, J.G. Bell, G. Zhao, X. Zhao and K.M. Thomas, Bottom-Up Fabrication of Ultrathin 2D Zr Metal–Organic Framework Nanosheets through a Facile Continuous Microdroplet Flow Reaction, *Chem Mater*, 30 (2018) 3048-3059.
- [178] C. Echaide-Górriz, C. Clément, F. Cacho-Bailo, C. Téllez and J. Coronas, New strategies based on microfluidics for the synthesis of metal–organic frameworks and their membranes, *Journal of Materials Chemistry A*, 6 (2018) 5485-5506.
- [179] N. Hao, Y. Nie and J.X.J. Zhang, Microfluidic Flow Synthesis of Functional Mesoporous Silica Nanofibers with Tunable Aspect Ratios, *ACS Sustainable Chemistry & Engineering*, 6 (2018) 1522-1526.
- [180] X. Wang, J. Liu, P. Wang, A. deMello, L. Feng, X. Zhu, W. Wen, R. Kodzius and X. Gong, Synthesis of Biomaterials Utilizing Microfluidic Technology, *Genes*, 9 (2018).
- [181] Z. Liu, T. Wakihara, N. Nomura, T. Matsuo, C. Anand, S.P. Elangovan, Y. Yanaba, T. Yoshikawa and T. Okubo, Ultrafast and Continuous Flow Synthesis of Silicoaluminophosphates, *Chem Mater*, 28 (2016) 4840-4847.
- [182] T. Vandermeersch, T.R.C. Van Assche, J.F.M. Denayer and W. De Malsche, A continuous flow reactor setup as a tool for rapid synthesis of micron sized NaA zeolite, *Micropor Mesopor Mat*, 226 (2016) 133-139.
- [183] Y. Hu, K. Wang, T. Wang and G. Luo, Ultrafast synthesis of TS-1 without extraframework titanium species in a continuous flow system, *Micropor Mesopor Mat*, 270 (2018) 149-154.

Table 1: Summary of methods and experimental parameters

Entry	Reactor	Experimental conditions	Parameters studied	LDH	React ^r vol. (mL)	Mixing	Heat ^{ing}	[M ²⁺ +M ³⁺] (mol.L ⁻¹)	Flow rate (mL.min ⁻¹)	T (°C)	P (MPa)	Adv ^{ge}	Ref.
Control of LDH composition, particle size and morphology													
1	Tank	- Steady-state - Magnetic stirring - pH control	- [cation] - Solvent - Res. t - pH - Nature anion	ZnAl	230	Magnetic stirrer (300 rpm)	no	3.10 ⁻³ - 3.10 ⁻¹		21	0.1		[80]
2	Cop ^{ion} chamber	- Vigorous stirring (turbulent regime) - In line pH control	Res. t	NiAl MgAl MgFe	6	high shear homog ^{er}	no	1				Flash cop. ^{ion}	[67, 81]
3	Counter-current flow	- Down-flow (base) and up-flow (Mg, Ca, Al salts) counter-currents (down:up flow = 2:1)	P (0 – 24 MPa); T (0 - 400 °C)	MgAl CaAl		no	Pre-heat ^r	0.1	20 (base) 10 (metal salts)	75-400	5; 24		[82]
4	Counter-current flow	- Down-flow (base) and up-flow (Ca, Al precursors) counter-currents (down:up flow = 2:1)	- P (5 – 20 MPa); T (75 - 200 °C) - [NaOH] = 0.01 – 1 M	CaAl		no	Pre-heat ^r	0.1		75 - 200	5 - 20		[83]

5	Meso-scale tubular	2 step process: - sol ^{ions} injected in the reactor in continuous flow (coprecipitation) - Mixture at the exit dripped into thermostated beaker (aging)	- Cationic composition - Aging T (65 and 80 °C)	MgAl MgAlFe MgAlCo MgAlNi MgAlCu MgAlZn		no	no	0.20	4	65 - 95	0.1	Similar residence and μ mixing times	[84]
6	T- and Y-shaped μ mixers	- Reactant injected in the restricted vol - Simultaneous mixing and segmentation - Flow rate: 0.4 – 1.15 mL s ⁻¹	- S ^(a) - Segment ^{ion} - Re ^(b) - Mixer config ^{ion}	MgAl	0.205	no	no		24 - 70	25	0.1		[85]
7	T-shaped μ mixer	Salts (M ²⁺ /Al = 2 - 4) and base sol ^{ions} pumped in the reactor through 2 inlets	[metal ions] = 0.1 - 4 mol L ⁻¹	MgAl NiAl ZnAl	4.10 ⁻³	no	no	0.3	20	25	0.1	Nack nanosheets obtained	[86]
8	Static mixer	sol ^{ions} pumped into a static spiral mixer then injected in a semi-continuous tubular centrifuge	[metal salts]; [NaOH]	MgAl			Elements rotating alternat ^{ly}	1.7		25	0.1	Integrated approach (synthesis, cleaning)	[87]

9	T-shaped mixer	sol ^{ions} pumped into the μ channel reactor		MgAl MgFe NiAl MgAlFe MgZnAl CuCoZn Al	$6.4 \cdot 10^{-3}$	no	Pre-heat ^t	300	80	0.1	Synthesis of \neq LDHs and Cl- and NO ₃ -LDH without inert gas protection	[68]	
10	Column	Preparation in 2 steps: 1) Seed growth in the reactor (160 °C, 20 min) 2) Flowing reaction sol ^{ion} (1 mL min ⁻¹ , 160 °C, 1.1 MPa, 4 h)		NiCo	33.2	no	Tube furnace	10 ⁻²	1	160	1.1	Synthesis of NiCo LDH	[88]
11	Column	Precursor sol ^{ions} flowed on alumina-coated substrate		ZnAl CoAl	33.2	no	Tube furnace	5.10 ⁻⁷ (Zn) 5.10 ⁻⁴ (Co)		95	0.1	growth screw-driven mechanism	[118]

Functional LDHs and LDH-based composites

12	Counter-current flow	Super-heated NaOH / NaNO ₃ sol ^{ion} passed down an inner nozzle pipe against metal sol ^{ion}	Post synthesis surf. modif. with PEA or DDA	MgAl		no	Pre-heat ^t	0.1	10	75 (down ⁿ fl ^w); 25 (up fl ^w)	5	Balance hydro ϕ / hydrophob.	[126]
13	T-shaped mixer	Salts (M ²⁺ /Al = 3) / Hb sol ^{ion} and NaOH pum ^d in the reactor at pH = 9	[metal ions] = 6 – 48 mmol.L ⁻¹	MgAl	$4 \cdot 10^{-3}$	no	no	10 ⁻³		25	0.1	Improv ^t Hb bioactivity	[127]

14	High pressure co-flow	- Salt sol ^{ion} in the inner tube ($\phi = 0.75$ mm); base s sol ^{ion} in the external tube ($\phi = 2.1$ mm) - Fl ^w rates: base : prec ^{ors} 2:1 - P = 20 MPa; T = 50 – 200 °C		MgAl NiAl ZnAl	1		Oil bath	$3.3 \cdot 10^{-2}$	7.5 – 10.8	50 - 200	20	Versatile functional LDHs	[128]
15	Column	2 steps: 1) seed growth of LDH on the Al alloy support 2) flow ^{ing} prec ^{or} sol ^{ion} (RGO, Zn,Al) on the supported seeds	[RGO]	ZnAl		no	Tube furnace	0.4	0.5	80	0.62	growth of RGO/LDH anticor ^{ion} film on alloy substrate	[129]

^(a) Supersaturation ; ^(b) Reynolds number

Table 2: Summaries of synthesis parameters, of structural properties of LDHs prepared and applications studied

Entry	Setup config ^{ion}	LDH	Res. t. (s) ^(a)	pH	Base	S ^(b)	D ₀₀₃₍₀₀₂₎ (nm) ^(c)	Nb stacked layers ^(d)	Lateral dim. (nm) ^(e) [morphology]	Application	Ref.
Control of LDH composition, particle size and morphology											
1	Tank	ZnAl	30 - 900	7- 11	NaOH+ Na ₂ CO ₃ / NaCH ₃ CO ₂ / NaC ₆ H ₅ CO ₂	H/L ^(f)	21– 57	28 - 75	80 - 200		[80]
2	Cop ^{ion} chamber	NiAl MgAl MgFe	1 – 36	10	NaOH+ Na ₂ CO ₃	H	4 – 7 ($\tau = 1 s$) 4 - 8 ($\tau = 12 s$)	5 – 9 ($\tau = 1 s$) 5 – 10 ($\tau = 12 s$)	< 10 [tightly aggregated polycrystals ($\tau = 1 s$) ~ 500 – 1000 [Hexagonal ($\tau = 12 s$)]]		[67, 81]
3	Counter- current flow	MgAl CaAl	4 4		NaOH + Na ₂ CO ₃ NaOH + Na ₂ CO ₃	H H	10 25 – 62	12 31 - 77	30 – 40 (5 MPa; 75 °C) [Nanowire] 1000 - 1500 (5 MPa; 75 °C) [Hexagonal]		[82]
4	Counter- current flow	CaAl	4		NaOH + NaNO ₃	H	30 – 80	35 - 93	2000 – 5000		[83]
5	Meso-scale reactor + thermostated beaker	MgAl MgAlFe MgAlCo MgAlNi MgAlCu MgAlZn	0.34	No contr ^l	NaOH + Na ₂ CO ₃	H	10.4(<i>MgAl</i>) ^(g) 11.9(<i>MgAlFe</i>) 11.7(<i>MgAlCo</i>) 9.5(<i>MgAlNi</i>) 9.8(<i>MgAlCu</i>) 11.1(<i>MgAlZn</i>)	13 15 15 12 13 14	20 – 30(<i>MgAl</i>) [Agglomerates of hexagonal platelets]		[84]

6	T- and Y-shaped μ mixers	MgAl	0.18 – 0.5	10 – 11	NaOH + Na ₂ CO ₃	H			7000 – 17000 [Agglomerates]	[85]	
7	T-shaped μ mixer	MgAl NiAl ZnAl	12.10 ⁻³		NH ₃ .H ₂ O		12 (<i>MgAl</i> (<i>f/c</i>)) 18.7 (<i>MgAl</i> (<i>p^d</i>))	1-2 (<i>MgAl</i> (<i>f</i>)) ^(h) 11 (<i>MgAl</i> (<i>f/c</i>)) ⁽ⁱ⁾ 21 (<i>MgAl</i> (<i>p^d</i>)) ⁽ⁱ⁾	15 – 30 (<i>MgAl</i> (<i>f</i>)) 60 – 120 (<i>MgAl</i> (<i>p^d</i>))	Synthesis nanohybrids	[86]
8	Static mixer + tubular centrifuge	MgAl	~ 3.5	13.2	NaOH + Na ₂ CO ₃	H/L			[Rounded shape] (H S) [Hexagonal] (L S + recryst ^{ion})	[87]	
9	T-shaped μ mixer	MgAl MgFe NiAl MgAlFe MgZnAl CuCoZn Al	1.3.10 ⁻³		NaOH + Na ₂ CO ₃		5 (<i>MgAl</i>)	7	20 – 100 (<i>MgAl</i>) 70 – 100 (<i>CuCoZnAl</i>) [Hexagonal]	Variety composition	[68]
10	Column	NiCo	~1800		NH ₃ .H ₂ O	L	~ 15	~ 18	500 – 1000 [Hexagonal]	Activity for OER ^(k)	[88]
11	Column	ZnAl CoAl			HMT Urea	vL	200 - 300	250 - 375	10000 – 20000 [Hexagonal]	Growth screw-driven mechanism	[118]
functional LDHs and LDH-based composites											
12	Counter-current flow	MgAl			NaOH + NaNO ₃	H			50	Heat sink action	[126]
13	T-shaped μ mixer	MgAl		9	NaOH	H	5	6	50 – 200 [Plate-like]	Oxid ^{ion} of ODP to 2,3-diaminophenazine	[127]

14	High P co-flow μ system	MgAl NiAl ZnAl	5 – 10	7-9	NaOH + Na ₂ CO ₃		11.5/5.6/17.5: Mg/Ni/ZnAl- CO ₃	15/7/23: Mg- /Ni-/ZnAl-CO ₃	36/9/200: Mg-/Ni- /ZnAl-CO ₃ [Rounded shape]	TK catalytic activity Cinnam ^{de} hydr ^{ion}	[128]
15	Column	ZnAl		5.6	NH ₃ .H ₂ O	L				Corrosion protection	[129]

^(a) $\tau = V_{\text{reactor}}/F_{\text{liquid}}$; ^(b) Supersaturation level; ^(c) From the Scherrer equation applied to the 003 (or 002) reflection; ^(d) $L_{003(002)}/d_{003(002)}$; ^(e) Determined by microscopy; ^(f) H: high; L: low; vL: very low; ^(g) all samples aged at 65 °C; ^(h) *f*: fresh; ⁽ⁱ⁾ *f/c*: fresh and centrifuged; ^(j) p^d: peptized; ^(k) oxygen evolution reaction.

Table 3 : Comparison of the properties of the LDH samples obtained using continuous-flow methods and static methods

Entry	LDH		Static method		Continuous-flow method	Continuous vs static method	Ref.
1	MgAl	Batch	~ 81 nm ^a , highly crystalline -S _{BET} : 6 m ² g ⁻¹	Steady-state conditions	- 20 – 60 nm ^a -S _{BET} : 16 – 62 m ² g ⁻¹	-Smaller particles -Preparation time decreased from 10 – 70 h to 3 – 9 h for same quantity of LDH	[80]
2	MgAl	Batch	38 nm ^b Broad particle size distribution	ILD method	4 – 11 nm ^b	Smaller particles	[81]
3	CaAl	Colloid mill	-14.7 ^c and 10.7 nm ^d -S _{BET} = 17.95 m ² g ⁻¹	Counter-current flow reactor	~ 50 - 75 nm ^c and 65 to 120 nm ^d	Larger particles and stacking	[83] [89]
4	MgAl	Stirred semi-batch	- 15 μm ^e - Prod ^{ion} 5 . 10 ³ kg: 3283 kW; 3 batches; V _{react.} = 0.7 m ³	Narrow-channel reactor	- 7 μm ^e - Prod ^{ion} 5 . 10 ³ kg: 280 kW; 25 narrow channels; V _{react.} = 0.205 . 10 ⁻⁶ m ³	- Smaller particles - Affords an intensified process	[85]
5	MgAl	PWD (beaker)	- ~80 nm ^f - Single layers	T-type μreactor [86]	- 20 - 30 nm; thick. 0.68 - 1.13 nm ^g - 1 – 2 layers	Nanosheets of smaller lateral size (suspensions)	[108] [86]
6	MgAl	Separated nucleation/aging (colloid mill)	60 - 80 nm ^f ; ~22 nm ^b	T-type μreactor	50 – 150 nm ^f	Larger particles due to dissolution-recrystallization during aging (avoided in the separated nucleation/aging method)	[72] [68]
7	NiCo	SHR	Thick. ~90 nm ⁱ Nanoplatelets	HCFR	Thick. ~15 nm ⁱ Nanoplatelets	-Better control of morphology and size -Higher activity for OER (lower onset overpotential and larger catalytic current density)	[88]
8	ZnAl CoAl	Sealed glass vial	Zn-Al and Co-Al: interpenetrated nanoplates	CFR column	-ZnAl: ø = 10 - 20 μm; thick. ~100 nm ⁱ	More uniform size and thickness	[118]

					-CoAl: $\phi = < 10 \mu\text{m}$; thick. $< 100 \text{ nm}^i$ -Screw dislocations in both		
9	Hb/MgAl	Classical coprecipitation	- 80 – 200 nm ^f (aggregated) -Hb immobilization rate: 66.5% -Bioactivity: 21.44%	T-type μ reactor	- 20 – 40 nm; thick. < 5 nm ^f -Hb immobilization rate: 90.5 – 95.8% -Bioactivity: 73.5 – 30.98%	- Smaller and more dispersed particles with edge-to-edge interactions - Higher bioactivity in the reaction of OPD with H ₂ O ₂ to 2,3- diaminophenazine	[127]

^a Average crystallite size from the Scherrer equation applied to the 006 reflection; ^b Average crystallite size from the Scherrer equation applied to the 003 reflection; ^c Average crystallite size from the Scherrer equation applied to the 002 reflection; ^d Average crystallite size from the Scherrer equation applied to the 030 reflection; ^e Particle size determined using light scattering technique; ^f Lateral size determined by TEM; ^g determined by AFM; ^h Average crystallite size from the Scherrer equation applied to the 110 reflection; ⁱ Determined by SEM

